Electronic Supplementary Material (ESI) for RSC Chemical Biology.

Supporting Information for:

Fluorescence lifetime predicts performance of voltage sensitive fluorophores in cardiomyocytes and neurons

Steven C. Boggess,[‡⁂] Julia R. Lazzari-Dean,[‡⁂] Benjamin K. Raliski,[‡⁂] Dong Min Mun,[‡] Amy Y. Li,[‡] Joshua L. Turnbull,[‡] and Evan W. Miller[‡§†*]

Departments of [‡]Chemistry and [§]Molecular & Cell Biology and [†]Helen Wills Neuroscience Institute. University of California, Berkeley, California 94720, United States.

* evanwmiller@berkeley.edu
⁂ These authors contributed equally and are listed in alphabetical order.

DOI: 10.1039/d0cb00152j.

Table of Contents

1. General methods for chemical synthesis and characterization

Chemical reagents and solvents (dry) were purchased from commercial suppliers and used without further purification. References to previously synthesized compounds are provided along with characterization data. Thin layer chromatography (TLC) (Silicycle, F254, 250 μm) and preparative thin layer chromatography (PTLC) (Silicycle, F254, 1000 μm) was performed on glass backed plates pre-coated with silica gel and were visualized by fluorescence quenching under UV light. Flash column chromatography was performed on Silicycle Silica Flash F60 (230–400 Mesh) using a forced flow of air at 0.5–1.0 bar. NMR spectra were measured on Bruker AVB-400 MHz, 100 MHz, AVQ-400 MHz, 100 MHz, Bruker AV-600 MHz, 150 MHz. NMR spectra measured on Bruker AVII-900 MHz, 225 MHz, equipped with a TCI cryoprobe accessory, were performed by Dr. Jeffrey Pelton (QB3). Chemical shifts are expressed in parts per million (ppm) and are referenced to $CDCl_3$ (7.26 ppm, 77.16 ppm) or DMSO (2.50 ppm, 39.52 ppm). Coupling constants are reported as Hertz (Hz). Splitting patterns are indicated as follows: s, singlet; d, doublet; t, triplet; q, quartet; dd, doublet of doublets; m, multiplet. High-resolution mass spectra (HR-ESI-MS) were measured by the QB3/Chemistry mass spectrometry service at University of California, Berkeley. High performance liquid chromatography (HPLC) and low resolution ESI Mass Spectrometry were performed on an Agilent Infinity 1200 analytical instrument coupled to an Advion CMS-L ESI mass spectrometer. The column used for the analytical HPLC was Phenomenex Luna 5 μm C18(2) (4.6 mm I.D. × 75 mm) with a flow rate of 1.0 mL/min. The mobile phases were MQ-H2O with 0.05% trifluoroacetic acid (eluent A) and HPLC grade acetonitrile with 0.05% trifluoroacetic acid (eluent B). Signals were monitored at 254, 350, and 480 nm over 10 min with a gradient of 10-100% eluent B unless otherwise noted. Ultra-high performance liquid chromatography (UHPLC) for purification of final compounds was performed using a Waters Acquity Autopurification system equipped with a Phenomenex Luna 10 μm C18(2) column (21.2 mm I.D. x 250 mm) with a flow rate of 30.0 mL/min, made available by the Catalysis Facility of Lawrence Berkeley National Laboratory (Berkeley, CA). The mobile phases were MQ-H2O with 0.05% trifluoroacetic acid (eluent A) and HPLC grade acetonitrile with 0.05% trifluoroacetic acid (eluent B). Signals were monitored at 254, 350, and 480 nm over 20 min with a gradient of 10-100% eluent B, unless otherwise noted.

2. Spectroscopic studies

Stock solutions of VoltageFluors were prepared in DMSO (500 μM-1 mM) by comparing the absorbance of the dichlorofluorescein peak of each VoltageFluor with the known extinction coefficient for this dye head.[1] These stock solutions were then diluted (1:1000) in the indicated solvent for each spectroscopic analysis. UV-Vis absorbance and fluorescence spectra were recorded using a Shimadzu 2501 Spectrophotometer (Shimadzu) and a Quantamaster Master 4 L-format scanning spectrofluorometer (Photon Technologies International). The fluorometer is equipped with an LPS-220B 75-W xenon lamp and power supply, A-1010B lamp housing with integrated igniter, switchable 814 photon-counting/analog photomultiplier detection unit, and MD5020 motor driver. Samples were measured in 1-cm path length quartz cuvettes (Starna Cells).

Relative quantum yields (Φ_{Fl}) were calculated by comparison to fluorescein (Φ_{Fl} = 0.93 in 0.1 M NaOH, Φ_{Fl} = 0.92 in Ethanol w/ 0.1 M KOH)[2,3] and rhodamine 6G (Φ_{Fl} = 0.95 in ethanol)[4] as references.[5] Stock solutions of standards were prepared in DMSO (0.25-1.25 mM) and diluted with appropriate solvent (1:1000 dilution). Absorption and emission (excitation = 485 nm) were taken at 5 concentrations. The absorption value at the excitation wavelength (485 nM) was plotted against the integration of the area of fluorescence curve (495-675 nm). For fluorescein, the integration of the area of the fluorescence curve was also taken with an excitation at 440 nm. The areas from 495-675 nm and 558-675 nm were used to extrapolate the area of the fluorescence curve with an excitation at 485 nm. This ensured the full fluorescence area of fluorescein excited at 485 nm was used for Φ_{Fl} calculations. The slope of the linear best fit of the data was used to calculate the relative

Φ_{Fl} by the equation $\Phi_{Fl(X)} = \Phi_{Fl(R)}(S_X/S_R)(\eta_X/\eta_R)^2$, where S_R and S_X are the slopes of the reference compound and unknown, respectively, and η is the refractive index of the solution. This method was validated by cross-referencing the reported Φ_{Fl} values of fluorescein and rhodamine 6G to the calculated Φ_{Fl} using the one standard as a reference for the other and vice versa. Calculated Φ_{Fl} values within 10% of the reported values for both standards ensured that Φ_{Fl} values calculated for the VoltageFluors were reliable within 10% error.

3. Preparation of POPC Vesicles

1-palmitoyl-2-oleoyl-glycero-3-phosphocholine (16:0-18:1 PC, POPC) was purchased as a $CHCl_3$ solution from Avanti Polar Lipids (Alabaster, AL). Stocks were aliquoted and stored at -80°C; all lipid solutions were handled in glassware cleaned with copious amounts of $CHCl_3$. For preparation of vesicles, 1-15 mg of POPC (at 4 mg/mL in $CHCl_3$) was dried down on a rotary evaporator at 45°C and 35 RPM to produce a film. The film was dried under vacuum at room temperature overnight and then rehydrated for 30-60 minutes with slow rotation (10-15 RPM) at room temperature in 1x Dulbecco's Phosphate Buffered Saline (dPBS, Gibco, composition in mM: 138 NaCl, 8 NaH_2PO4, 2.7 KCl, 1.5 KH_2PO_4, pH approx. 7.1). Unilamellar vesicles were formed by extrusion through a 0.1 µm pore size polycarbonate membrane with the Mini Extruder Set at room temperature (Avanti) as per the manufacturer's protocol. Vesicles were kept at room temperature and used within a few hours of formation.
Vesicle formation was verified by dynamic light scattering (DLS) with a Zetasizer Nano ZS (Malvern Instruments). Vesicle diameters ranged from 125.9-160.3 nm between batches; all batches were monodisperse, with one primary size peak. For DLS measurements, vesicle suspensions were used directly or diluted 1:1 in dPBS before measurement. 100-200 uL of vesicle suspension were placed into a Zen 0040 cuvette. Refractive indices of 1.450 (material) and 1.332 (dispersant) were used in the Zetasizer software to obtain size distributions. Vesicle size distributions were measured in both naïve POPC vesicles and in POPC vesicles incubated with VoltageFluor; results were indistinguishable.

4. Cell Culture

All animal procedures were approved by the UC Berkeley Animal Care and Use Committees and conformed to the NIH Guide for the Care and Use of Laboratory Animals and the Public Health Policy.

4a. Human embryonic kidney (HEK) 293T cells

HEK293T cells were acquired from the UC Berkeley Cell Culture Facility and were verified by STR (short tandem repeat) profiling. Cells were routinely checked for mycoplasma contamination. HEK293T cells were maintained in Dulbecco's modified eagle medium (DMEM, Gibco) supplemented with 4.5 g/L D-glucose, 10% fetal bovine serum (FBS, Seradigm), and 2 mM GlutaMAX (Gibco). Cells were passaged every few days into fresh media following dissociation with 0.05% Trypsin-EDTA (Gibco). All cells were discarded after 30 passages. For imaging experiments, 12 mm and 25 mm glass coverslips (Electron Microscopy Sciences) were prepared by acid washing (1 M HCl, approx. 5 hours), followed by three overnight washes in ethanol and three overnight washes in water. Coverslips were sterilized by heating at 150°C for 2-4 hours. To facilitate cell attachment, sterilized coverslips were coated with Poly-D-Lysine (PDL; 1 mg/mL; Sigma-Aldrich) for 1-24 hours at 37°C, followed by two washes with water and two washes with phosphate-buffered saline. For general imaging, cells were seeded onto prepared coverslips in complete DMEM at a 42,000 cells/cm^2 and used approximately 24 hours after plating. For electrophysiology, cells were seeded at a density of 21,000 cells/cm^2 in low glucose DMEM (1 g/L glucose, 10% FBS, 1 mM pyruvate, 2 mM GlutaMAX) and used approximately 16 hours after plating.

4b. Rat hippocampal neurons.

Hippocampi were dissected from embryonic day 18 Sprague Dawley rats (Charles River Laboratory) in cold sterile HBSS (zero Ca^{2+}, zero Mg^{2+}). All dissection products were supplied by Invitrogen, unless otherwise stated. Hippocampal tissue was treated with trypsin (2.5%) for 15 min at 37 °C. The tissue was triturated using fire polished Pasteur pipettes, in minimum essential media (MEM) supplemented with 5% fetal bovine serum (FBS; Thermo Scientific), 2% B-27, 2% 1M D-glucose (Fisher Scientific), and 1% glutamax. The dissociated cells were plated onto 12 mm diameter coverslips (Electron Microscopy Sciences, prepared as above) at a density of 27,000 cells per coverslip in MEM supplemented media. Neurons were maintained at 37 °C in a humidified incubator with 5% CO_2. At 1 day in vitro (DIV) half of the MEM supplemented media was removed and replaced with Neurobasal media containing 2% B-27 supplement and 1% glutamax. Functional imaging was performed on 14-17 DIV neurons.

4c. Differentiation of hiPSC into cardiomyocytes and culture.

hiPSCs (WTC11)[6] were cultured on Matrigel (1:100 dilution; Corning)-coated 12 well-plates in StemFlex medium (Gibco). When the cell confluency reached 80–90%, which is referred as day 0, the medium was switched to RPMI 1640 medium (Life Technologies) containing B27 minus insulin supplement (Life Technologies) and 10 µM CHIR99021 GSK3 inhibitor (Peprotech). At day 1, the medium was changed to RPMI 1640 medium containing B27 minus insulin supplement only. At day 3, medium was replaced to RPMI 1640 medium containing B27 supplement without insulin, and 5 µM IWP4 (Peprotech) for 2 days without medium change. On day 5, medium was replaced to RPMI 1640 medium containing B27 minus insulin

supplement for 2 days without medium change. On day 7, medium was replaced with RPMI 1640 containing B27 with insulin supplement. After day 7, the medium was changed every two days. Confluent contracting sheets of beating cells appear between days 7 to 15.[7]
Beating sheets were treated with collagenase II for 60-75 minutes. The collagenase solution was carefully transferred to cold DMEM, making sure cardiac sheets were not disturbed. Trypsin (0.25%) was added to dissociated sheets for 4-8 minutes and plated onto 6 well-plates coated with Matrigel (1:100 dilution) in RPMI 1640 medium containing B27 supplement plus ROCK inhibitor Y-27632. 24 hours later, the medium was replaced with fresh RMPI/B27 without ROCK inhibitor. Cardiomyocytes were maintained for 7 days, replacing media every other day, and then were switched to RPMI 1640 medium (-glucose) supplemented with 4 mM sodium lactate (Sigma Aldrich). Cells were maintained in this media for 7 days, replacing every other day, then switched back to RPMI/B27 containing glucose.[8] These purified cardiomyocytes were then used for imaging.
Lactate purified sheets were dissociated with 0.25% trypsin-EDTA (4-8 minutes, depending on density and quality of tissue) and plated onto Matrigel (1:100)-coated Ibidi ® 24 well µ-plates (cat no. 82406) in RPMI 1640 medium containing B27 supplement (containing insulin). Medium was changed every 3 days until imaging. For loading hiPSC cardiomyocytes, voltage dyes were diluted 1 in 1000 in RPMI 1640 with B27 supplement minus Phenol Red to the desired final concentration. Cardiomyocytes were incubated in this solution for 20 minutes at 37 °C, then exchanged with dye-free RPMI 1640 with B27 supplement minus Phenol Red.

5. VoltageFluor stocks and cellular loading

VoltageFluors were stored as 0.5-1 mM DMSO stocks at -20°C or as a solid at room temperature. For cellular loading in HEK293T, DMSO stocks were diluted to the indicated concentration in imaging buffer (IB; composition in mM: 139.5 NaCl, 10 HEPES, 5.6 D-glucose, 5.3 KCl, 1.3 $CaCl_2$, 0.49 $MgCl_2$, 0.44 KH_2PO_4, 0.41 $MgSO_4$, 0.34 Na_2HPO_4; 290 mOsm/kg, pH 7.25). HEK293T cells were incubated in the VF-IB solution for 20-25 minutes in a humidified incubator at 37°C. Cells were washed once in IB and transferred to fresh IB for imaging. Hippocampal neurons were loaded with VoltageFluor at the indicated concentration in HBSS and incubated in the VF-HBSS solution for 20 minutes in a humidified incubator at 37°C. For imaging evoked activity, the hippocampal neurons were then transferred to a HBSS solution containing the synaptic blockers 10 µM 2,3-Dioxo-6-nitro-1,2,3,4-tetrahydrobenzo[f]quinoxaline-7-sulfonamide (NBQX; Santa Cruz Biotechnology) and 25 µM D-2-Amino-5-phosphonopentanoic acid (APV; Sigma-Aldrich) to prevent recurrent activity. Cardiomyocytes were loaded with VoltageFluor in RPMI-B27 with no phenol red (instead of IB). The loading solution was exchanged for fresh RPMI-B27 without phenol red (and without VF) before imaging. All imaging was conducted under ambient atmosphere; no imaging samples were used for longer than an hour.

For assessment of the concentration dependence of fluorescence lifetime, the indicated concentration of VoltageFluor was used (**Fig. S6**). From these data, an optimal working concentration that minimized concentration quenching but retained adequate signal was selected. This concentration was used for all other experiments in HEK293T unless indicated. Optimal concentrations for VF2.1.Cl and VF2.0.Cl were previously determined;[9] where indicated, we also include some data at 300 nM (3x higher concentration) for comparison. Working concentration values are tabulated below (**Table S1**):

Table S1: Optimized working concentrations for the VoltageFluors used in this study.

VoltageFluor	Optimized Concentration
JuloVF	500 nM
IndoVF	300 nM
^{i}PrVF	300 nM
VF2.1.Cl	100 nM
NN26VF	300 nM
VF2.0.Cl	100 nM

Table S2: Cellular measurements in HEK293T cells with VF2.1.Cl and VF2.0.Cl at 100 nM and 300 nM.

Dye	Concentration	Rel. brightness (HEK293T)	%ΔF/F	$\Delta\tau_{fl}$ per mV (ps)	τ_{fl} at 0 mV (ns)
VF2.1.Cl	100 nM	0.36 ± 0.01	23 ± 3	3.11 ± 0.04	1.68 ± 0.04
	300 nM	1.0 ± 0.1	26 ± 3	3.05 ± 0.08	1.57 ± 0.03
VF2.0.Cl	100 nM	0.62 ± 0.06	-0.30 ± 0.01	0.02 ± 0.03	3.44 ± 0.01
	300 nM	1.8 ± 0.2	-0.20 ± 0.01	0.00 ± 0.03	3.36 ± 0.03

Table S3: SNR values for cellular voltage measurements with VF2.1.Cl and VF2.0.Cl at 100 nM and 300 nM.

VoltageFluor	Concentration	HEK293T[a]	Cardio	Neuron
VF2.1.Cl	100 nM	100 ± 5	130 ± 5	7.8 ± 0.6
	300 nM	200 ± 10	440 ± 10	13 ± 1
VF2.0.Cl	100 nM	1.8 ± 0.1	---	---
	300 nM	2 ± 1	---	---

Data are mean SNR ± SEM. [a]per 100 mV.

6. Fluorescence intensity imaging parameters

For all experiments, excitation light for the epifluorescence intensity image was generated by a Spectra-X Light engine LED (Lumencor) using the cyan LED (475/34 nm bandpass filter). Light was collected with an emission filter (bandpass 540/50 nm) after passing through a dichroic mirror (510 nm LP). Images were captured with an OrcaFlash4.0 sCMOS camera (Hamamatsu). More detailed imaging information for each fluorescence intensity application is expanded below.

6a. Membrane staining, voltage sensitivity, and photostability in HEK293T cells

HEK293T cells were imaged on an inverted Zeiss AxioObserver Z-1. Fluorescence was collected with a 40x oil immersion objective (EC-Plan-NEOFLUAR 40x/1.3 NA; Zeiss). For membrane staining, images (2048x2048 px^2, pixel size 0.16 x 0.16 μm^2). For voltage sensitivity experiments, images (100x100 px^2, pixel size 0.64 x 0.64 μm^2) were collected continuously with constant LED illumination (9.53 mW/mm^2) and a sampling rate of 0.5 kHz. For photostability experiments, images (2048 x 2048 px^2, pixel size 0.16 x 0.16 μm^2) were taken every 1 second for 5 minutes with constant illumination of LED (30.4 mW/mm^2; 50 ms exposure time).

6b. Evoked activity in rat hippocampal neurons

Evoked activity imaging was performed on an upright AxioExaminer Z-1 (Zeiss), equipped with a Spectra-X light engine LED light (Lumencor), and controlled with µManager (V1.4, open-source, Open Imaging).[10] Images were acquired using a W-Plan-Apo/1.0 NA 20x water immersion objective (Zeiss). Images (2048x400 px^2, pixel size: 0.325 x 0.325 μm^2) were collected continuously on an OrcaFlash4.0 sCMOS camera (sCMOS; Hamamatsu) at a sampling rate of 0.5 kHz, with 4x4 binning, and a cyan excitation light power of 13.22 mW/mm^2. Extracellular field stimulation was delivered by a Grass Stimulator connected to a recording chamber containing two platinum electrodes (Warner), with triggering provided through a Digidata 1440A digitizer and pCLAMP 10 software (Molecular Devices). Action potentials were triggered by 1 ms 80 V field potentials delivered at 5 Hz.

6c. Spontaneous activity in human induced pluripotent stem cell derived cardiomyocytes (iCMs)

Functional recordings of VoltageFluors were performed on an inverted AxioObserver Z-1 (Zeiss), equipped with a Spectra-X Light engine LED light (Lumencor), controlled with µManager (V1.4, open-source, Open Imaging).[10] Images were acquired using a Plan-Apochromat 20x/0.8 NA air objective (Zeiss). Images were focused onto an OrcaFlash4.0 sCMOS camera (sCMOS; Hamamatsu). Images (512 x 125 px^2, pixel size 0.64 x 0.64 μm^2) were taken continuously at 0.2 kHz for ten seconds with constant LED illumination (11.1 mW/mm^2).
Phototoxicity of VoltageFluor dyes was assessed in cardiomyocyte monolayers exposed to constant illumination from the excitation LED (9.53 mW/mm^2) for up to ten minutes (or until automaticity was lost), while typical ten second fluorescence recordings were made at the beginning of each minute.

7. Fluorescence intensity image analysis

7a. Voltage sensitivity in HEK293T cells (%ΔF/F)

Analysis of voltage sensitivity in HEK293T cells was performed using ImageJ (FIJI). Briefly, a region of interest (ROI) encompassing the cell body was selected and average fluorescence intensity was calculated for each frame. For background subtraction, a ROI encompassing a region without cells was selected and the average pixel intensity was calculated for each frame. A linear fit to the background trace was calculated and applied to the background, and this was used to subtract background signal from the fluorescence intensity trace. F/F_0 values were calculated by dividing the background subtracted trace by the median value of fluorescence when the cell is held at -60 mV. ΔF/F values were calculated by plotting the change in fluorescence (ΔF) vs the applied voltage step and finding the slope of a linear best-fit.

7b. Spontaneous activity in iCMs

Analysis of action potential (AP) data from hiPSC cardiomyocytes was performed using in-house MATLAB scripts based on previously developed software by the Efimov lab (Washington University, St. Louis, MO).[11,12] Scripts are

available upon request. Briefly, raw OME-tiffs recorded in µManager were read directly into MATLAB for batch-processing of large datasets (>30 Gb per experiment). The mean pixel intensity of the entire image was calculated for each frame and a mean fluorescence trace was extracted for the entire stack. Photobleach correction was performed by subtracting an asymmetric least-squares fit of the data from the mean trace.[13] This spline was used to estimate and compare the rate of photobleaching of VoltageFluors in cardiomyocytes (**Figure S20b**). No subtraction of background was possible due to staining of the entire monolayer. Individual AP events were identified through threshold detection based on a Schmidtt trigger. Action potential duration (APD) values were calculated for each AP by finding the activation time (time of the maximum derivative of the AP upstroke) and the time the signal returns to 70% and 10% of the maximum depolarization (APD30 and APD90, respectively). APD values were corrected for variation due to spontaneous beat rate by Fridericia's formula (Eq. 1). CL is the cycle length, calculated as the time period from the beginning of one beat to the beginning of the succeeding beat.[14]

$$\mathrm{cAPD} = \frac{APD}{\sqrt[3]{CL}}$$

7c. Evoked activity in rat hippocampal neurons

For analysis of evoked voltage responses in neurons, regions of interest encompassing cell bodies were drawn in ImageJ and the mean fluorescence intensities for each frame were extracted. ΔF/F values were calculated in the following manner. First, a mean background value was subtracted from all raw fluorescence frames, bypassing the noise amplification which arises from subtracting background for each frame, to give a background corrected trace. A least squares regression was then fit to the background corrected trace. A bleaching curve, derived from the slope of the regression, was then subtracted from the background corrected trace to correct for photobleaching and yield a bleach-corrected trace. The median of the bleach-corrected trace was subtracted from each timepoint of the bleach-corrected trace to yield a ΔF trace. The ΔF trace was then divided by the median of the bleach-corrected trace to give a ΔF/F trace. No averaging has been applied to any voltage traces. Signal-to-noise ratios were calculated by dividing the ΔF/F value of the frame containing the first spike of evoked activity by the standard deviation of the previous 10 frames in the ΔF/F trace.

7d. Photobleaching studies

For photostability experiments HEK293T cells were loaded as outlined above. Images (2048 x 2048 px^2, pixel size 0.16 μm × 0.16 μm) were taken every 1 second for 5 minutes with constant illumination of LED (30.4 mW/mm^2; 50 ms exposure). The obtained fluorescence curves were normalized with the fluorescence intensity at t = 0 and averaged (three different cell rafts for each dye).

Phototoxicity of VoltageFluor dyes was assessed in cardiomyocyte monolayers incubated with 0.3 µM of indicator (and 0.1 µM for VF2.1.Cl). These were exposed to constant illumination from the excitation LED (475/34; bandpass) for up to 10 minutes, while typical ten second fluorescence recordings were made at the beginning of each minute. Initial photobleach was compared using splines calculated from the asymmetric least squares fits of the baselines (**Figure S20**).

The bleach rates of VoltageFluors in neurons are the slopes of the least squares regressions fit to the background corrected traces (**7c**). The bleach rates of VoltageFluors in HEK293T cells, cardiomyocytes, and neurons were compared in **Figure S20**.

8. Fluorescence lifetime data acquisition

8a. Microscopy configuration

Fluorescence lifetime data were obtained as described previously.[9] Briefly, fluorescence lifetime data were acquired on an inverted LSM 510 (Zeiss) scanning confocal microscope equipped with a Becker and Hickl SPC-150N photon counting card. Pulsed excitation light was supplied by a MaiTai HP Ti:Sapphire laser (SpectraPhysics) tuned to 958 nm and frequency doubled to 479 nm. Average power at the sample ranged from 5-25 µW. Photons were collected with a 40x oil immersion objective (1.3 NA Plan-Neofluar, Zeiss) and detected with an HPM-100-40 hybrid detector (Becker and Hickl) after passing through a 488 nm long pass dichroic (Zeiss) and a 550/49 nm bandpass emission filter (Semrock, Rochester, NY). Fluorescence lifetime data were acquired using SPCM software (Becker and Hickl). To maximize photon signal but retain some optical sectioning, the confocal pinhole was set to 2.5-3.5 AU (~2.5 µm optical section). Proper functioning of the fluorescence lifetime imaging system was routinely measured with the standards erythrosin B and fluorescein in 0.1 N NaOH. The instrument response function (IRF) was recorded at least hourly during data acquisition from a solution of quenched fluorescein (500 µM fluorescein, 12 M NaI, 0.1 N NaOH).[15]

8b. Data acquisition – solution phase measurements

POPC vesicles in 1x dPBS were incubated with VoltageFluor at the indicated concentration at room temperature for 20-30 minutes. The final concentration of DMSO was kept at or below 0.2%. After incubation, vesicle suspensions with dye were transferred to a clean 25 mm coverslip in an Attofluor imaging chamber (Thermo Fisher Scientific). Fluorescence lifetime images were acquired for 60 seconds and generally contained >10^6 photons per recording. Data from the image were combined into a global decay with 256 time channels in the fluorescence decay before analysis (see below).

8c. Data acquisition – cellular measurements

HEK293T loaded with VF were transferred to an Attofluor imaging chamber containing imaging buffer. Fluorescence lifetime images were recorded with 256x256 px^2 of spatial resolution (112 x 112 μm^2 image size; see below for binning during lifetime fitting) and 256 time channels. Images for evaluating concentration dependence were acquired for 75-90 seconds; results are the sum of approximately 12 scans across the field of view. For tandem electrophysiology and fluorescence lifetime imaging, data were recorded with 64x64 px^2 of spatial resolution (56.3 x 56.3 μm^2 image size) and 256 time channels. Images with concurrent electrophysiology were acquired for 30 seconds, summing multiple frames recorded from the same field of view.

9. Fluorescence lifetime data analysis

Time-resolved fluorescence decays I(t) of VoltageFluors were fit to a single exponential decay or to a sum of two or three exponential decays (eqn. 2, n=1, 2, or 3). Fits were optimized in custom Matlab code (MathWorks, Natick, MA) using the weighted least squares method to minimize the reduced chi squared χ^2 (eqn. 3). The interior-point algorithm from the built-in Matlab optimization routine fmincon was used for optimization. Code is available upon request.

$$I(t) = \sum_{i=1}^{n} a_i e^{-t/\tau_i} \quad [2]$$

To calculate χ^2, the difference between the observed value y_m and the calculated value z_m for each time channel m was determined, with Poisson weighting based on the square root of the calculated number of counts in each channel. χ^2 was adjusted for the total number of time channels *N* included in the fit, as well as the number of parameters *p* in the model (coefficients a_i and decay constants τ_i).

$$\chi^2 = \sum_{m=1}^{N} \frac{(y_m - z_m)^2}{z_m(N-p)} \quad [3]$$

Where only one fluorescence decay term was used, the reported τ_{fl} is simply the decay constant τ. Where more than one exponential decay term was used, τ_{fl} data are presented as the amplitude weighted average of the two (eqn. 4) or three (eqn. 5) coefficients a_i and decay constants τ_i.

$$\tau_{fl} = \frac{a_1\tau_1 + a_2\tau_2}{a_1 + a_2} \quad [4]$$

$$\tau_{fl} = \frac{a_1\tau_1 + a_2\tau_2 + a_3\tau_3}{a_1 + a_2 + a_3} \quad [5]$$

The number of fluorescence decay terms was chosen to balance the reduction in χ^2 against the need to minimize fit noise (**Fig. S13, S14**). The number of terms selected for each probe is indicated below (**Table S2**).

Table S4: Number of exponential terms selected to describe VF time-resolved fluorescence decays.

VoltageFluor	Number of exponential decay terms
JuloVF	3
IndoVF	3
^{i}PrVF	2
VF2.1.Cl	2
NN26VF	1
VF2.0.Cl	1

10. Electrophysiology

For electrophysiological experiments in HEK293T, pipettes were pulled from borosilicate glass with filament (Sutter Instruments, BF150-86-10) with a P-97 pipette puller (Sutter Instruments) to a resistance of 4-7 MΩ. Pipettes were filled with an internal solution (composition, in mM): 125 potassium gluconate, 10 HEPES, 10 KCl, 5 NaCl, 2 ATP disodium salt, 1 EGTA, 0.3 GTP sodium salt (pH 7.25, 285 mOsm). Pipettes were positioned with an MP-225 micromanipulator (Sutter Instruments). Electrophysiological recordings were obtained with an Axopatch 200B amplifier (Molecular Devices) at room

temperature. The signals were digitized with a Digidata 1550B, sampled at 50 kHz, filtered at 5 kHz, and recorded with pCLAMP 10 software (Molecular Devices).

Electrophysiology was performed in the whole cell voltage clamp configuration. After gigaseal formation and break-in, recordings were only pursued if series resistance in voltage clamp was less than 30 MΩ and the recording maintained a 30:1 ratio of membrane resistance to access resistance throughout all voltage steps. No series resistance compensation was applied. Fast capacitance was compensated in the cell attached configuration. All voltage clamp protocols were corrected for the calculated liquid junction (-14 mV, Liquid Junction Potential Calculator in pClamp).[16] For tandem electrophysiology and fluorescence intensity recordings, cells were held at -60 mV and de- and hyper- polarizing steps were applied from +100 to -100 mV in 20 mV increments, with each step lasting 100 ms. For tandem electrophysiology and fluorescence lifetime recordings, the potentials -80, -40, 0, and +40 mV were randomly applied in four sequential 30 second recordings, followed by a 30 second recording at +80 mV. Cells were only included if the aforementioned patch quality criteria were retained throughout the first 4 steps; the 5th step to +80 mV was included if it also met the quality criteria (true for ~3/4 of cells).

11. Synthesis

Scheme S1.

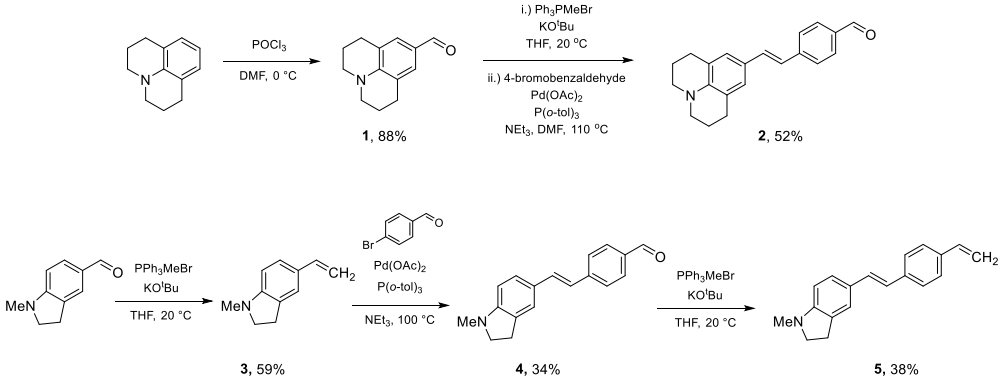

Scheme S2.

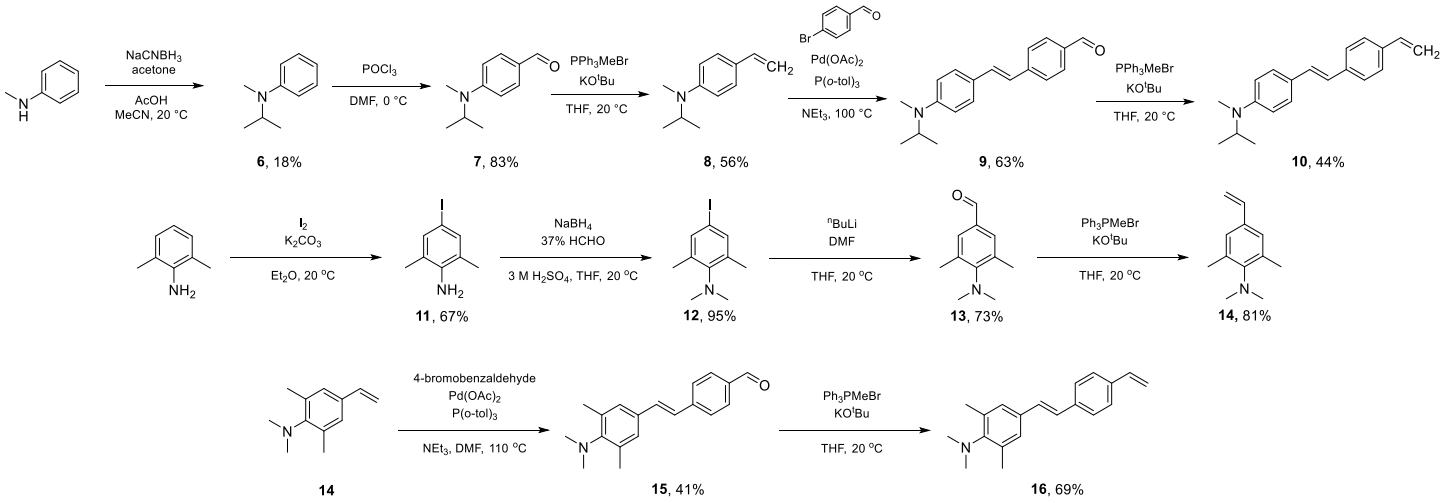

Scheme S3.

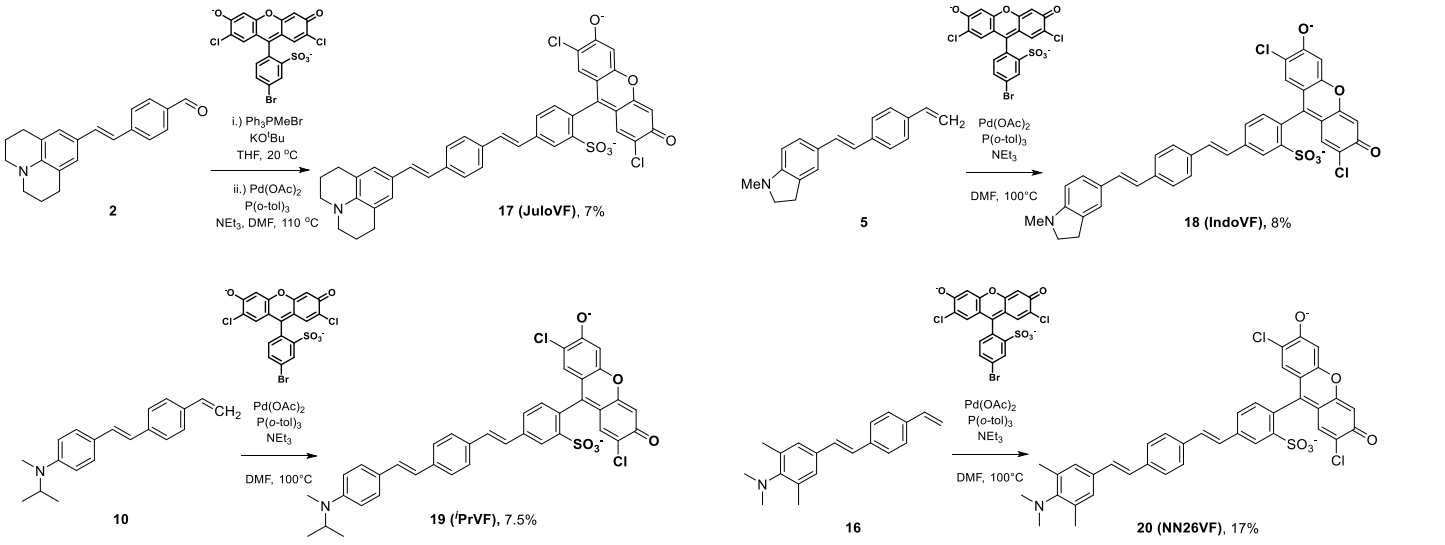

Preparation of molecular wires:

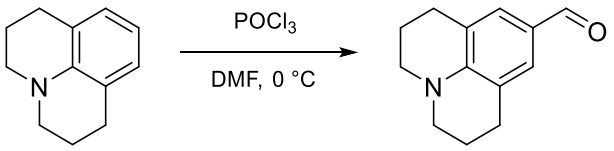

1, 88%

Synthesis of 2,3,6,7-tetrahydro-1H,5H-pyrido[3,2,1-ij]quinoline-9-carbaldehyde, 1:
$POCl_3$ (1.2 mL, 12.7 mmol) was slowly added to ice-cold anhydrous DMF (20 mL) and set to stir for 30 minutes at room temperature. This solution was added to 2,3,6,7-tetrahydro-1H,5H-pyrido[3,2,1-ij]quinoline (2.0 g, 11.5 mmol) and stirred at 90° C under N_2 for 16 hours. The reaction mixture was cooled to room temperature, added to ice cold water, neutralized with saturated $NaHCO_3$ and extracted with EtOAc (3x). The organic layers were collected, dried with Na_2SO_4, and concentrated to dryness *in vacuo*. The residue was taken up in 1:1 EtOAc:hexanes and run through a silica plug to afford **1** as an orange powder (2.0 g, 88**%** yield).

^{1}H NMR (400 MHz, Chloroform-d) δ 9.58 (s, 1H), 7.28 (s, 2H), 3.28 (t, J = 5.9 Hz, 4H), 2.75 (t, J = 6.3 Hz, 4H), 1.95 (p, J = 6.1 Hz, 4H).

^{13}C NMR (101 MHz, Chloroform-d) δ 190.22, 147.98, 129.60, 124.05, 120.39, 50.11, 27.74, 21.33.

HRMS (ESI+) Calculated for $C_{13}H_{16}O_1N_1$ $[M+H]^+$ 202.1226; Found 202.1225.

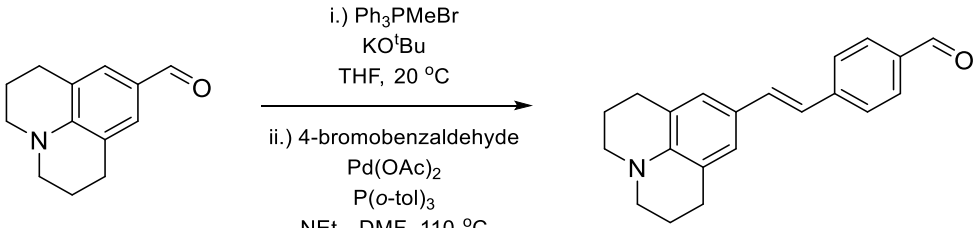

1 **2**, 52%

Synthesis of (E)-4-(2-(2,3,6,7-tetrahydro-1H,5H-pyrido[3,2,1-ij]quinolin-9-yl)vinyl)benzaldehyde, 2:
Ph_3PMeBr (2.44 g, 6.82 mmol) and KO^tBu (920 mg, 8.19 mmol) were combined with anhydrous THF (38 mL) and set to stir at room temperature for one hour. Compound **1** (1.1 g, 5.46 mmol) was then dissolved in anhydrous THF (10 mL) and added to the reaction mixture, which was set to stir at room temperature for four hours. The reaction was then added to water and extracted with EtOAc (3x). The organic layers were collected, washed twice with brine, dried with Na_2SO_4, and concentrated to dryness *in vacuo* to give an orange solid. This crude material was combined with 4-bromobenzaldehyde (957 mg, 5.46 mmol), $Pd(OAc)_2$ (61 mg, 0.27 mmol), and $P(o\text{-}tol)_3$ (167 mg, 0.55 mmol) in a flame-dried Schlenk flask. The flask was evacuated/backfilled with N_2 (3x). Anhydrous DMF (11 mL) and anhydrous triethylamine (11 mL) were added, the flask was sealed, and the solution was stirred at 110° C for 40 hours. The reaction was then cooled to room temperature, diluted with EtOAc, and filtered. The filtrate was concentrated to dryness *in vacuo*. The residue was purified by flash chromatography (10% EtOAc in hexanes), affording **2** as an orange powder (1.7 g, 52% yield).

^{1}H NMR (400 MHz, Chloroform-d) δ 9.94 (s, 1H), 7.81 (d, J = 8.4 Hz, 2H), 7.56 (d, J = 8.2 Hz, 2H), 7.12 (d, J = 16.2 Hz, 1H), 7.01 (s, 2H), 6.86 (d, J = 16.2 Hz, 1H), 3.20 (t, J = 5.6 Hz, 4H), 2.78 (t, J = 6.4 Hz, 4H), 1.98 (p, J = 6.3 Hz, 4H).

^{13}C NMR (101 MHz, Chloroform-d) δ 191.73, 144.96, 143.56, 134.30, 133.00, 130.38, 126.16, 126.13, 123.80, 121.76, 121.39, 50.05, 27.85, 21.95.

HRMS (ESI+) Calculated for $C_{21}H_{22}O_1N_1$ $[M+H]^+$ 304.1696; Found 304.1693.

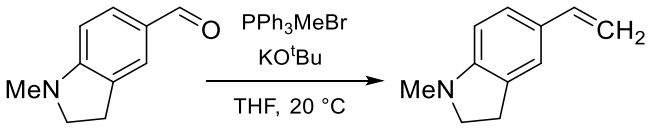

3, 59%

Synthesis of 1-methyl-5-vinylindoline, 3:
KO^tBu (3.3 g, 9.1 mmol) and Ph_3PMeBr (3.3 g, 9.1 mmol) were combined in anhydrous THF (10 mL) stirred at 20 °C for 30 minutes. N-methylindoline carbaldehyde (0.82 g, 5.1 mmol) was added and stirred for 12 hours. This was then suspended in hexanes and filtered over celite. Filtrate was concentrated onto celite, then purified by flash column chromatography with basic alumina as a support (1-5% ethyl acetate in hexanes). **3** was isolated as a yellow oil (0.48 g, 59%).

^{1}H NMR (400 MHz, Chloroform-d) δ 7.22 (q, J = 1.3 Hz, 1H), 7.14 – 7.10 (m, 1H), 6.63 (dd, J = 17.5, 10.9 Hz, 1H), 6.42 (d, J = 8.0 Hz, 1H), 5.52 (dd, J = 17.5, 1.0 Hz, 1H), 5.00 (dd, J = 10.9, 1.1 Hz, 1H), 3.33 (t, J = 8.2 Hz, 2H), 2.95 (t, J = 8.1 Hz, 2H), 2.77 (s, 3H).

^{13}C NMR (101 MHz, $CDCl_3$) δ 153.33, 137.05, 130.73, 127.82, 126.57, 121.66, 109.10, 106.64, 56.12, 36.07, 28.54.

HRMS (ESI+) m/z: $[M+H]^+$ calculated for $C_{11}H_{14}N$: 160.1121; found 160.1121

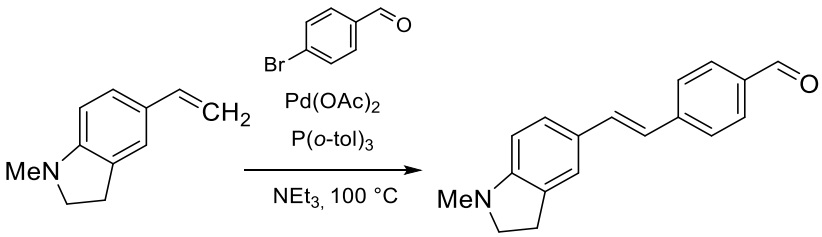

3 **4,** 34%

Synthesis of (E)-4-(2-(1-methylindolin-5-yl)vinyl)benzaldehyde, 4:
$Pd(OAc)_2$ (19 mg, 0.084 mmol), P(*o*-tol)$_3$ (51 mg, 0.17 mmol), and 4-bromo-benzaldehyde (0.31 g, 1.7 mmol) were added into flame dried Schlenk flask. This was evacuated and backfilled with N_2 (3x). Anhydrous triethylamine (3 mL) and **3** (0.4 g, 2.5 mmol) were then added and stirred at 95°C. After 18 hours, the reaction was cooled and diluted in dichloromethane, washed with sat. ammonium chloride (1X) and brine (1X). This was dried with $MgSO_4$, and concentrated. This was triturated with hexanes and filtered, affording **4** as an orange solid (153 mg, 34%).

^{1}H NMR (600 MHz, Chloroform-*d*) δ 9.95 (s, 1H), 7.82 (dd, 2H), 7.58 (d, *J* = 8.2 Hz, 2H), 7.34 (d, *J* = 1.8 Hz, 1H), 7.24 (dd, *J* = 8.0, 1.8 Hz, 1H), 7.19 (d, *J* = 16.2 Hz, 1H), 6.91 (d, *J* = 16.1 Hz, 1H), 6.43 (d, *J* = 8.1 Hz, 1H), 3.39 (t, *J* = 8.2 Hz, 2H), 2.99 (t, *J* = 8.2 Hz, 2H), 2.81 (s, 3H).

^{13}C NMR (151 MHz, $CDCl_3$) δ 191.59, 153.96, 144.64, 134.46, 132.99, 130.97, 130.27, 128.13, 126.33, 126.21, 122.39, 122.26, 106.44, 55.74, 35.50, 28.35

HRMS (ESI+) calculated for $C_{18}H_{18}NO$ $[M+H)^+$ m/z: 264.1383; found: 264.1383
.

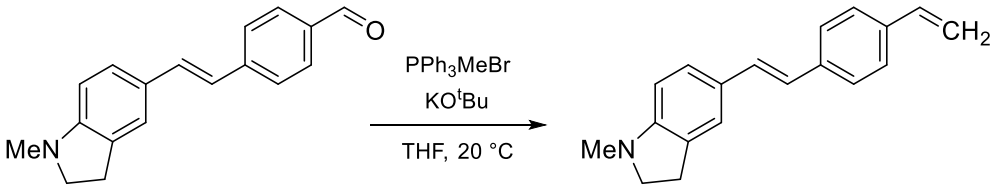

4 **5,** 38%

Synthesis of (E)-1-methyl-5-(4-vinylstyryl)indoline, 5:
Potassium tert-butoxide (0.28 g, 2.5 mmol) and Ph_3PMeBr (0.32 g, 0.89 mmol) were stirred in anhydrous THF (3 mL) at 20 °C for 30 minutes. **4** (0.13 g, 0.49 mmol) was then added and stirred for 12 hours. The reaction was then concentrated to dryness, resuspended in dichloromethane, and filtered over basic alumina. The filtrate was concentrated onto silica and purified by flash chromatography (10% ethyl acetate in hexanes) affording **5** a yellow solid (49 mg, 38%)

^{1}H NMR (600 MHz, Chloroform-*d*) δ 7.44 (d, *J* = 8.3 Hz, 2H), 7.39 (d, *J* = 8.3 Hz, 2H), 7.33 (s, 1H), 7.23 (dd, *J* = 8.0, 1.8 Hz, 1H), 7.06 (d, *J* = 16.2 Hz, 1H), 6.90 (d, *J* = 16.2 Hz, 1H), 6.72 (dd, *J* = 17.6, 10.9 Hz, 1H), 6.45 (d, *J* = 8.0 Hz, 1H), 5.78 – 5.72 (m, 1H), 5.25 – 5.21 (m, 1H), 3.37 (t, *J* = 8.1 Hz, 2H), 2.99 (t, *J* = 8.2 Hz, 2H), 2.80 (s, 3H).

^{13}C NMR (151 MHz, $CDCl_3$) δ 153.29, 137.89, 136.64, 135.96, 130.91, 129.29, 127.36, 127.21, 126.51, 126.13, 123.74, 121.96, 113.09, 106.73, 55.98, 35.88, 28.51.

HRMS (ESI+) m/z $[M+H]^+$ calculated for $C_{19}H_{20}N$: 262.1590; found 262.1591

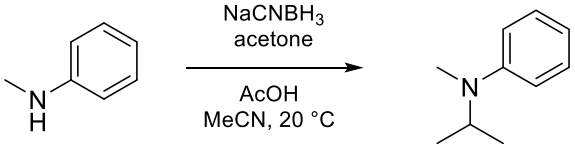

6, 18%

Synthesis of N-isopropyl-N-methylaniline, 6:
N-methylaniline (1.0 g, 9.3 mmol) was stirred in ACN (10 mL). Reagent grade acetone (5.4 g, 93 mmol) was added and stirred for 4 hours at 0°C. $NaCNBH_3$ (2.3 g, 37 mmol) was then added in four portions and glacial acetic acid (1.5 mL) was added. After two hours of stirring at 0°C, more glacial acetic acid (1 mL) was added, and the reaction was stirred for 12 hours and allowed to warm to 20 °C. The reaction was poured into ice and diluted with saturated $NaHCO_3$. This was then extracted in ethyl acetate, washed with brine, dried with $MgSO_4$, and concentrated onto celite. This was purified by flash chromatography on basic alumina (5% EtOAc in hexanes), affording **6** as a yellow oil (0.24 g, 18%).

^{1}H NMR (400 MHz, Chloroform-*d*) δ 7.23 (dd, *J* = 8.9, 7.2 Hz, 2H), 6.83 – 6.76 (m, 2H), 6.69 (tt, *J* = 7.1, 1.1 Hz, 1H), 4.10 (hept, *J* = 6.6 Hz, 1H), 2.73 (s, 3H), 1.16 (d, *J* = 6.6 Hz, 6H).

^{13}C NMR (101 MHz, $CDCl_3$) δ 150.28, 129.15, 116.45, 113.39, 48.96, 29.81, 19.35.

HRMS (ESI+) m/z $[M+H]^+$ calculated for $C_{10}H_{16}N$: 150.1277; found 150.1277

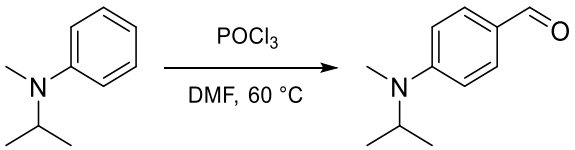

6 **7,** 83%

Synthesis of 4-(isopropyl(methyl)amino)benzaldehyde, 7:
N,N-Dimethylformamide (2 mL) was stirred at 0°C and phosphorus oxychloride (0.4 mL) was added dropwise, then stirred for 15 minutes. **6** (0.24 g, 1.6 mmol) was then added into solution and stirred for 15 hours at 60 °C. The reaction was then poured into ice. This was extracted with ethyl acetate, washed with 1M KOH and brine, and dried with $MgSO_4$. The organic layer was concentrated *in vacuo* to yield compound **7** as a yellow oil (0.24 g, 83%).

^{1}H NMR (400 MHz, Chloroform-*d*) δ 9.72 (s, 1H), 7.72 (dd, *J* = 8.9 Hz, 2H), 6.76 (dd, 2H), 4.23 (hept, *J* = 6.6 Hz, 1H), 2.85 (s, 3H), 1.22 (d, *J* = 6.6 Hz, 6H).

^{13}C NMR (101 MHz, $CDCl_3$) δ 190.10, 154.15, 132.14, 125.08, 111.27, 48.42, 29.94, 19.66.

HRMS (ESI+) m/z $[M+H]^+$ calculated for $C_{11}H_{16}NO$: 178.1226; found 178.1228

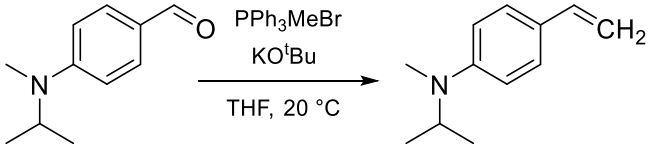

7 **8,** 56%

Synthesis of N-isopropyl-N-methyl-4-vinylaniline, 8:
KO^tBu (0.73 g, 6.5 mmol) and Ph_3PMeBr (0.83 g, 2.3 mmol) were combined in anhydrous THF (4 mL) and stirred at 20 °C for 30 minutes. **7** (0.23 g, 1.3 mmol) was added and stirred for 12 hours. This was then suspended in hexanes and filtered over celite. The filtrate was taken up in ethyl acetate, then filtered again over basic alumina, repeating once more. **8** was isolated as a yellow oil (0.13 g, 56%).

^{1}H NMR (400 MHz, Chloroform-*d*) δ 7.33 – 7.27 (m, 2H), 6.77 – 6.71 (m, 2H), 6.63 (dd, *J* = 17.6, 10.9 Hz, 1H), 5.53 (dd, *J* = 17.6, 1.1 Hz, 1H), 5.01 (dd, *J* = 10.9, 1.1 Hz, 1H), 4.11 (hept, *J* = 6.6 Hz, 1H), 2.74 (s, 3H), 1.17 (d, *J* = 6.6 Hz, 6H).

^{13}C NMR (101 MHz, $CDCl_3$) δ 149.88, 136.62, 127.23, 126.03, 112.91, 109.17, 48.81, 29.81, 19.37.

HRMS (ESI+) m/z $[M+H]^+$ calculated for $C_{12}H_{18}N$: 176.1434; found 176.1433

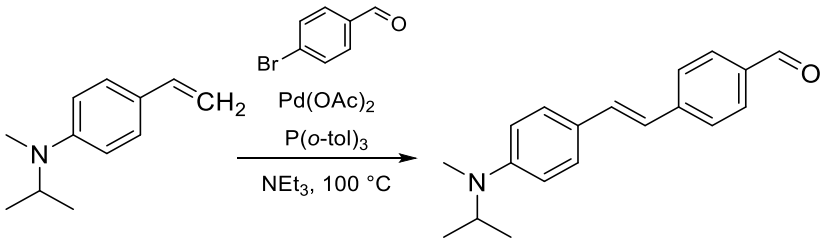

8 **9,** 63%

Synthesis of (E)-4-(4-(isopropyl(methyl)amino)styryl)benzaldehyde, 9:
4-bromobenzaldehyde (120 mg, 0.66 mmol), $Pd(OAc)_2$ (7.4 mg, 33 µmol), and P(*o*-tol)$_3$ (20 mg, 66 µmol) were added to a flame dried Schlenk flash, then evacuated and backfilled with N_2 (3X). **8** (115 mg, 0.66 mmol) was added as a solution in anhydrous triethylamine (3 mL). This was stirred for 18 hours at 100 °C, then diluted in dichloromethane. This was washed with NH_4Cl and brine before drying with $MgSO_4$. This was concentrated to a yellow solid, taken up in a small portion of dichloromethane, and triturated. Filtration afforded **9** as a yellow solid (115 mg, 63%).

^{1}H NMR (600 MHz, Chloroform-*d*) δ 9.96 (s, 1H), 7.83 (d, *J* = 8.3 Hz, 2H), 7.59 (d, *J* = 8.2 Hz, 2H), 7.46 – 7.42 (m, 2H), 7.20 (d, *J* = 16.2 Hz, 1H), 6.93 (d, *J* = 16.2 Hz, 1H), 6.77 (d, *J* = 8.9 Hz, 2H), 4.16 (hept, *J* = 6.6 Hz, 1H), 2.79 (s, 3H), 1.20 (d, *J* = 6.6 Hz, 6H).

^{13}C NMR (151 MHz, $CDCl_3$) δ 191.56, 150.25, 144.59, 134.39, 132.49, 130.22, 128.25, 126.17, 124.47, 122.42, 112.65, 77.21, 77.00, 76.79, 48.54, 29.74, 19.45.

HRMS (ESI+) m/z $[M+H]^+$ calculated for $C_{19}H_{22}NO$: 280.1696; found 280.1695

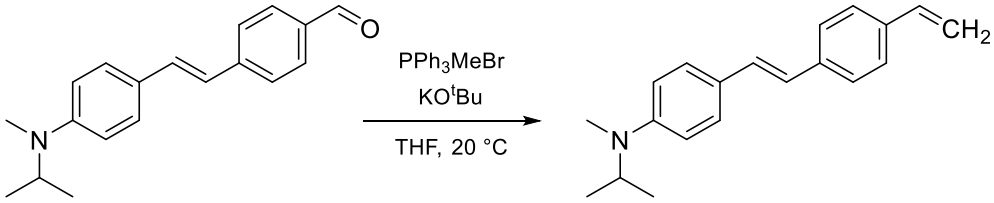

9 **10,** 44%

Synthesis of (E)-N-isopropyl-N-methyl-4-(4-vinylstyryl)aniline, 10:
Potassium tert-butoxide (0.2 g, 1.8 mmol) and methyltriphenylphosphonium bromide (0.23 g, 0.64 mmol) were stirred in anhydrous THF (4 mL) at 20 °C for 30 minutes. **9** (0.1 g, 0.36 mmol) was then added and stirred for 12 hours. The reaction was diluted in hexanes, then filtered over celite. This was concentrated, then suspended in ethyl acetate and filtered over basic alumina. This was concentrated to afford **10** as a yellow solid (44 mg, 44%).

^{1}H NMR (600 MHz, Chloroform-*d*) δ 7.45 – 7.42 (m, 2H), 7.41 – 7.35 (m, 4H), 7.04 (d, *J* = 16.2 Hz, 1H), 6.89 (d, *J* = 16.2 Hz, 1H), 6.79 – 6.75 (m, 2H), 6.71 (dd, *J* = 17.6, 10.9 Hz, 1H), 5.74 (dd, *J* = 17.6, 0.9 Hz, 1H), 5.21 (dd, *J* = 10.8, 0.9 Hz, 1H), 4.14 (p, *J* = 6.6 Hz, 1H), 2.77 (s, 3H), 1.19 (d, *J* = 6.6 Hz, 6H).

^{13}C NMR (151 MHz, $CDCl_3$) δ 149.78, 137.89, 136.62, 135.92, 128.82, 127.67, 126.48, 126.10, 125.53, 123.77, 113.05, 112.96, 48.73, 29.78, 19.41.

HRMS (ESI+) m/z $[M+H]^+$ calculated for $C_{20}H_{24}N$: 278.1903; found 278.1902

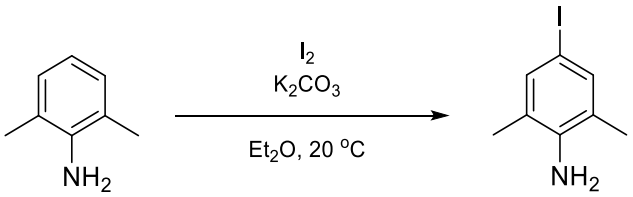

11, 67%

Synthesis of 4-iodo-2,6-dimethylaniline, 11:
2,6-dimethylaniline (1.5 g, 12.4 mmol), Iodine (3.3 g, 13.0 mmol), and K_2CO_3 (3.4 g, 24.75 mmol) were combined with diethyl ether (22 mL) and set to stir under N_2 in the absence of light for 16 hours. The reaction mixture was then diluted with diethyl ether and washed with water, an aqueous solution of $Na_2S_2O_3 \cdot 5H_2O$ (3.2 g, 13.0 mmol), water, and brine. The organic layer was then dried with Na_2SO_4 and concentrated to dryness *in vacuo*. The residue was purified by flash chromatography (silica deactivated with Et_3N, 15% to 20% EtOAc in hexanes) to afford **11** as a purple oil (2.04 g, 67% yield).

^{1}H NMR (500 MHz, Chloroform-d) δ 7.24 (s, 2H), 3.58 (s, 2H), 2.13 (s, 6H).

^{13}C NMR (126 MHz, Chloroform-d) δ 142.67, 136.54, 124.21, 79.23, 17.36.

HRMS (ESI+) Calculated for $C_8H_{11}N_1I_1$ $[M+H]^+$ 247.9931; Found 247.9930.

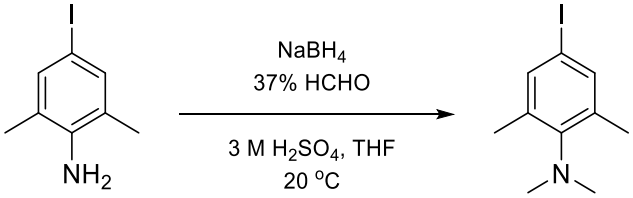

11 **12**, 95%

Synthesis of 4-iodo-N,N,2,6-tetramethylaniline, 12:
11 (1 g, 4 mmol), 37 wt.% aqueous HCHO (1.3 mL, 12 mmol), 3 M H_2SO_4 (2.4 mL), and THF (10.76 mL) were combined and set to stir in an ice bath. $NaBH_4$ (605 mg, 16 mmol) was added portionwise to the solution with strong stirring. After one hour, the reaction was quenched with a saturated aqueous solution of $NaHCO_3$ and basified to a pH of 8. The reaction mixture was extracted with EtOAc (3x). The organic layers were washed with brine, dried with Na_2SO_4, and concentrated to dryness *in vacuo* to afford **12** as a brown oil with an orange hue (1.06 g, 95% yield).

^{1}H NMR (500 MHz, Chloroform-d) δ 7.32 (s, 2H), 2.78 (s, 6H), 2.23 (s, 6H).

^{13}C NMR (126 MHz, Chloroform-d) δ 149.77, 139.70, 137.55, 89.31, 42.45, 18.89.

HRMS (ESI+) Calculated for $C_{10}H_{15}N_1I_1$ $[M+H]^+$ 276.0244; Found 276.0242.

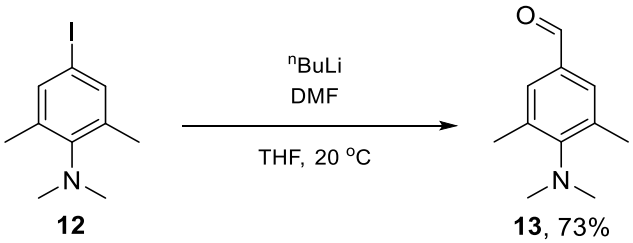

12 **13**, 73%

Synthesis of 4-(dimethylamino)-3,5-dimethylbenzaldehyde, 13:
A solution of **12** (510 mg, 1.87 mmol) in anhydrous THF (11.2 mL) was added to a flame-dried Schlenk flask under inert atmosphere and cooled to -78 °C using a bath of dry ice in acetone. A solution of 1.6 M ^{n}BuLi in hexane (1.73 mL, 2.8 mmol)) was added dropwise to the flask. After 1 hr, anhydrous DMF (217 μL, 2.8 mmol) was added dropwise to the flask. After 15 minutes, the reaction mixture was brought to room temperature and quenched with saturated aqueous NH_4Cl (~10 mL). This solution was extracted with EtOAc (3x). The organic layers were washed with brine, dried with Na_2SO_4, and concentrated to dryness *in vacuo*. The residue was purified by flash chromatography (silica deactivated with Et_3N, 10% EtOAc in hexanes) to afford **13** as a clear, yellow oil (242 mg, 73% yield).

^{1}H NMR (500 MHz, Chloroform-d) δ 9.86 (s, 1H), 7.50 (s, 2H), 2.87 (s, 6H), 2.34 (s, 6H).

^{13}C NMR (126 MHz, Chloroform-d) δ 191.99, 156.38, 136.70, 132.28, 130.83, 42.55, 19.66.

HRMS (ESI+) Calculated for $C_{11}H_{16}O_1N_1$ $[M+H]^+$ 178.1226; Found 178.1224.

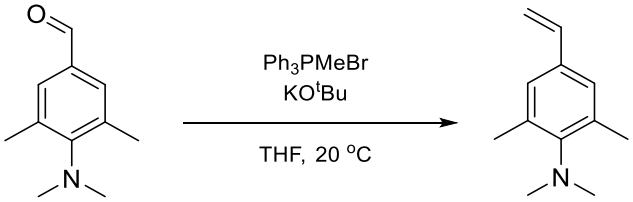

13 **14,** 81%

Synthesis of N,N,2,6-tetramethyl-4-vinylaniline, 14:
Ph_3PMeBr (917 mg, 2.57 mmol) and KO^{t}Bu (345 mg, 3.081 mmol) were added to a flask and the flask was evacuated/backfilled with N_2 (3x). Anhydrous THF (14 mL) was added to the reaction mixture and the solution was set to stir at room temperature for 30 minutes. **13** (364 mg, 2.05 mmol) was then dissolved in anhydrous THF (4 mL) and added to the flask. The mixture was set to stir at room temperature for 16 hours. The reaction was then added to water and extracted with EtOAc (3x). The organic layers were washed with brine, dried with Na_2SO_4, and concentrated to dryness *in vacuo*. The residue was purified by flash chromatography (silica deactivated with Et_3N, 10% to 20% EtOAc in hexanes) to afford **14** as a clear, yellow oil (291 mg, 81% yield).

^{1}H NMR (500 MHz, Chloroform-d) δ 7.05 (s, 2H), 6.62 (dd, J = 17.6, 10.9 Hz, 1H), 5.64 (d, J = 17.6 Hz, 1H), 5.14 (d, J = 10.9 Hz, 1H), 2.81 (s, 6H), 2.29 (s, 6H).

^{13}C NMR (126 MHz, Chloroform-d) δ 137.14, 136.67, 133.94, 126.77, 112.70, 42.64, 19.34.

HRMS (ESI+) Calculated for $C_{12}H_{18}N_1$ $[M+H]^+$ 176.1434; Found 176.1432.

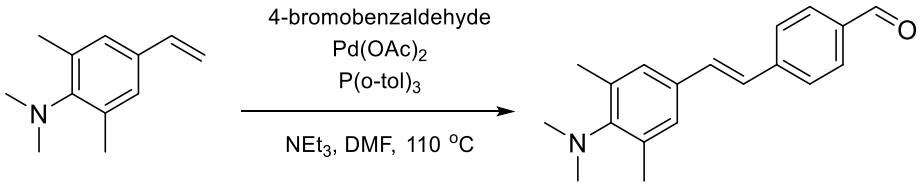

14 **15**, 41%

Synthesis of (E)-4-(4-(dimethylamino)-3,5-dimethylstyryl)benzaldehyde, 15:
14 (98 mg, 0.56 mmol), 4-bromobenzaldehyde (104 mg, 0.56 mmol), $Pd(OAc)_2$ (6.3 mg, 0.03 mmol), and $P(o\text{-}tol)_3$ (17 mg, 0.06 mmol) were combined in a flame-dried Schlenk flask. The flask was evacuated/backfilled with N_2 (3x). Triethylamine (1.1 mL) and DMF (1.1 mL) were then added to the flask. The reaction was set to stir at 110 °C for 16 hours. The mixture was then concentrated to dryness *in vacuo* and purified by flash chromatography (silica deactivated with Et_3N, 5% to 8% EtOAc in hexanes to afford **15** as a yellow solid (64 mg, 41% yield).

^{1}H NMR (400 MHz, Chloroform-d) δ 9.98 (s, 1H), 7.85 (d, J = 8.2 Hz, 2H), 7.62 (d, J = 8.2 Hz, 2H), 7.22 – 7.00 (m, 4H), 2.84 (s, 6H), 2.33 (s, 6H).

^{13}C NMR (101 MHz, Chloroform-d) δ 191.72, 150.60, 143.98, 137.28, 135.10, 132.71, 132.17, 130.34, 127.57, 126.78, 126.10, 42.63, 19.43.

HRMS (ESI+) Calculated for $C_{19}H_{22}O_1N_1$ $[M+H]^+$ 280.1696; Found 280.1694.

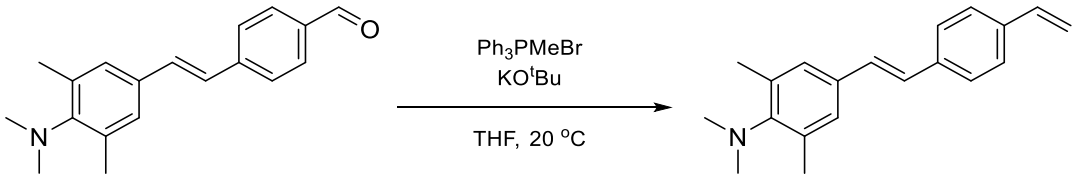

15 **16**, 69%

Synthesis of (E)-N,N,2,6-tetramethyl-4-(4-vinylstyryl)aniline, 16:
Ph_3PMeBr (256 mg, 0.72 mmol) and KO^{t}Bu (96.5, 0.86 mmol) were added to a flask and the flask was evacuated/backfilled with N_2 (3x). Anhydrous THF (4 mL) was added to the reaction mixture and the solution was set to stir at room temperature for 30 minutes. **15** (160 mg, 0.573 mmol) was then dissolved in anhydrous THF (1 mL) and added to the flask. The mixture was set to stir at room temperature for 16 hours. The reaction was then added to water and extracted with EtOAc (3x). The organic layers were washed with brine, dried with Na_2SO_4, and concentrated to dryness *in vacuo*. The residue was purified by flash chromatography (silica deactivated with Et_3N, 15% EtOAc in hexanes) to afford **16** as an orange solid (109 mg, 69% yield).

^{1}H NMR (500 MHz, Chloroform-d) δ 7.48 – 7.38 (m, 4H), 7.16 (s, 2H), 7.01 (d, J = 3.0 Hz, 2H), 6.72 (dd, J = 17.6, 10.9 Hz, 1H), 5.76 (d, J = 17.6 Hz, 1H), 5.24 (d, J = 10.9 Hz, 1H), 2.83 (s, 6H), 2.32 (s, 6H).

^{13}C NMR (126 MHz, Chloroform-d) δ 149.76, 137.41, 137.26, 136.63, 128.54, 127.18, 127.11, 126.65, 126.62, 113.64, 42.68, 19.42.

HRMS (ESI+) Calculated for $C_{20}H_{24}N_1$ $[M+H]^+$ 278.1903; Found 278.1900.

Preparation of voltage indicators:

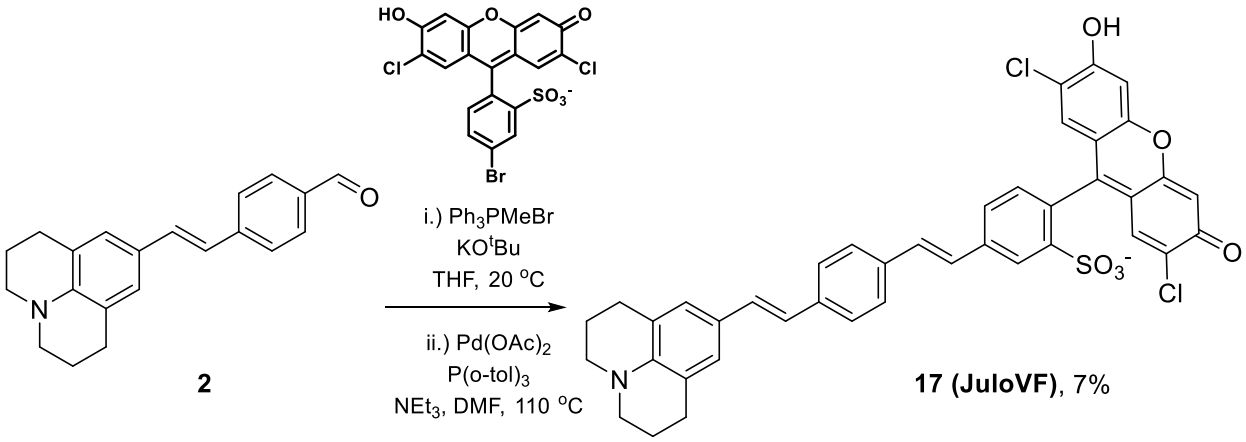

Synthesis of 17 (JuloVF):
Ph_3PMeBr (146 mg, 0.41 mmol) and KO^tBu (56 mg, 0.5 mmol) were combined with anhydrous THF (2 mL) and set to stir at room temperature for one hour. Compound **2** (100 mg, 0.33 mmol) was then dissolved in anhydrous THF (1 mL), added to the reaction mixture, and set to stir at room temperature for 16 hours. The reaction was then added to water and extracted with EtOAc (3x). The organic layers were collected, washed with brine, dried with Na_2SO_4, and concentrated to dryness *in vacuo* to give a red-orange solid. This crude material was combined with 5-bromo-(2',7')-dichloro-sulfofluorescein (**A**, 155 mg, 0.30 mmol), $Pd(OAc)_2$ (3 mg, 0.015 mmol), and $P(o\text{-}tol)_3$ (9 mg, 0.030 mmol) in a flame-dried Schlenk flask. The flask was evacuated/backfilled with N_2 (3x). Anhydrous DMF (1.4 mL) and anhydrous triethylamine (339 µL) were added, the flask was sealed, and the solution was stirred at 110° C for 16 hours. The reaction was then cooled to room temperature and concentrated to dryness *in vacuo*. The crude residue was taken up in 1:1 MeOH/ACN (100 mL) and filtered through Celite. The filtrate was concentrated to dryness *in vacuo*. The residue was taken up in a minimal amount of 1:1 MeOH/ACN and precipitated in ether. The precipitate was purified by preparative-HPLC (Water/MeCN + 0.05% TFA) to afford **17** as a red-orange powder (15 mg, 7% yield).

^{1}H NMR (400 MHz, DMSO-d_6) δ 8.17 (s, 1H), 7.79 (d, *J* = 8.0 Hz, 1H), 7.66 (d, *J* = 7.7 Hz, 2H), 7.54 (d, *J* = 7.8 Hz, 2H), 7.48 – 7.35 (m, 2H), 7.25 (d, *J* = 7.9 Hz, 1H), 7.18 – 6.82 (m, 6H), 6.77 (s, 2H), 3.28 – 3.01 (m, 4H), 2.87 – 2.58 (m, 4H), 1.99 – 1.78 (m, 4H).

HRMS (ESI-) Calculated for $C_{41}H_{30}O_6N_1Cl_2S_1$ $[M\text{-}H]^-$ 734.1176; Found 734.1168.

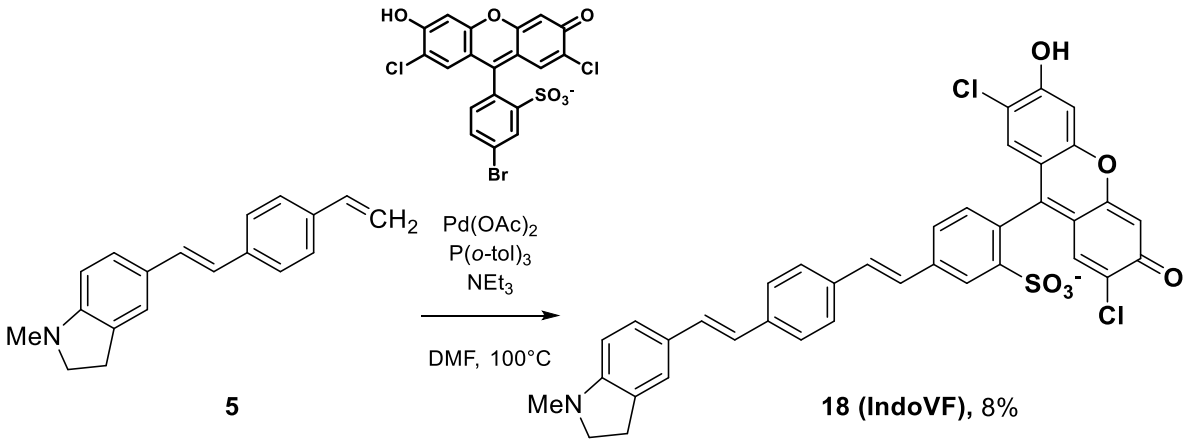

5 **18 (IndoVF),** 8%

Synthesis of 18 (IndoVF):
5 (30 mg, 0.11 mmol), 5-bromo-(2',7')-dichloro-sulfofluorescein (**A**, 54 mg, 0.1 mmol), $Pd(OAc)_2$ (0.5 mg, 2 µmol), and P(*o*-tol)$_3$ (1.5 mg, 5 µmol) were combined in anhydrous DMF (2 mL). Anhydrous triethylamine (0.21 g, 2.1 mmol) was added, the flask was sealed, and the reaction was stirred at 110 °C for 18 hours. The reaction was then concentrated to dryness *in vacuo*, then the crude material was taken up in 1:1 dicholoromethane:methanol, and precipitated in ether. The precipitate was purified by preparative-HPLC (Water/MeCN + 0.05% TFA) to afford **18** as a red-orange powder (6 mg, 8% yield).

^{1}H NMR (400 MHz, DMSO-d_6) δ 8.15 (s, 1H), 7.76 (d, *J* = 7.8 Hz, 1H), 7.64 (d, *J* = 8.0 Hz, 2H), 7.53 (d, *J* = 7.9 Hz, 2H), 7.42 – 7.32 (m, 3H), 7.22 (dd, *J* = 8.1, 4.2 Hz, 2H), 7.16 (d, *J* = 16.5 Hz, 1H), 6.97 (d, *J* = 10.3 Hz, 3H), 6.73 (s, 2H), 6.47 (d, *J* = 8.0 Hz, 1H), 3.29 (t, *J* = 8.2 Hz, 3H), 2.89 (t, *J* = 8.3 Hz, 2H), 2.71 (s, 3H).

HRMS (ESI-) m/z: $[M-H]^-$ calculated for $C_{38}H_{26}CL_2NO_6S$ 694.0863; found 694.0859.

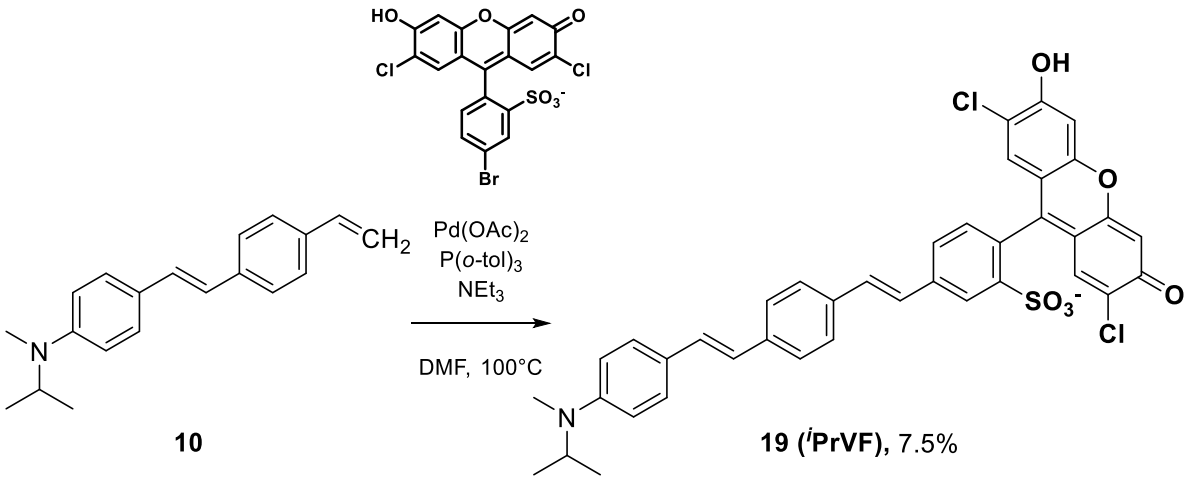

10 **19 (*i*PrVF),** 7.5%

Synthesis of 19 (*i*PrVF):
10 (40 mg, 0.14 mmol), 5-bromo-(2',7')-dichloro-sulfofluorescein (**A**, 68 mg, 0.13 mmol), $Pd(OAc)_2$ (0.6 mg, 3 µmol), and $P(o\text{-tol})_3$ (1.6 mg, 5 µmol) were combined in anhydrous DMF (1 mL). Anhydrous triethylamine (0.27 g, 2.6 mmol) was added, the flask was sealed, and the reaction was stirred at 100 °C for 18 hours. The reaction was then concentrated to dryness *in vacuo*, then the crude material was taken up in 1:1 dicholoromethane:methanol, and precipitated in ether. The precipitate was purified by preparative-TLC (15% methanol in dichloromethane + 1% acetic acid) to afford **19** as a red solid (7 mg, 7% yield). We identified the presence of an impurity: the starting material, dichlorobromosulfonofluorescein **A** (see Spectrum S38). The presence of **A** had no effect on cellular loading (see Figure S22).

^{1}H NMR (900 MHz, DMSO-d_6) δ 8.16 (d, *J* = 1.9 Hz, 1H), 7.71 (dd, *J* = 7.9, 1.9 Hz, 1H), 7.66 (d, *J* = 7.9 Hz, 2H), 7.56 (d, *J* = 8.0 Hz, 2H), 7.44 (d, *J* = 8.3 Hz, 2H), 7.41 (d, *J* = 16.3 Hz, 1H), 7.37 – 7.34 (m, 1H), 7.18 (d, *J* = 16.3 Hz, 1H), 7.12 (d, *J* = 7.7 Hz, 1H), 6.99 (d, *J* = 16.3 Hz, 1H), 6.79 (d, *J* = 8.5 Hz, 2H), 6.74 (s, 2H), 6.12 (s, 2H), 4.16 (q, *J* = 6.6 Hz, 1H), 2.72 (s, 3H), 1.13 (d, *J* = 6.5 Hz, 6H).

HRMS (ESI-) m/z: $[M-H]^-$ calculated for $C_{39}H_{30}Cl_2NO_6$ 710.1176; found 710.1172.

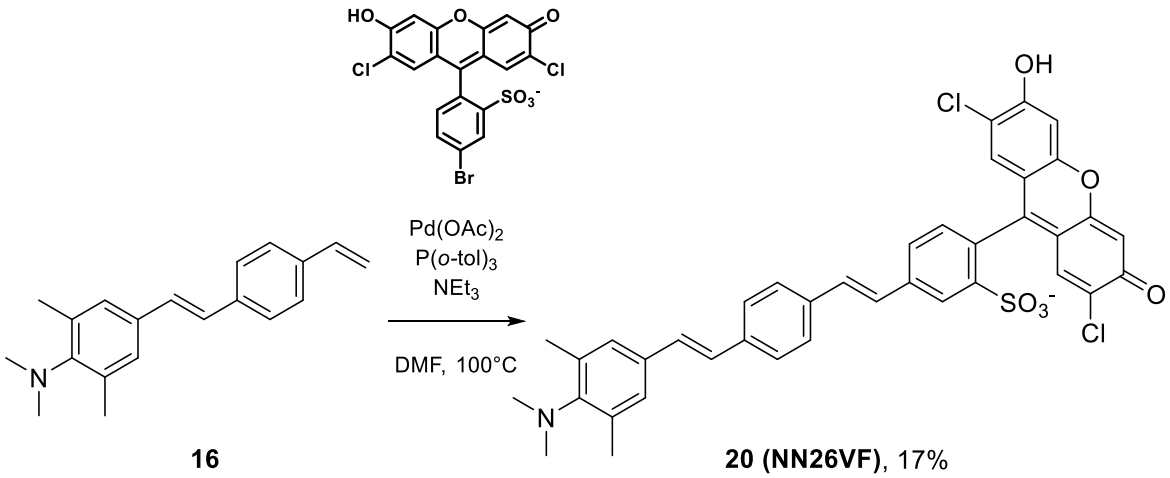

16 **20 (NN26VF)**, 17%

Synthesis of 20 (NN26VF):
16 (18 mg, 0.065 mmol), 5-bromo-(2',7')-dichloro-sulfofluorescein (**A**, 20 mg, 0.039 mmol), $Pd(OAc)_2$ (0.5 mg, 0.002 mmol), and P(o-tol)$_3$ (1.2 mg, 0.004 mmol) were combined in a flame-dried Schlenk flask. The flask was evacuated/backfilled with N_2 (3x). Anhydrous DMF (750 µL) and anhydrous triethylamine (187.5 µL) were added, the flask was sealed, and the solution was stirred at 110° C for 16 hours. The reaction was then cooled to room temperature, diluted with 1:1 MeOH/DCM (10 mL), and filtered through Celite. The filtrate was concentrated to dryness *in vacuo*. The residue was purified by preparative-TLC (silica deactivated with Et_3N, 10% MeOH in DCM) to afford **20** as a red-orange powder (4.6 mg, 15% yield). We identified the presence of an impurity: the starting material, dichlorobromosulfonofluorescein **A** (see Spectrum S40 and S41). The presence of **A** had no effect on cellular loading (see Figure S22).

^{1}H NMR (900 MHz, DMSO-d_6) δ 8.17 (d, *J* = 1.8 Hz, 1H), 7.73 (dd, *J* = 7.8, 1.8 Hz, 1H), 7.69 (d, *J* = 7.9 Hz, 2H), 7.61 (d, *J* = 7.9 Hz, 2H), 7.44 (d, *J* = 16.4 Hz, 1H), 7.37 (d, *J* = 16.4 Hz, 1H), 7.24 (s, 2H), 7.19 – 7.15 (m, 2H), 7.13 (d, *J* = 7.8 Hz, 1H), 6.75 (s, 2H), 6.16 (s, 2H), 2.78 (s, 6H), 2.28 (s, 6H).

HRMS (ESI-) Calculated for $C_{39}H_{30}O_6N_1Cl_2S_1$ $[M-H]^-$ 710.1176; Found 710.1172.

12. Supplementary Figures

Figure S1. Absorbance, Emission, and Excitation Spectra of Aniline VFs.

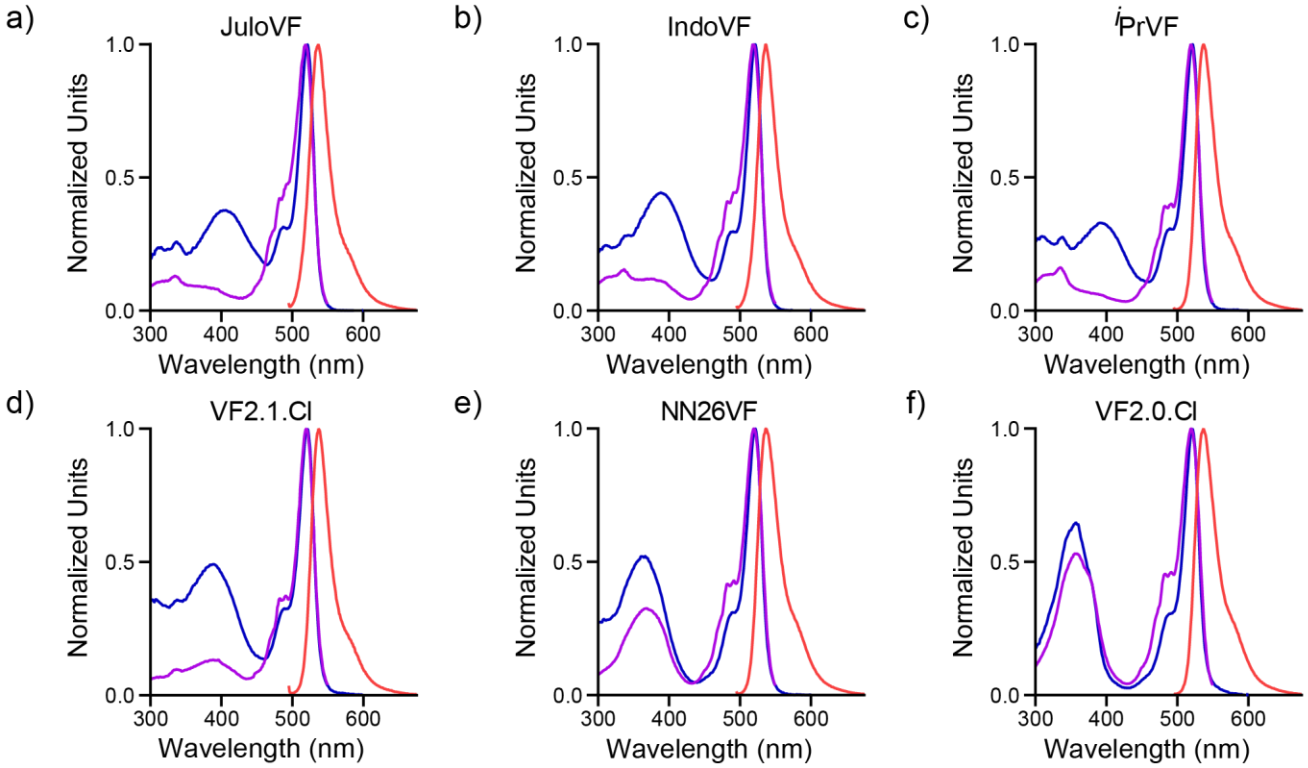

Figure S1. Absorbance, Emission, and Excitation Spectra of Aniline VFs.
Absorbance spectra (blue), emission spectra (red), and excitation spectra (purple) for JuloVF (a), IndoVF (b), ^{i}PrVF (c), VF2.1.Cl (d), NN26VF(e), and VF2.0.Cl (f) in ethanol with 0.1 M KOH. The VoltageFluors were diluted from DMSO stocks (500 µM-1 mM) to either 1 µM (JuloVF, IndoVF, ^{i}PrVF, VF2.1.Cl, NN26VF) or 500 nM (VF2.0.Cl) in ethanol with 0.1 M KOH. VF2.0.Cl was measured at 500 nM as the emission of 1 mM VF2.0.Cl was higher than the range of the detector for wavelengths near the emission maximum. Spectra were taken using the equipment described above in section **2**. Absorbance measurements were recorded at 1 nm intervals from 300 nm to 600 nm. Emission measurements were recorded at 1 nm intervals from 495 nm to 675 nm while exciting the VoltageFluors with 485 nm light. Excitation measurements were recorded by measuring the emission of each VoltageFluor at 570 nm while the excitation light was varied from 300 nm to 550 nm. 2 nm slit widths were used for each measurement. Each absorbance, emission, and excitation trace was normalized to the maximum value of absorbance, emission, or excitation respectively.

Figure S2. **^{13}C NMR shifts of the para-carbon in aniline series precursors.**

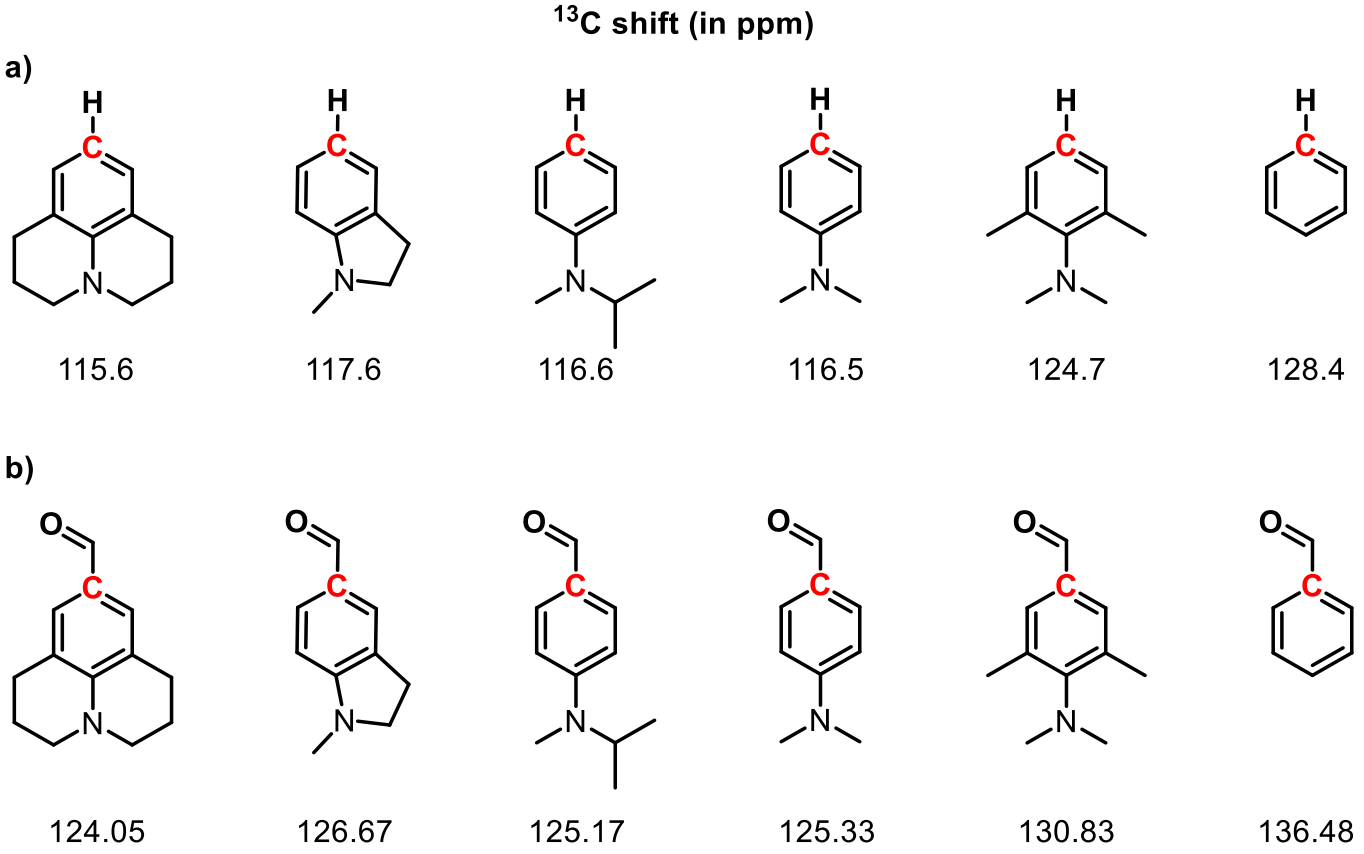

Figure S2. ^{13}C NMR shifts of the para-carbon in aniline series precursors.
^{13}C NMR shifts (in ppm) for the carbons labeled above in red. a) (from left to right): Julolidine[17], N-methylindoline[18], N-methyl-N-isopropylaniline[19], N,N-dimethylaniline[20–22], N,N,2,6-tetramethylaniline[23], and benzene[24]. Values are taken from literature. All were acquired in $CDCl_3$. b) (from left to right): Compound **1** (**Spectrum S2**), 1-methylindoline-5-carbaldehyde (**Spectra S41-S43**), Compound **7** (**Spectrum S14**), 4-(dimethylamino)benzaldehyde (**Spectrum S44**), Compound **13** (**Spectrum S26**), and benzaldehyde (**Spectrum S45**). All spectra were taken in $CDCl_3$ (chloroform peak referenced to 77.16 ppm).

Figure S3. Calculated HOMO energy levels of aniline series precursors and correlations to measured dye properties.

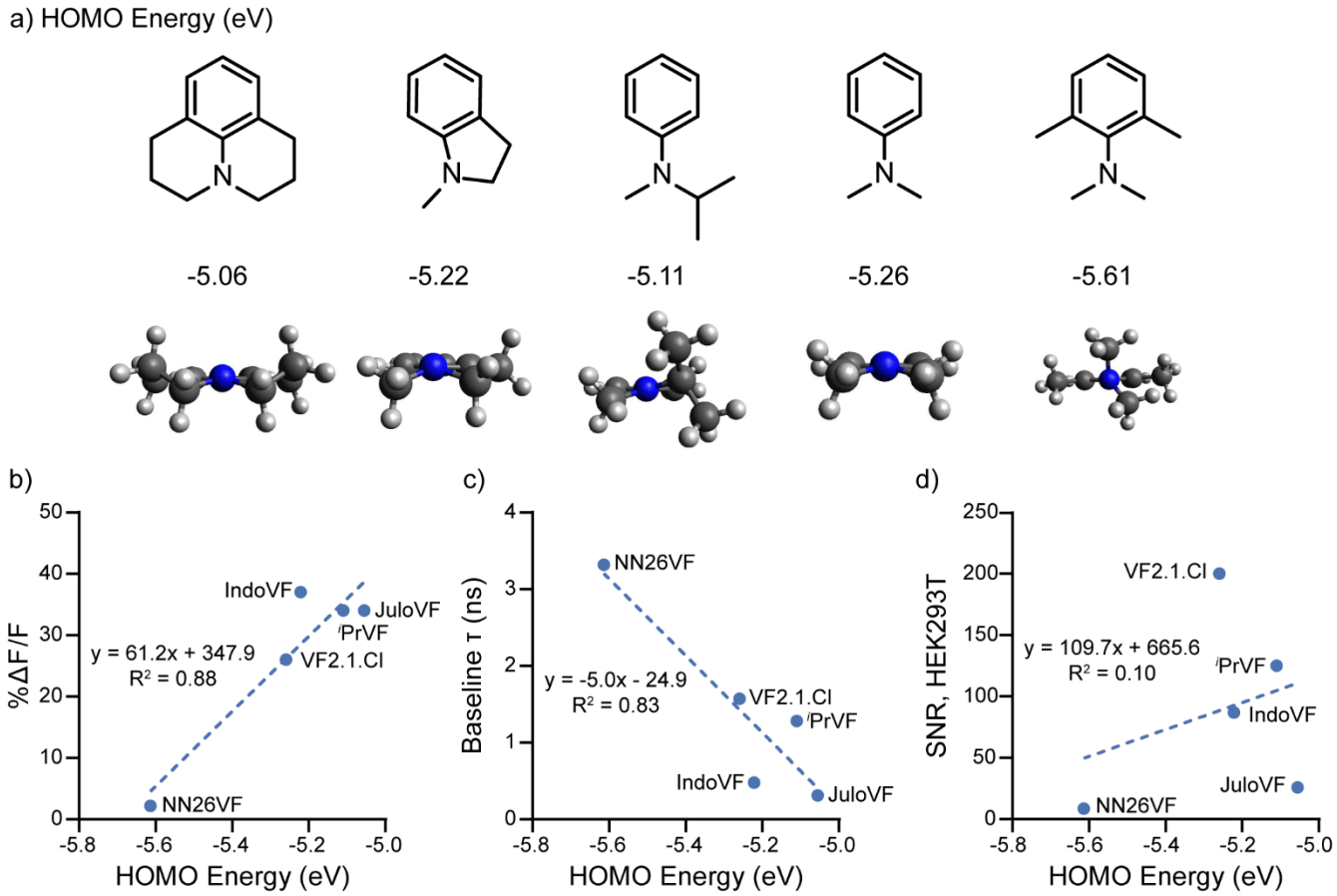

Figure S3. Calculated HOMO energy levels of aniline series precursors and correlations to measured dye properties. **a**) Calculated HOMO energies (in eV) and optimized geometries of aniline precursors. All calculations were performed at the B3LYP-D3(BJ)/6-311G* level of theory. All geometries were confirmed to be true minima (zero imaginary frequencies). Correlations between the calculated HOMO energies of aniline precursors and the measured b) %ΔF/F values, c) fluorescence lifetimes at 0 mV, and d) signal-to-noise ratios (SNRs) for a 100 mV step in HEK293T cells for VF dyes derived from the associated aniline precursors.

Figure S4. Full spectra for pH titrations.

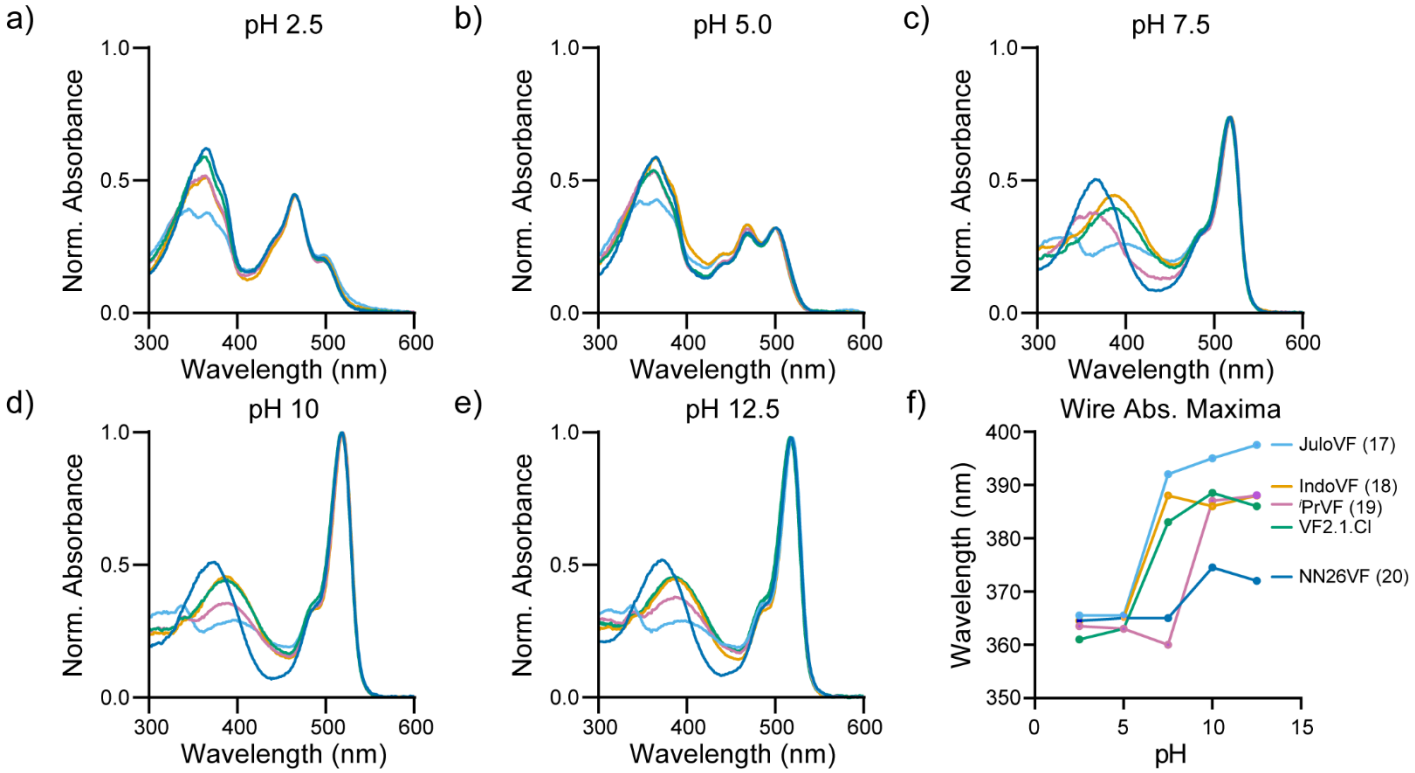

Figure S4. Full spectra for pH titrations.
Absorbance spectra for JuloVF (light blue), IndoVF (orange), ^{i}PrVF (pink), VF2.1.Cl (green), and NN26VF (dark blue) in buffered solutions with defined pH. All buffer solutions contain 0.1% w/v SDS to help solubilize the VoltageFluors. The VoltageFluors were diluted from DMSO stocks (500 µM-1 mM) to 500 nM in the following solutions. a) Absorbance spectra in 10 mM phosphate buffer which was adjusted to pH 2.5 with HCl/NaOH and adjusted to 56 mOsm with NaCl. b) Absorbance spectra in 10 mM acetate buffer which was adjusted to pH 5.0 with HCl/NaOH and adjusted to 56 mOsm with NaCl. c) Absorbance spectra in 10 mM phosphate buffer which was adjusted to pH 7.5 with HCl/NaOH and adjusted to 56 mOsm with NaCl. d) Absorbance spectra in 10 mM carbonate buffer which was adjusted to pH 10.0 with HCl/NaOH and adjusted to 56 mOsm with NaCl. e) Absorbance spectra in 10 mM KCl/NaOH buffer which was adjusted to pH 12.5 with HCl/NaOH and adjusted to 56 mOsm with NaCl. f) Plot of the wavelength of maximum absorbance for the wire peak of each VoltageFluor versus the pH of the solution. Absorbance measurements were recorded at 0.5 nm intervals from 300 nm to 600 nm. 2 nm slit widths were used for each measurement. The absorbance traces were first normalized to their respective absorbance values at 519 nm (pH 7.5, 10.0, and 12.5), 500 nm (pH 5.0), or 470 nm (pH 2.5). The absorbance of chloro-fluorescein varies as a function of pH and these wavelengths are the absorbance maxima for the chloro-fluorescein peaks at the respective pH values. Finally, the absorbance traces were multiplied by the ratio of the average raw absorbance values at the chloro-fluorescein peak for a given pH to the average raw absorbance values at 519 nm for the pH 10 traces. The pH 10 traces had the highest raw absorbance values at 519 nm.

Figure S5. Concentration dependence of VoltageFluor fluorescence lifetimes in vesicles and in basic ethanol.

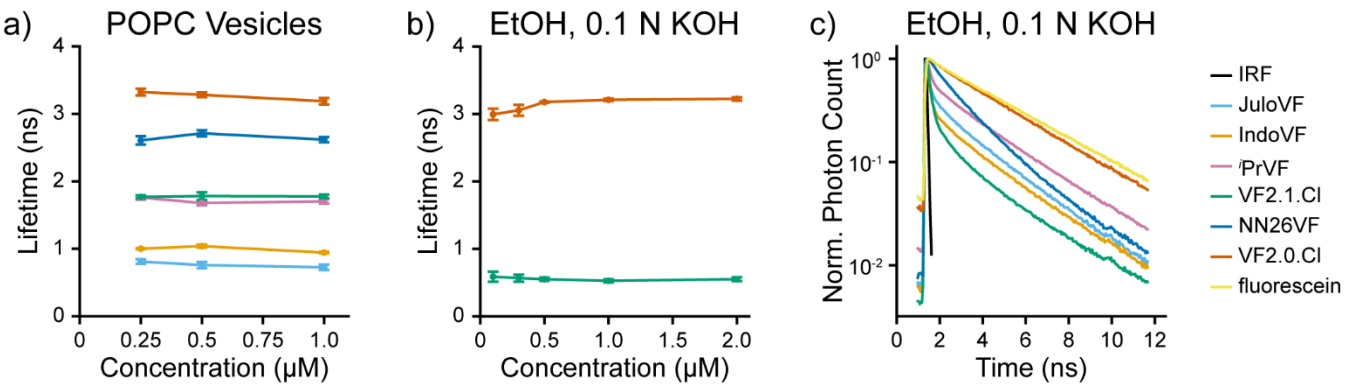

Figure S5. Concentration dependence of VoltageFluor fluorescence lifetimes in vesicles and in basic ethanol. Fluorescence lifetime data for VoltageFluors in POPC vesicles and in ethanol with 0.1 N KOH (EtOH-KOH). In all cases, 500 nM was selected as the optimal working concentration. The fluorescence lifetime of VF2.0.Cl was modeled as a sum of two exponential components; all other probes were modeled with three exponential components (see **Methods**). a) Concentration dependence of VF fluorescence lifetime in POPC vesicles. Data were tested for homoscedasticity (Levene's test on the median, $p>0.05$ for 5/6 probes, $p>0.01$ for ^{i}PrVF). Differences between concentrations for each probe were evaluated with Fisher's one-way ANOVA. No significant differences were found between groups for 5 of the 6 probes ($p>0.05$). For IndoVF, significant differences were observed between groups ($F(2,24)=9.00$, $p<0.01$). Tukey-Kramer post hoc tests revealed significant differences between 500 nM IndoVF and 1μM IndoVF ($p<0.05$), as well as between 250 nM IndoVF and 1 μM IndoVF ($p<0.001$). b) Concentration dependence of the fluorescence lifetime of VF2.0.Cl and VF2.1.Cl in EtOH-KOH. The data for each probe were tested for homoscedasticity (Levene's test on the median, $p>0.05$ in both cases). Differences between concentrations were assessed via Fisher's one-way ANOVA. No significant differences were observed between VF2.1.Cl concentrations ($F(4,32)=0.254$, $p=0.91$). Significant differences were observed between VF2.0.Cl concentrations ($F(4,20)=3.61$, $p=0.023$). Tukey-Kramer post hoc tests revealed significant differences between 100 nM and 1 μM VF2.0.Cl and between 100 nM and 2 μM VF2.0.Cl ($p<0.05$); all other comparisons did not yield significant differences ($p>0.05$). c) Representative time-resolved fluorescence intensity of the library of VFs at 500 nM VF in EtOH-KOH. Color coding for VF identity is consistent throughout all plots. IRF= instrument response function. Data in (a) and (b) are displayed as the mean ± SEM of data taken on 3 or 4 independent samples, each with 1-3 technical replicates.

Figure S6. HEK293T intensity patching and relative brightness.

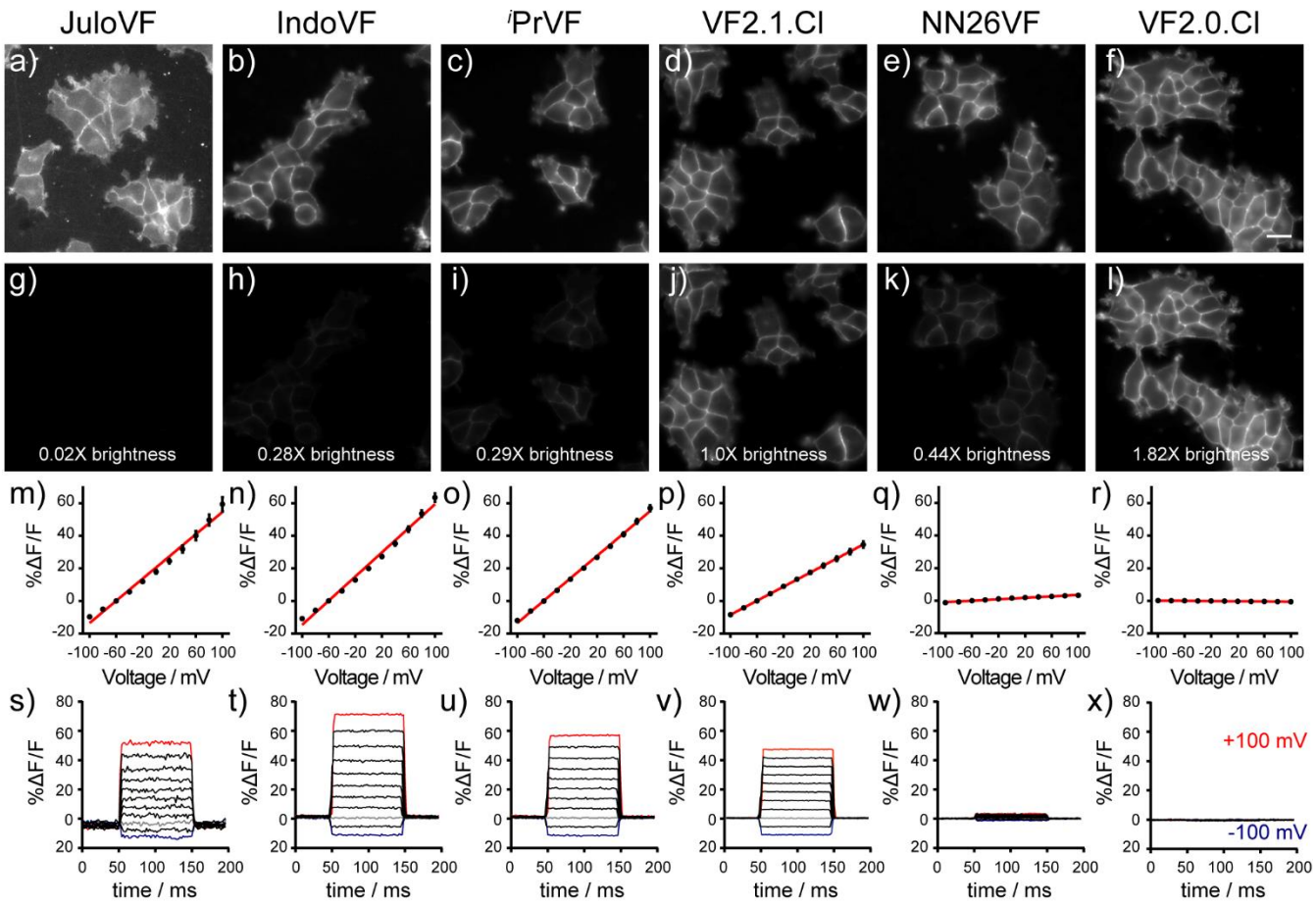

Figure S6. HEK293T intensity patching and relative brightness.

Voltage sensitivity and relative brightness comparison of VoltageFluor indicators in HEK293T cells with intensity-based imaging. Relative brightness was compared at a working concentration of 300 nM for all dyes. All brightness values are relative to VF2.1.Cl (d,j, 1.0X brightness), and were calculated as the difference between cell signal and the surrounding background (signal-background). Scale bar represents 20 µm. Top row (a-f) images are the same as Figure 2a-f, and display membrane localization for each indicator. The second row (g-l) features the same images, but with consistent pixel histograms across each image to illustrate the relative brightness of membrane staining. Linear plots (m-r) of the percent change in fluorescence versus V_{mem} from whole-cell voltage clamp (m, n=8 cells; n, n=4 cells; o, n=4 cells; p, n=8 cells; q, n=3 cells; r, n=5 cells). For whole-cell voltage clamp experiments, cells were loaded at 300 nM. Representative concatenated traces from a single patched cell (s-x) show the percent change in fluorescence over time as the holding potential is changed from +100 mV (red) to -100 mV (blue) in 20 mV increments.

Figure S7. V_{mem} sensitivity of the fluorescence lifetime of JuloVF.

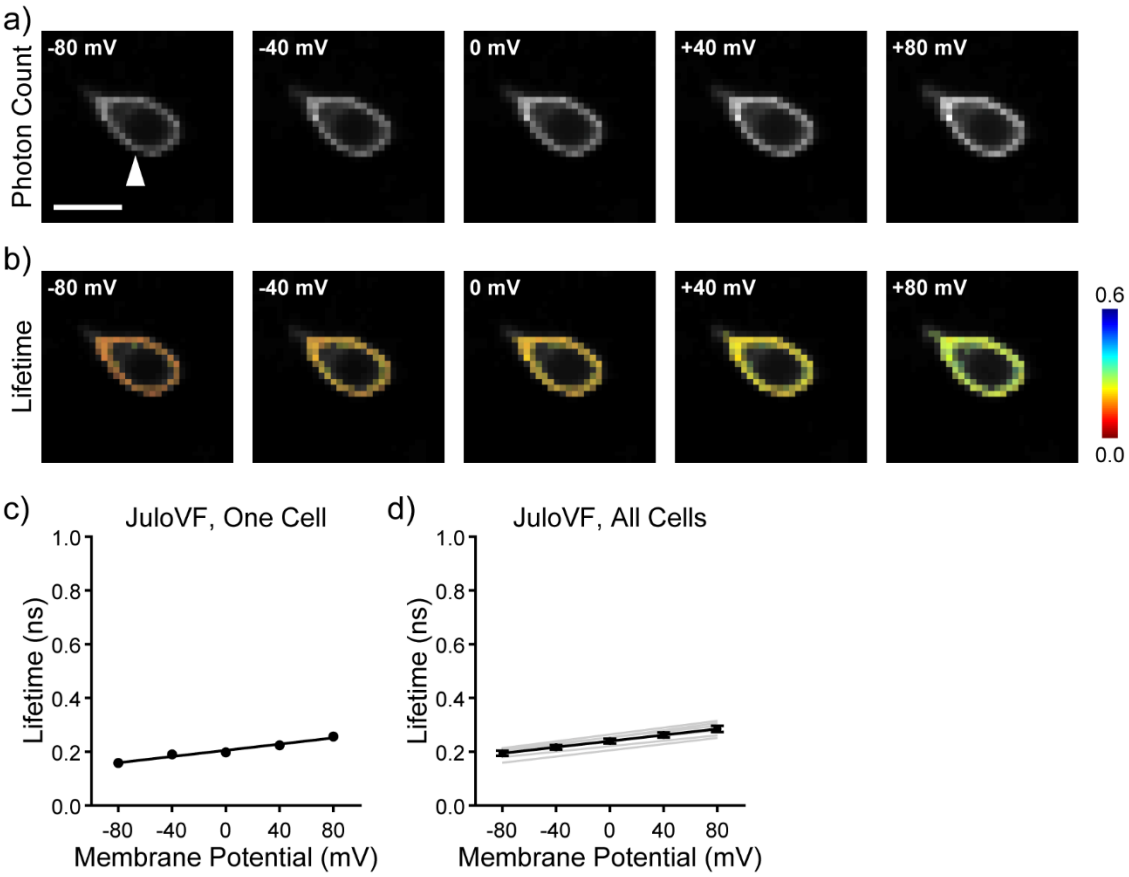

Figure S7. V_{mem} sensitivity of the fluorescence lifetime of JuloVF.
a) Photon count images of JuloVF in a HEK293T cell held at the indicated V_{mem} by whole cell patch clamp electrophysiology. The white arrow indicates the patch pipette; scale bar represents 20 µm. b) Lifetime-intensity overlay images of JuloVF as in (a). The time-resolved fluorescence decay for JuloVF was modeled as a sum of three exponential terms; the weighted average is shown here. Lifetime scale is in ns. c) Quantification of average lifetime at the plasma membrane for the individual cell shown in (a-b). The line of best fit for τ_{fl} vs. V_{mem} is shown in black. d) The average τ_{fl}-V_{mem} relationship for JuloVF (black line), as well as lines of best fit for each individual patched cell (gray, n=6 cells).

Figure S8. V_{mem} sensitivity of the fluorescence lifetime of IndoVF.

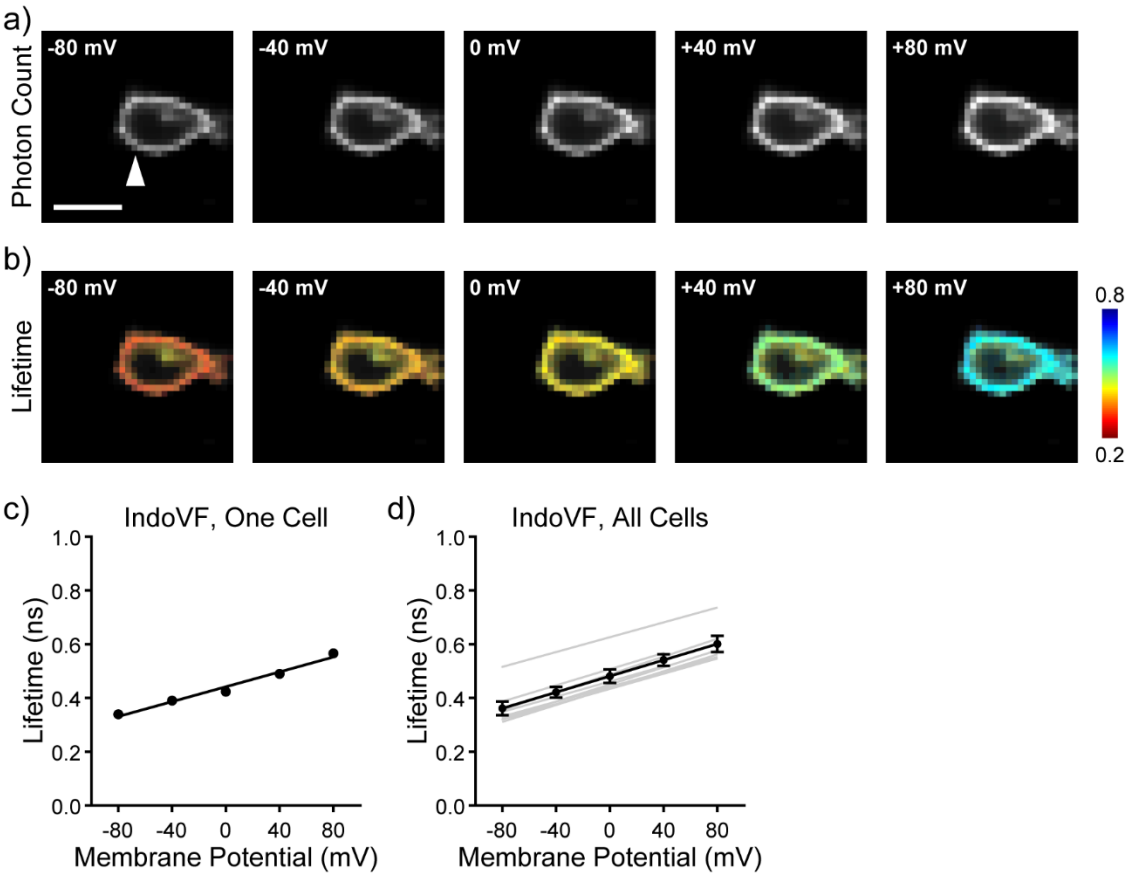

Figure S8. V_{mem} sensitivity of the fluorescence lifetime of IndoVF.
a) Photon count images of IndoVF in a HEK293T cell held at the indicated V_{mem} by whole cell patch clamp electrophysiology. The white arrow indicates the patch pipette; scale bar represents 20 µm. b) Lifetime-intensity overlay images of IndoVF as in (a). The time-resolved fluorescence decay for IndoVF was modeled as a sum of three exponential terms; the weighted average is shown here. Lifetime scale is in ns. c) Quantification of average lifetime at the plasma membrane for the individual cell shown in (a-b). The line of best fit for τ_{fl} vs. V_{mem} is shown in black. d) The average τ_{fl}-V_{mem} relationship for IndoVF (black line), as well as lines of best fit for each individual patched cell (gray, n=8 cells).

Figure S9. V_{mem} sensitivity of the fluorescence lifetime of ^{i}PrVF.

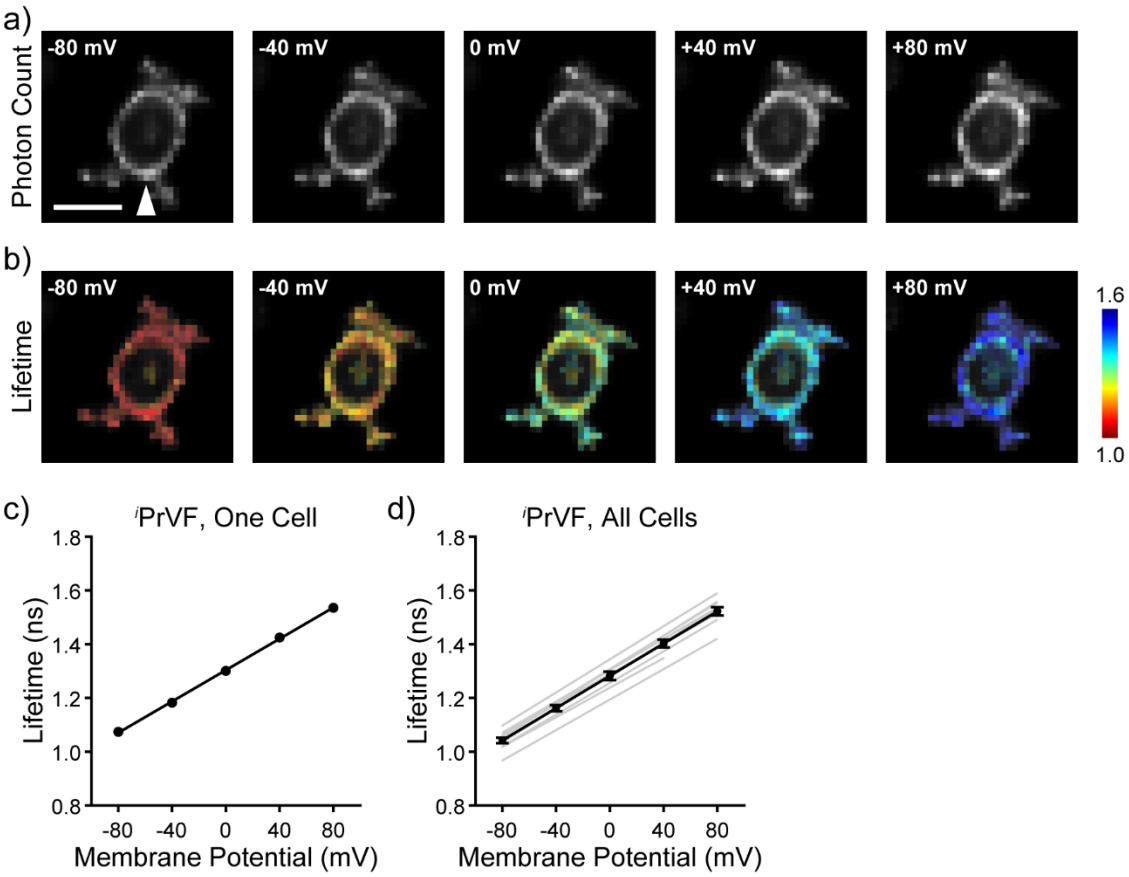

Figure S9. V_{mem} sensitivity of the fluorescence lifetime of ^{i}PrVF.
a) Photon count images of ^{i}PrVF in a HEK293T cell held at the indicated V_{mem} by whole cell patch clamp electrophysiology. The white arrow indicates the patch pipette; scale bar represents 20 µm. b) Lifetime-intensity overlay images of ^{i}PrVF as in (a). The time-resolved fluorescence decay for ^{i}PrVF was modeled as a sum of two exponential terms; the weighted average is shown here. Lifetime scale is in ns. c) Quantification of average lifetime at the plasma membrane for the individual cell shown in (a-b). The line of best fit for τ_{fl} vs. V_{mem} is shown in black. d) The average τ_{fl}-V_{mem} relationship for ^{i}PrVF (black line), as well as lines of best fit for each individual patched cell (gray, n=10 cells).

Figure S10. V_{mem} sensitivity of the fluorescence lifetime of VF2.1.Cl.

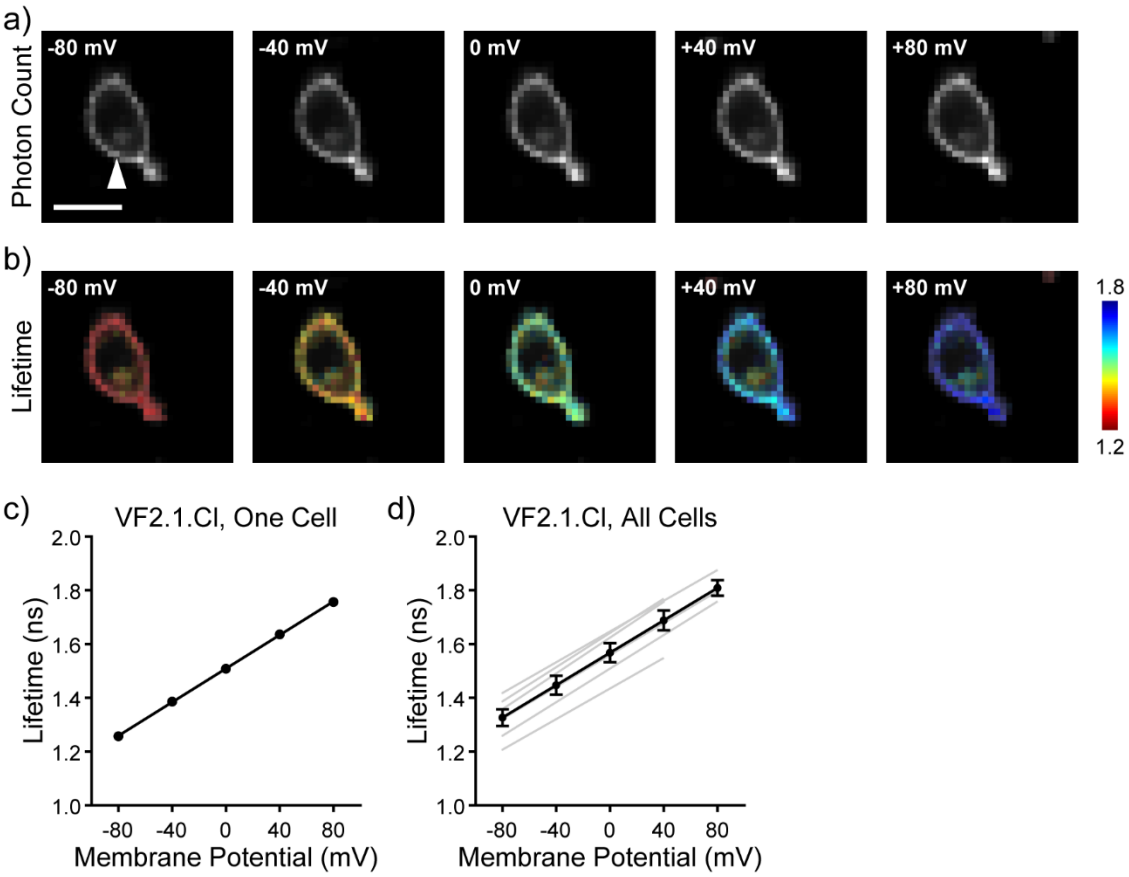

Figure S10. V_{mem} sensitivity of the fluorescence lifetime of VF2.1.Cl.
The relationship between fluorescence lifetime and V_{mem} for VF2.1.Cl was previously reported by our lab;[9] we repeated the experiment here at 300 nM dye loading for maximum comparability with the rest of the VF series presented here. These results are in good agreement with our previous work using 100 nM VF2.1.Cl. a) Photon count images of VF2.1.Cl in a HEK293T cell held at the indicated V_{mem} by whole cell patch clamp electrophysiology. The white arrow indicates the patch pipette; scale bar represents 20 µm. b) Lifetime-intensity overlay images of VF2.1.Cl as in (a). The time-resolved fluorescence decay for VF2.1.Cl was modeled as a sum of two exponential terms; the weighted average is shown here. Lifetime scale is in ns. c) Quantification of average lifetime at the plasma membrane for the individual cell shown in (a-b). The line of best fit for τ_{fl} vs. V_{mem} is shown in black. d) The average τ_{fl}-V_{mem} relationship for VF2.1.Cl (black line), as well as lines of best fit for each individual patched cell (gray, n=6 cells).

Figure S11. V_{mem} sensitivity of the fluorescence lifetime of NN26VF.

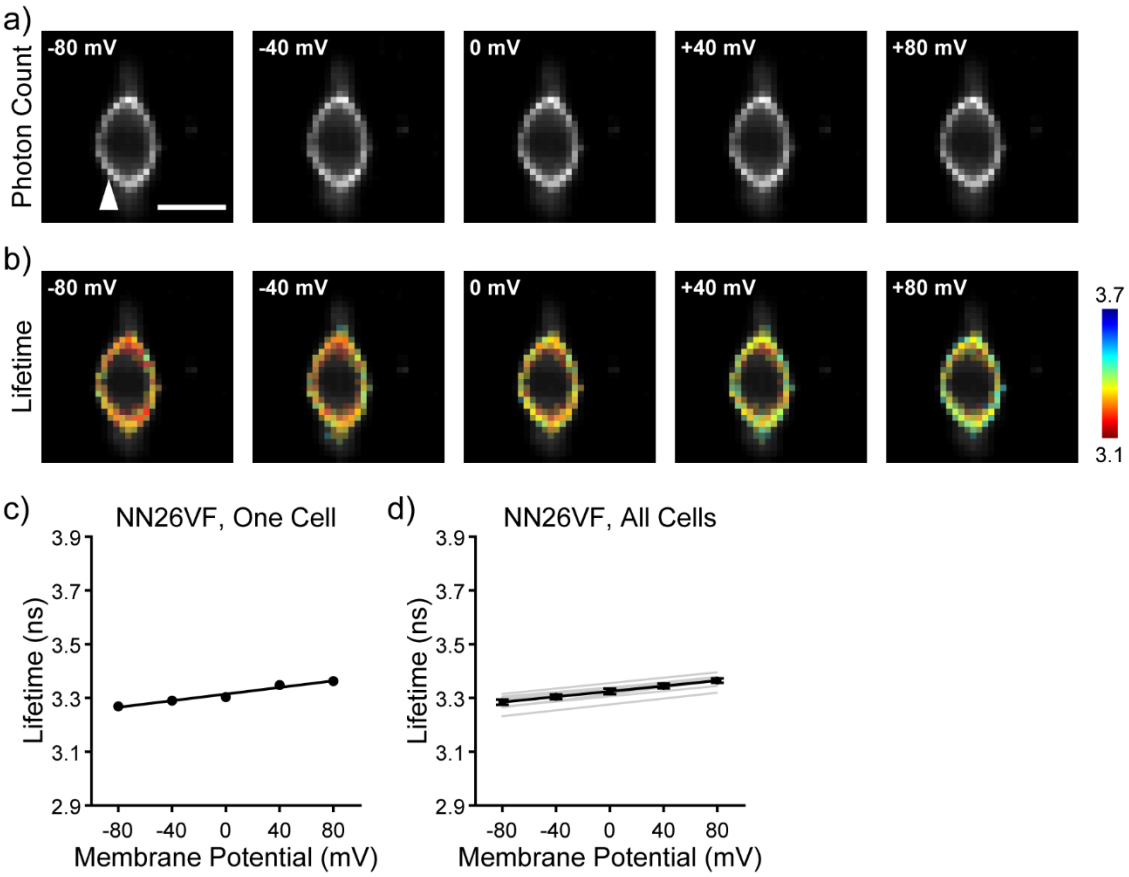

Figure S11. V_{mem} sensitivity of the fluorescence lifetime of NN26VF.
a) Photon count images of NN26VF in a HEK293T cell held at the indicated V_{mem} by whole cell patch clamp electrophysiology. The white arrow indicates the patch pipette; scale bar represents 20 µm. b) Lifetime-intensity overlay images of NN26VF as in (a). The time-resolved fluorescence decay for NN26VF was described by a single exponential decay term. Lifetime scale is in ns. c) Quantification of the NN26VF fluorescence lifetime at the plasma membrane for the individual cell shown in (a-b). The line of best fit for τ_{fl} vs. V_{mem} is shown in black. d) The average τ_{fl}-V_{mem} relationship for NN26VF (black line), as well as lines of best fit for each individual patched cell (gray, n=8 cells).

Figure S12. The fluorescence lifetime of VF2.0.Cl is not sensitive to V_{mem}.

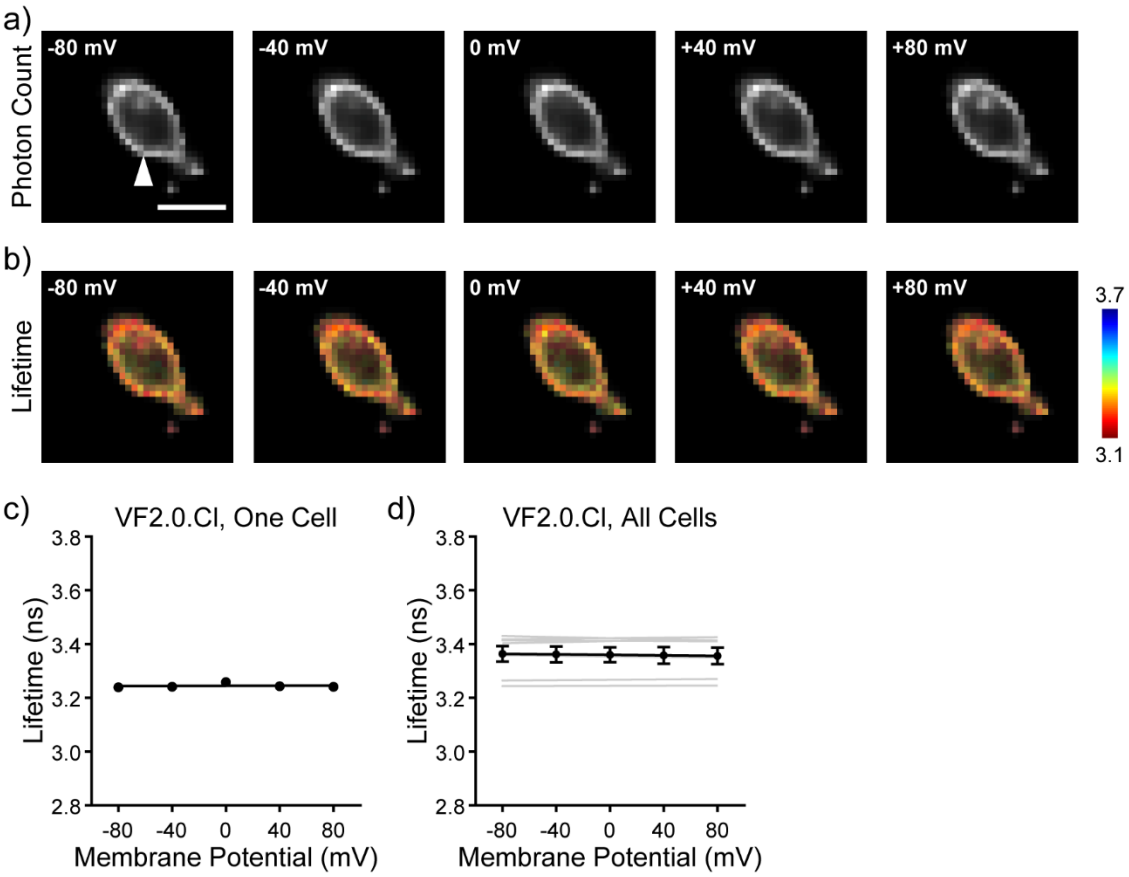

Figure S12. The fluorescence lifetime of VF2.0.Cl is not sensitive to V_{mem}.
The voltage-insensitivity of the fluorescence lifetime of VF2.0.Cl was previously reported by our lab;[9] we repeated the experiment here with 300 nM dye for maximum comparability with the rest of the VF series presented here. These results are in good agreement with our previous work with 100 nM VF2.0.Cl. a) Photon count images of VF2.0.Cl in HEK293T cells held at the indicated V_{mem} by whole cell patch clamp electrophysiology. The white arrow indicates the patch pipette; scale bar represents 20 µm. b) Lifetime-intensity overlay images of VF2.1.Cl as in (a). The time-resolved fluorescence decay for VF2.0.Cl was modeled with a single exponential term. Lifetime scale is in ns. c) Quantification of average lifetime at the plasma membrane for the individual cell shown in (a-b). The line of best fit for τ_{fl} vs. V_{mem} is shown in black. d) The average τ_{fl}-V_{mem} relationship for VF2.0.Cl (black line), as well as lines of best fit for each individual patched cell (gray, n=7 cells).

Figure S13. Percent change in τ_{fl} and goodness of linear fit for V_{mem}-τ_{fl} calibrations.

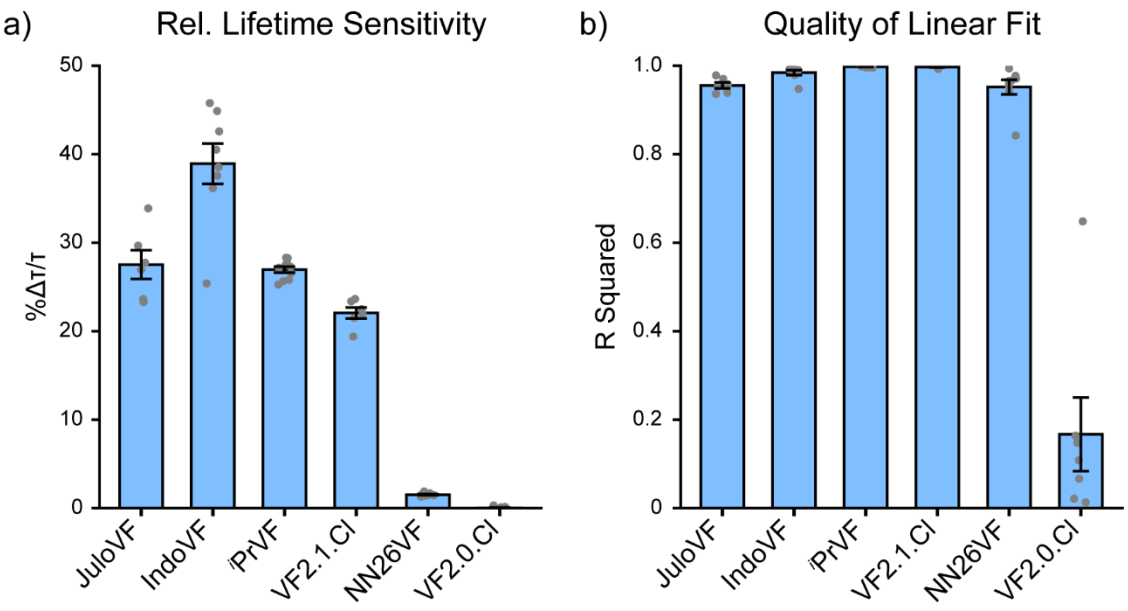

Figure S13. Percent change in τ_{fl} and goodness of linear fit for V_{mem}-τ_{fl} calibrations.
This supplement accompanies **Figure 3**. a) Percent change in τ_{fl} per 100 mV change, relative to the lifetime at -60 mV. b) Quality of the linear fit (as evaluated by the squared correlation coefficient, r^2) for the V_{mem}-τ_{fl} relationship of each VF. Each gray dot represents an individual patched HEK293T cell; bars represent mean ± SEM. Sample sizes (number of individual HEK293T cells): JuloVF 6, IndoVF 8, ^{i}PrVF 10, VF2.1.Cl 6, NN26VF 8, VF2.0.Cl 7. All dyes were loaded at 300 nM, except for JuloVF, where 500 nM dye was used because of brightness limitations.

Figure S14. Effect of fit model on the value and the V_{mem} sensitivity of the VF2.1.Cl fluorescence lifetime.

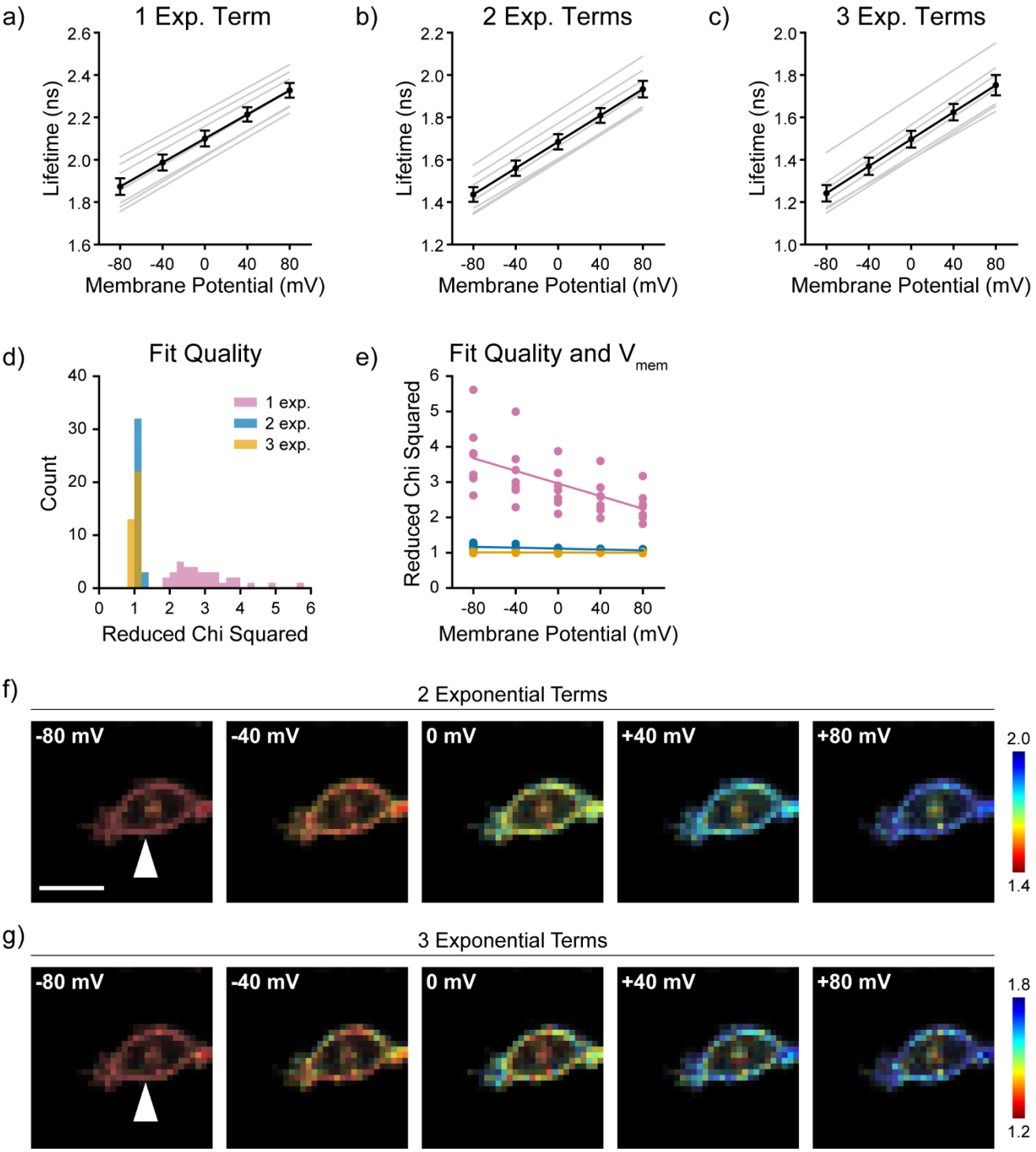

Figure S14. Effect of fit model on the value and the V_{mem} sensitivity of VF2.1.Cl fluorescence lifetime.
The relationship between V_{mem} and τ_{fl} of VF2.1.Cl in HEK293T was confirmed by whole cell patch clamp electrophysiology in HEK293T cells. V_{mem} was set with whole cell voltage clamp electrophysiology; the patch electrode is indicated by the white arrow. Previously reported τ_{fl} data for VF2.1.Cl was modeled with two exponential components;[9] here we show in details the process of selecting a satisfactory number of terms in a fluorescence lifetime decay model. a-c) The relationship between τ_{fl} and V_{mem} for VF2.1.Cl in HEK293T when VF2.1Cl τ_{fl} is described by a sum of one, two, or three exponential components (n=7 cells). The overall relationship is preserved, although the 0 mV lifetime shifts considerably across the three models. d) The quality of the exponential fit, as described by the reduced chi squared (χ^2, see **Methods**). Each value in the histogram is an individual measurement at a particular V_{mem}; therefore, each patch is represented by 4 or 5 values in the histogram). e) V_{mem} dependence of the fit quality of the exponential fit. Each point represents an individual measurement as in (d); each line represents the line of best fit for χ^2 vs V_{mem}. If a fit model adequately describes the V_{mem} sensitivity of a

VoltageFluor, there should be no V_{mem} dependence in χ^2. f-g) Representative images of the fluorescence lifetime of VF2.1.Cl fit pixel-by-pixel in a HEK293T cell. Increased variability between nearby pixels is observed when a third exponential component is added. VF2.1.Cl was used at 100 nM in these data. Scale bar represents 20 µm.

Figure S15. Fluorescence lifetime fit model selection for all VF derivatives.

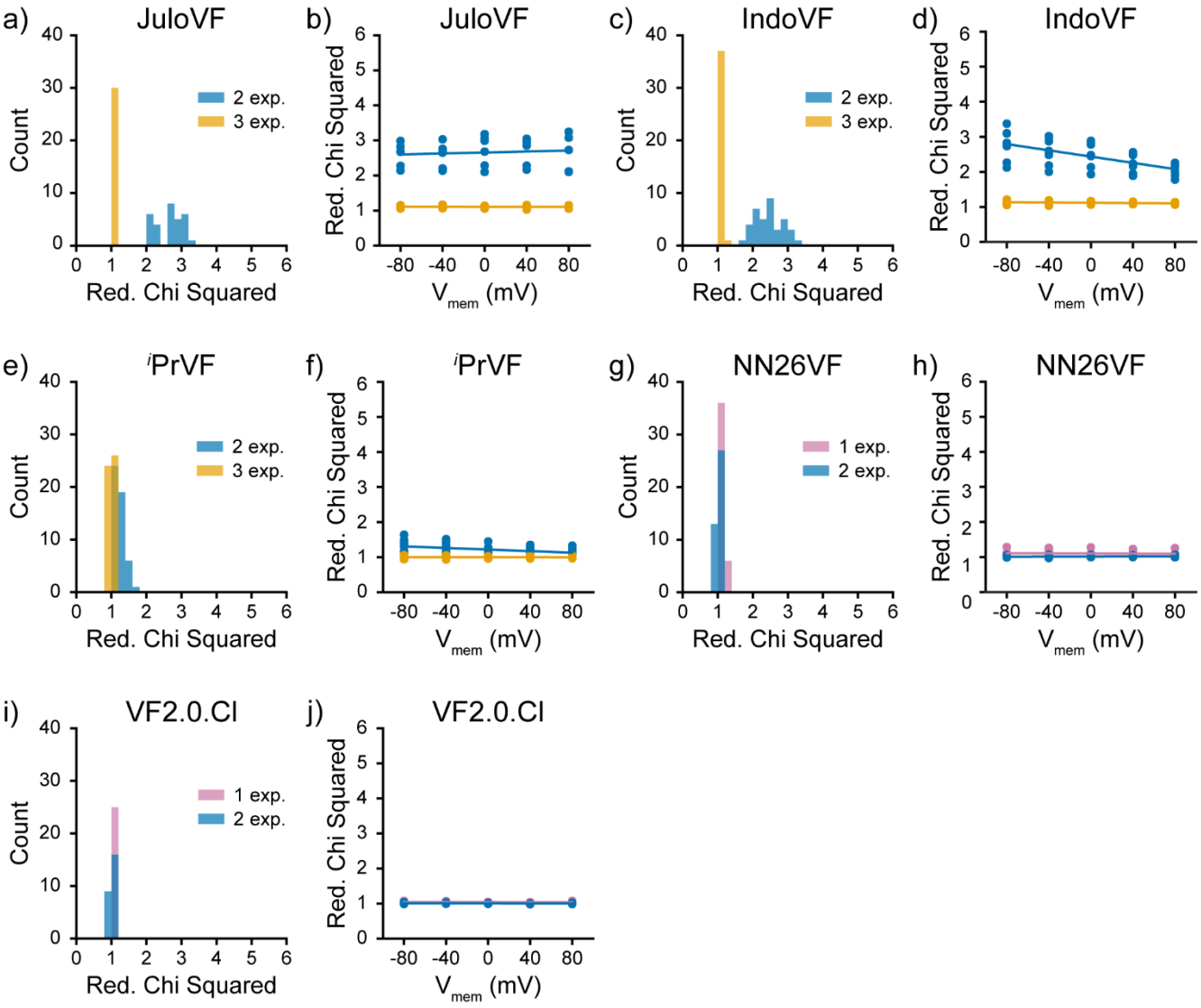

Figure S15. Fluorescence lifetime fit model selection for all VF derivatives.
Selection of the appropriate number of exponential terms in the fluorescence lifetime decay model was based on minimization of reduced chi squared χ^2 and avoidance of V_{mem} dependence in χ^2. These data are reproduced in **Fig. 3 and S7-12**. a) Comparison of χ^2 when the time resolved fluorescence decay of JuloVF is modeled as a sum of two or three exponential components. b) Relationship between V_{mem} χ^2 for JuloVF. Measurements from individual cells are shown as markers; for closely spaced results, markers may overlap. The line of best fit for χ^2 vs. V_{mem} for each fit model is shown. c-d) Evaluation of χ^2 overall as it relates to V_{mem} for IndoVF when its fluorescence lifetime is modeled as a sum of two or three exponential terms. e-f) Evaluation of χ^2 overall as it relates to V_{mem} for ^{i}PrVF when modeled as a sum of two or three exponential terms. g-h) Evaluation of χ^2 overall as it relates to V_{mem} for NN26VF when modeled as a single exponential decay or as a sum of two exponential terms. i-j) Evaluation of χ^2 overall as it relates to V_{mem} for VF2.0.Cl when the fluorescence lifetime of VF2.0.Cl is modeled as a single exponential decay or as a sum of two exponential terms. Each measurement on each cell at a given potential is represented individually (i.e. each patch has 4 or 5 values in the histogram, one for each recorded V_{mem}). Number of cells patched: JuloVF (500 nM) 6, IndoVF (300 nM) 8, ^{i}PrVF (300 nM) 10, NN26VF (300 nM) 8, VF2.0.Cl (100 nM) 5.

Figure S16. Concentration dependence of τ_{fl} for four new VFs in HEK293T cells.

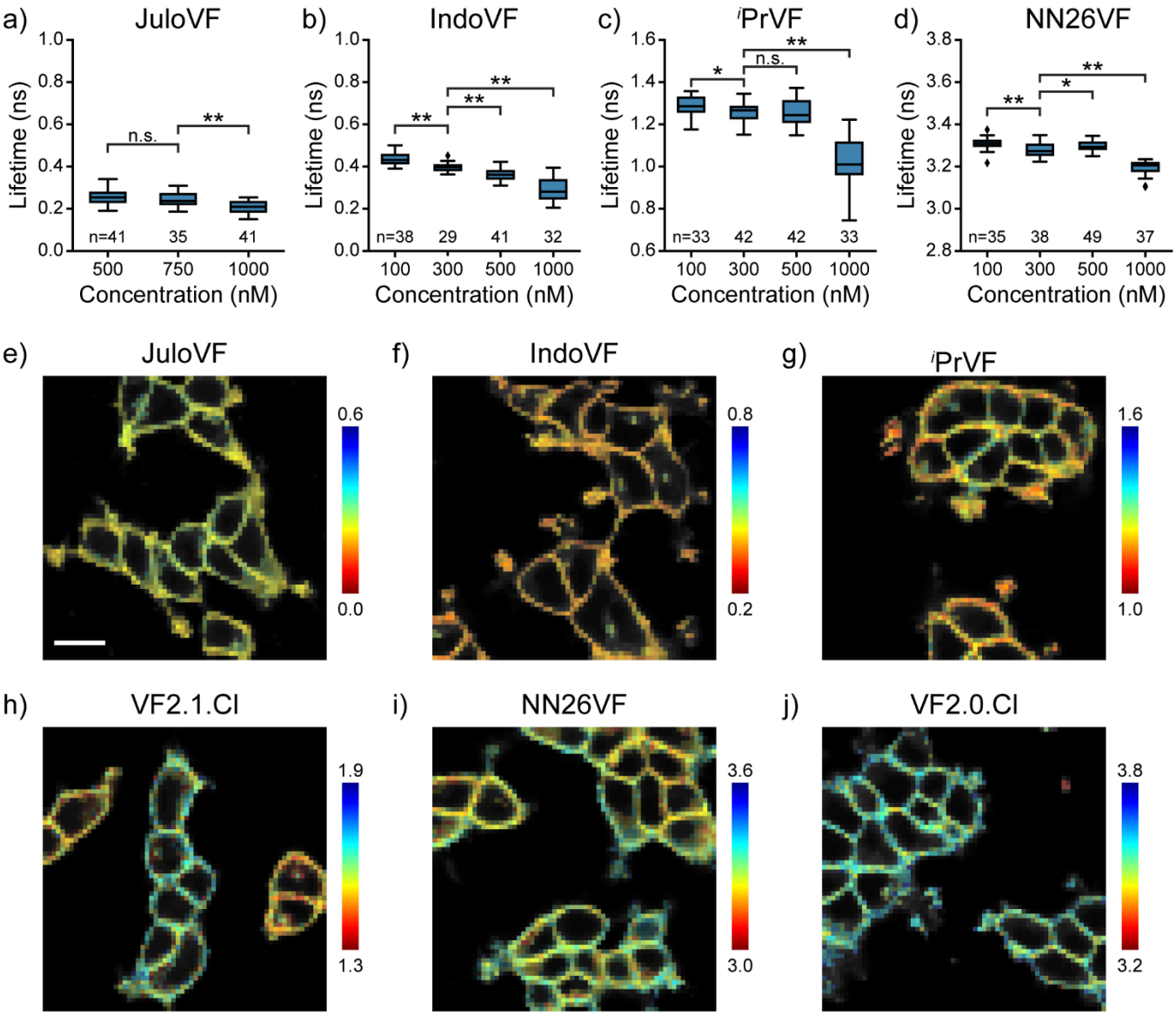

Figure S16. Concentration dependence of τ_{fl} for four new VFs in HEK293T cells.
a-d) Box plots showing the effect of JuloVF, IndoVF, *i*PrVF, or NN26VF concentration on fluorescence lifetime in HEK293T cells at rest in imaging buffer. Diamonds represent datapoints more than 1.5 times the interquartile range past an edge of the box. Data were tested for homoscedasticity (Levene's test on the median, many with $p<0.05$). The statistical significance of differences between concentrations were evaluated with Welch's ANOVA, in all cases resulting in $p<0.05$. Asterisks indicate the significance level of Games-Howell post hoc tests (n.s. $p>0.05$, * $p<0.05$, ** $p<0.01$, *** $p<0.001$). For clarity, only the significance level of post hoc comparisons involving the concentration used in this study is shown (300 nM for all probes except JuloVF, where 500 nM was used). e-j) Representative fluorescence lifetime images overlaid on the fluorescence intensity for all six VFs used in this study. Probe concentrations in lifetime images: JuloVF 500 nM, IndoVF 300 nM, *i*PrVF 300 nM, VF2.1.Cl 100 nM, NN26VF 300 nM, VF2.0.Cl 100 nM. Lifetimes are scaled across the same range for electrophysiological studies (**Fig. 3, Fig S7-12**). Scale bar represents 20 µm.

Figure S17. Comparison of fluorescence lifetime and molecular wire absorbance in different environments.

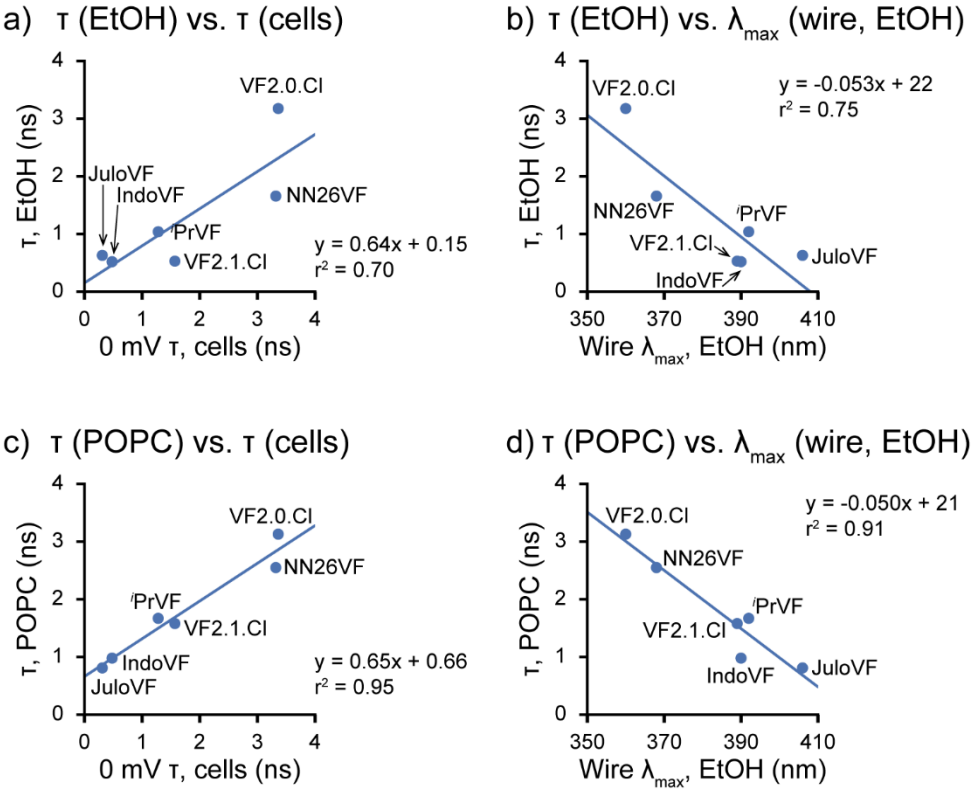

Figure S17. Comparison of fluorescence lifetime and molecular wire absorbance in different environments. Data are aggregated from Table 1. a) Probe lifetime in ethanol is somewhat correlated with 0 mV lifetime in cells, although various probes deviate considerably from the line of best fit. b) Probe lifetime in ethanol is somewhat inversely correlated with the absorbance maximum of the molecular wire in ethanol, again with considerable deviation from the line of best fit. c) Probe lifetime in POPC vesicles is strongly correlated with 0 mV lifetime in cells. d) Probe lifetime in POPC vesicles is strongly inversely correlated with the absorbance maximum of the molecular wire in ethanol. For (a)-(d), all measurements in ethanol or POPC were performed with probes at 500 nM; measurements in cells were performed with 300 nM probe for all probes except for JuloVF, which was used at 500 nM because of brightness limitations. Slope, y-intercept, and goodness-of-fit for all trendlines are indicated on the plots. Error bars are omitted for clarity.

Figure S18. Functional comparison of VoltageFluor indicators in hiPSC-CMs.

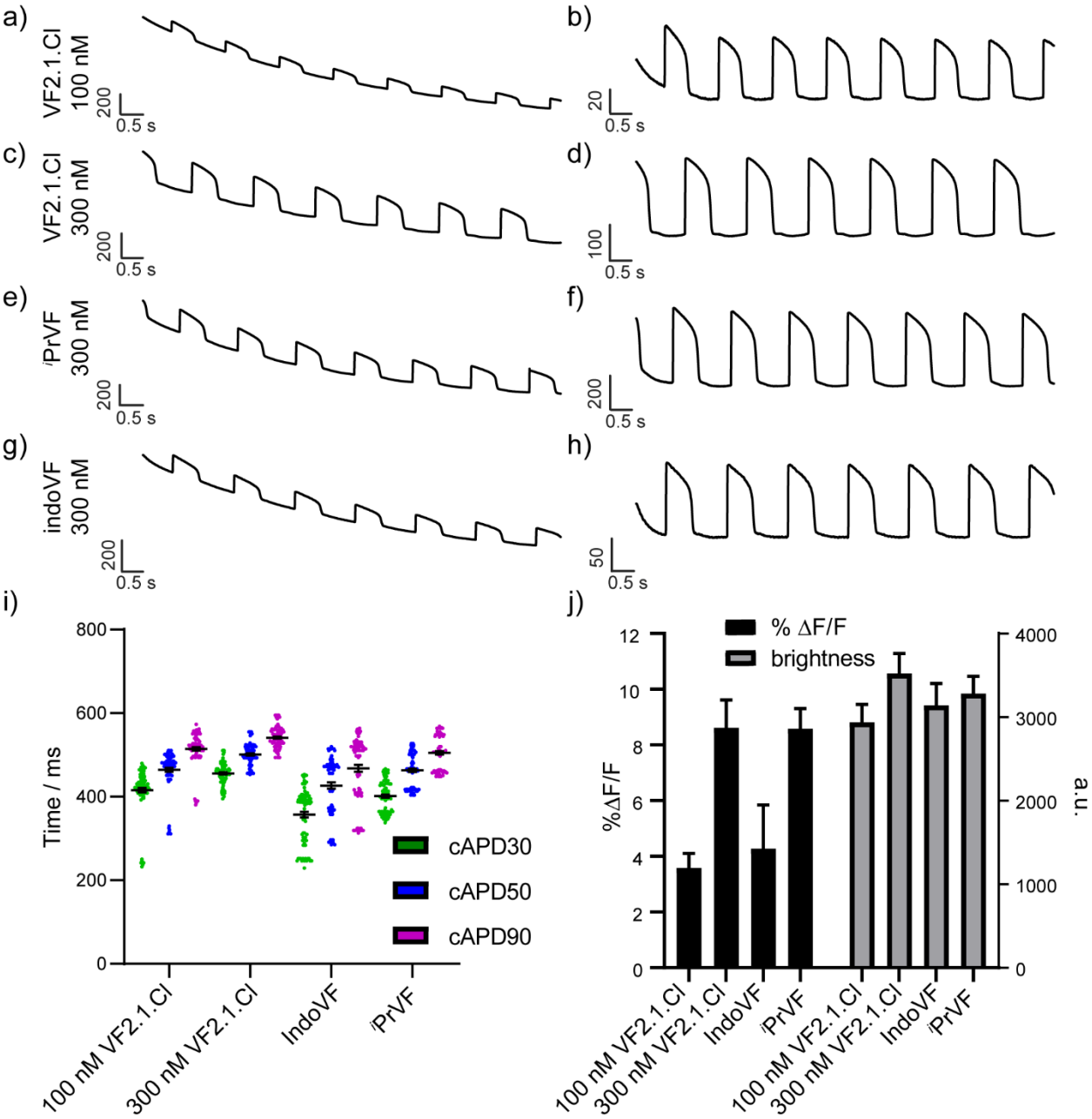

Figure S18. Functional comparison of VoltageFluor indicators in hiPSC-CMs.
Representative uncorrected (a,c,e,g) and bleach-corrected (b,d,f,h) functional recordings of spontaneous activity in hiPSC-CMs. Recordings were made for 10 seconds. Bleach correction was made by subtracting the exponential decay calculated by an asymmetric least-squares fit to the raw trace. Of the VoltageFluors tested, each has a similar photobleach decay (see **Figure S20**). i) Scatter plot of corrected action potential duration (cAPD) values at 30, 50, and 90% of the repolarization recorded with VoltageFluors. cAPD, and action potential morphology, was not affected by the identity of VoltageFluor used in these studies. Bars represent mean ± SEM. Samples were taken from 3 wells per condition, with 5 fields of view per well for a total of 15 recordings per condition. Sample size (number of individual action potentials recorded): 100 nM – VF2.1.Cl 100, 300 nM – VF.2.1.Cl 103, indoVF 89, *i*PrVF 102. j) Bar plot of mean %ΔF/F (left y-axis, black bars), and mean brightness (right y-axis, grey bars). Brightness was calculated as the average pixel intensity of the baseline of the fluorescence trace. IndoVF and *i*PrVF were loaded at a concentration of 300 nM. As with SNR (**Figure 4**), IndoVF performs similarly in %ΔF/F and has a similar brightness to VF2.1.Cl loaded at 100 nM, and *i*PrVF performs similarly to VF2.1.Cl loaded at 300 nM.

Figure S19. Functional comparison of VoltageFluor indicators in rat hippocampal neurons.

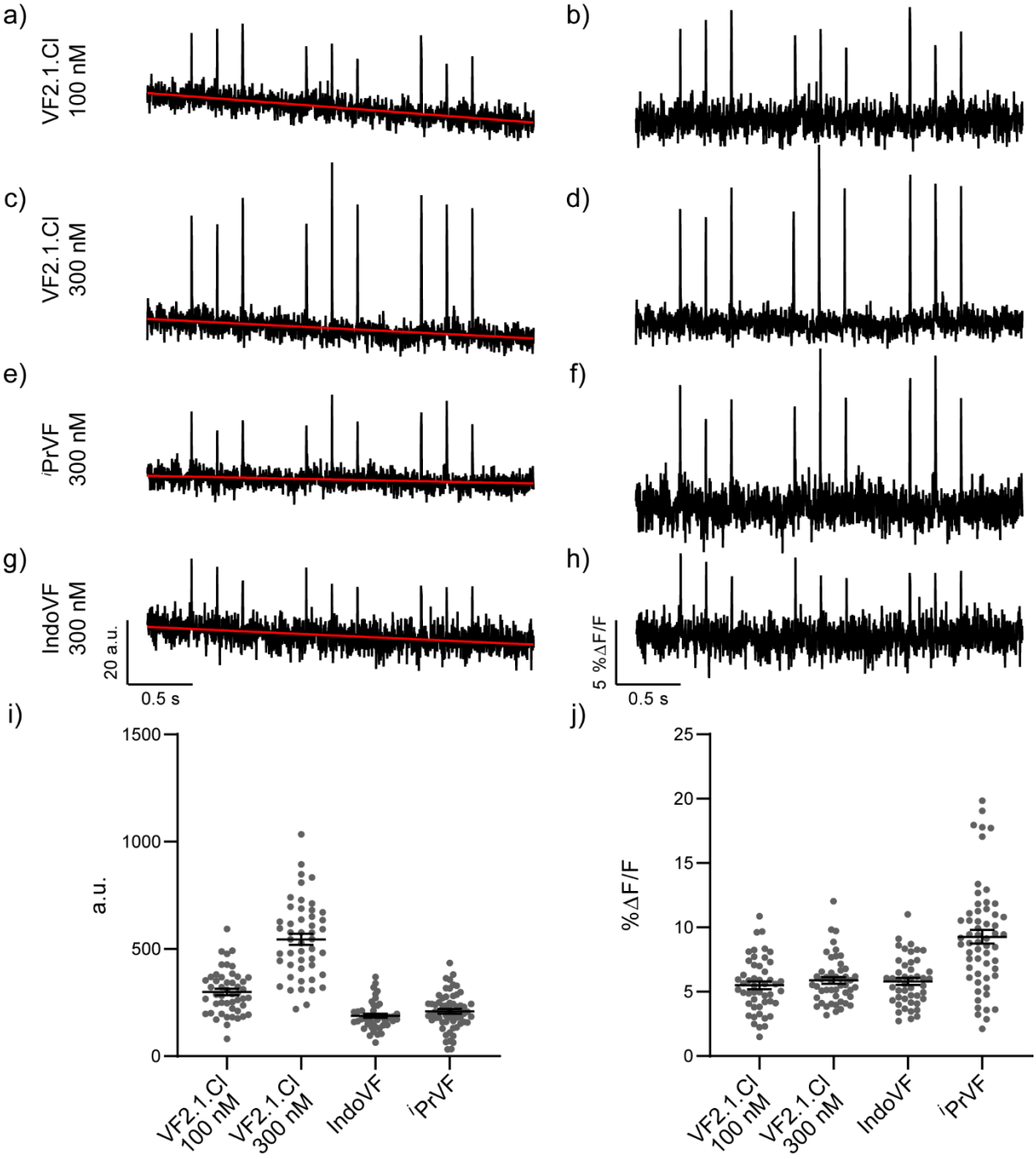

Figure S19. Functional comparison of VoltageFluor indicators in rat hippocampal neurons.
a,c,e,g) Representative background-corrected traces (black) of evoked activity in rat hippocampal neurons and regression lines (red) fit to the respective traces for VF2.1.Cl 100 nM (a), VF2.1.Cl 300 nM (c), *i*PrVF 300 nM (e), and IndoVF 300 nM (g). b,d,f,h) %ΔF/F traces (black) of evoked activity in rat hippocampal neurons for VF2.1.Cl 100 nM (b), VF2.1.Cl 300 nM (d), *i*PrVF 300 nM (f), and IndoVF 300 nM (h). %ΔF/F traces were obtained from the background corrected traces using the methodology described above in **7c. Evoked activity in rat hippocampal neurons**. i) Plot of the raw background corrected fluorescence values of each dye in rat hippocampal neurons. Each grey dot represents a background corrected fluorescence value for the first frame of one measurement of evoked activity; bars represent mean ± SEM. j) Plot of the %ΔF/F values for evoked activity in rat hippocampal neurons. Each grey dot represents the %ΔF/F value of the first action potential in one measurement of evoked activity; bars represent mean ± SEM.

Figure S20. Cardiotoxicity with prolonged illumination of VoltageFluors

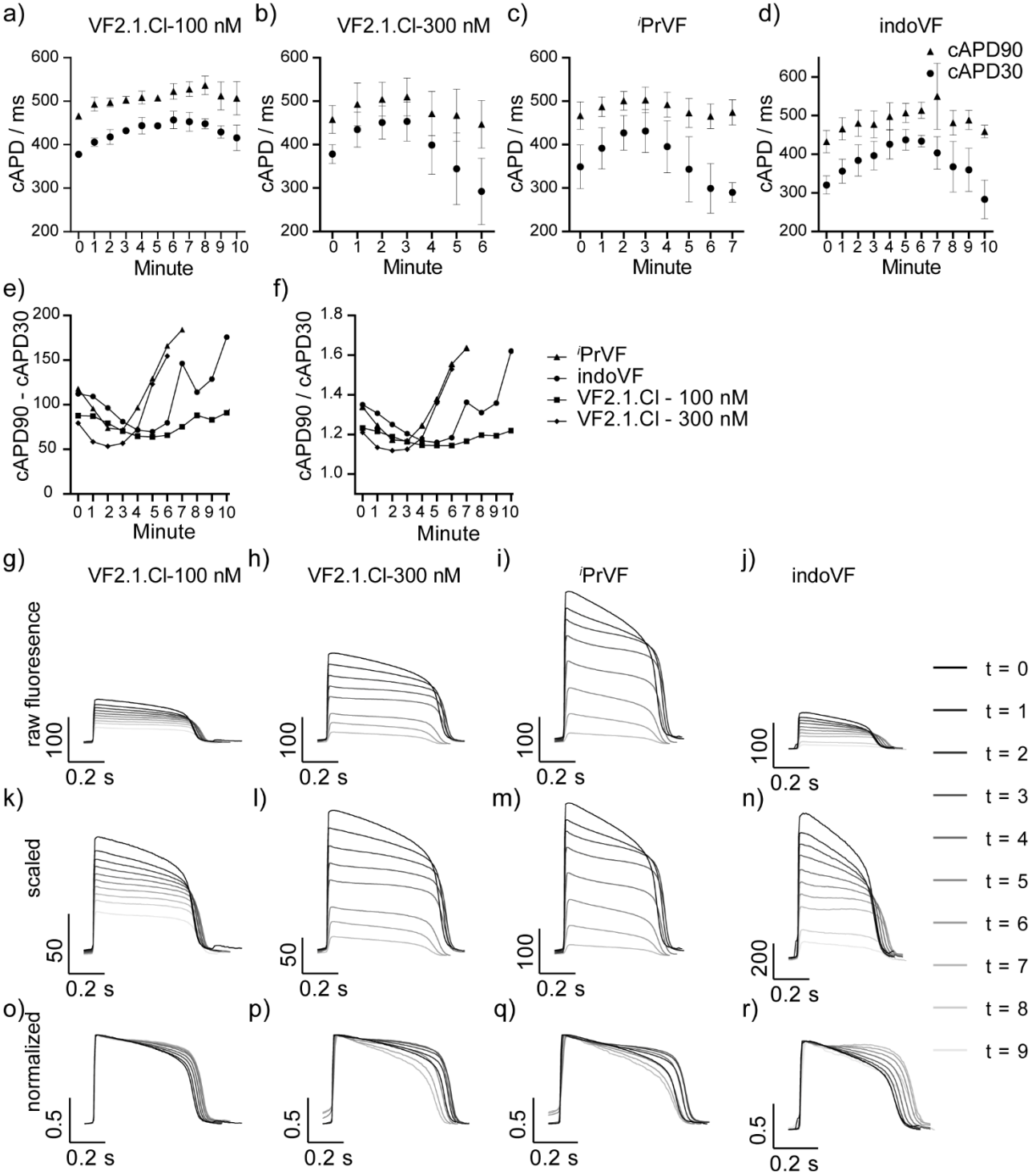

Figure S20. Cardiotoxicity with prolonged illumination of VoltageFluors

The phototoxicity of VoltageFluors was examined in hiPSC-CMs by prolonged, continuous exposure to the excitation LED. Action potential morphology was monitored through 10 second recordings made each minute (a-d) and quantified using cAPD. Deviations in cAPD from starting values (recording made at 0 minutes) can be interpreted as an action potential morphology change, which is indicative of potential phototoxic effects. As previously observed,[12] decreasing the concentration of VF2.1.Cl to 100 nM (a) from 300 nM (b) permits recordings over extended times with minimal change to action potential morphology. *i*PrVF (c, 300 nM) performs similarly to VF2.1.Cl loaded at 300 nM (b), permitting recordings for 3 minutes of constant illumination before AP morphology changes are seen. indoVF (d, 300 nM) resembles VF2.1.Cl loaded at a lower concentration (a, 100 nM), as AP morphology changes are not observed until extended illumination periods. AP morphology changes were also quantified by the difference (e) and ratio (f) of cAPD90 and cAPD30. Deviations from initial values indicate changes to AP morphology. In the case of the VoltageFluors tested, both the difference and ratio of cAPD90 and cAPD30 increases over prolonged exposure to excitation light, indicating a prolongation of phase 2 in the

cardiac AP and an overall increase in duration. (g-j) Representative fluorescence traces from a single trial, each action potential is the mean trace from a single 10 second recording. As time progresses (purple to cream), the amplitude of the cardiac action potential decreases regardless of VoltageFluor used due to photobleaching. (k-n) Scaled fluorescence traces more clearly show the decrease in amplitude for each VoltageFluor. (o-r) Normalized fluorescence traces show the change in action potential morphology with increased illumination.

Figure S21. Comparison of VF bleach rate in HEK293T, iCMs, and rat hippocampal neurons.

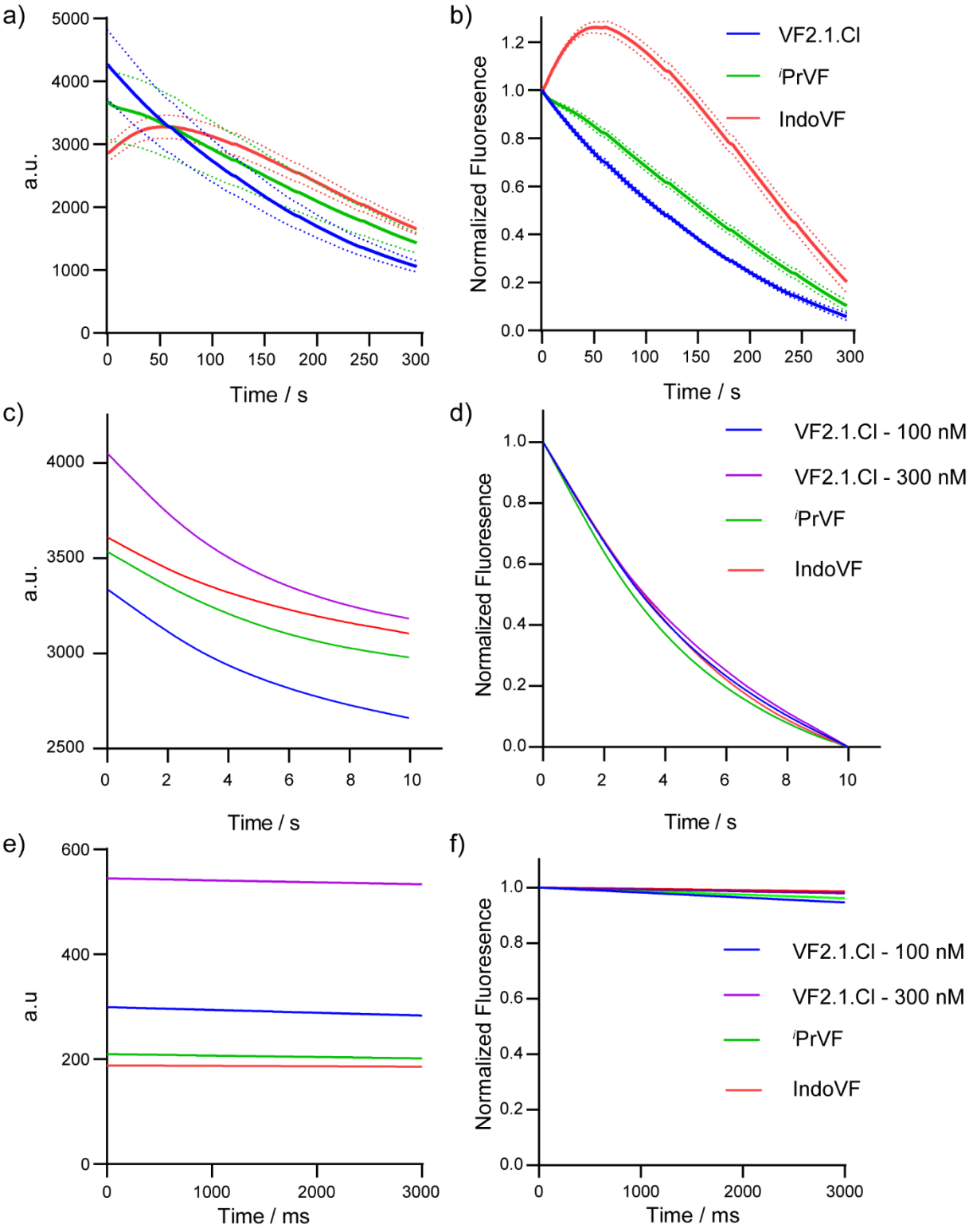

Figure S21. Comparison of VF bleach rate in HEK293T, iCMs, and rat hippocampal neurons.
a) Photobleaching in HEK293T cells, sampled at 1 Hz for five minutes. b) Normalized values in HEK293T cells. c) Average splines used for photobleach correction by asymmetric least-square fit (**Methods**) of the first ten seconds of recording in iPSC-CMs. d) Average bleach splines from (c) normalized to show relative rates of decay. e) Average bleaching traces for evoked activity experiments in neurons. The y-intercept is the average fluorescence value of the first frame of the background corrected traces for each dye. The slope is the average slope of the regression lines which were fit to the background corrected traces for each dye and used to correct for bleaching. f) Each trace from (e) normalized.

Figure S22. Sulfonofluorescein A does not stain HEK cells.

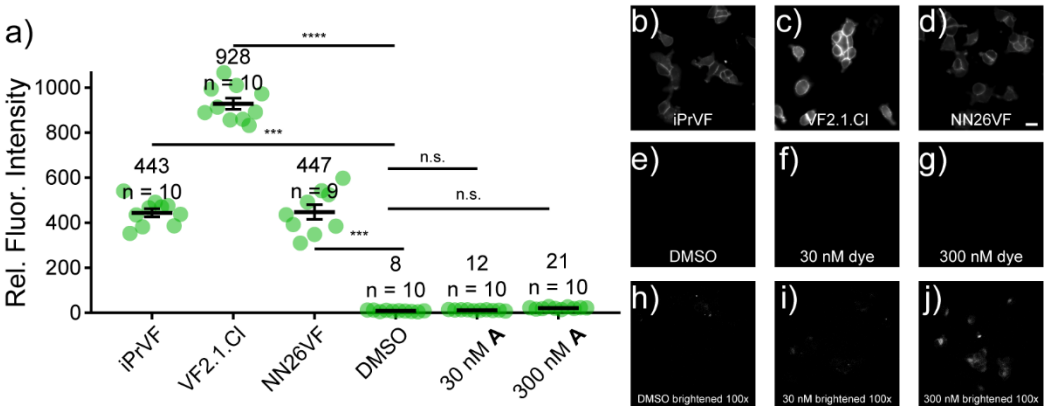

Figure S22. Sulfonofluorescein A does not stain HEK cells. **a)** Plot of relative cellular fluorescence intensity in HEK cells stained VF dyes and starting material with 300 nM ^{i}PrVF, VF2.1.Cl, NN26VF, DMSO control, 30 nM **A**, or 300 nM **A**. Data are mean ± S.E.M. for the indicated number of images. Each image contained between 20 to 50 cells. Labels indicate the mean fluorescence intensity of cells. **b-j)** Example images used for quantification in panel a. HEK cells stained with the following compounds **b)** ^{i}PrVF (300 nM), **c)** VF2.1.Cl (300 nM), **d)** NN26VF (300 nM), **e)** DMSO only as a negative control, **f)** 30 nM of **A** ("dye"), or **g)** 300 nM **A** ("dye"). **h-j)** These panels are the same images from e-g, brightened by applying a 100x multiplication to the image. Scale bar for all images is 20 μm. Statistical tests are Kruskal-Wallis test, followed by Dunn's multiple comparisons test against DMSO. Values are as follows: DMSO vs. ^{i}PrVF, $p = 0.0001$; DMSO vs. VF2.1.Cl, $p < 0.0001$; DMSO vs. NN26VF, $p = 0.001$; DMSO vs 30 nM **A**, $p > 0.9999$; DMSO vs 300 nM **A**, $p = 0.0891$.

13. NMR Spectra

Spectrum S1. ^{1}H spectrum of 2,3,6,7-tetrahydro-1H,5H-pyrido[3,2,1-ij]quinoline-9-carbaldehyde, 1:

^{1}H NMR (400 MHz, Chloroform-*d*) δ 9.58 (s, 1H), 7.28 (s, 2H), 3.28 (t, *J* = 5.9 Hz, 4H), 2.75 (t, *J* = 6.3 Hz, 4H), 1.95 (p, *J* = 6.1 Hz, 4H).

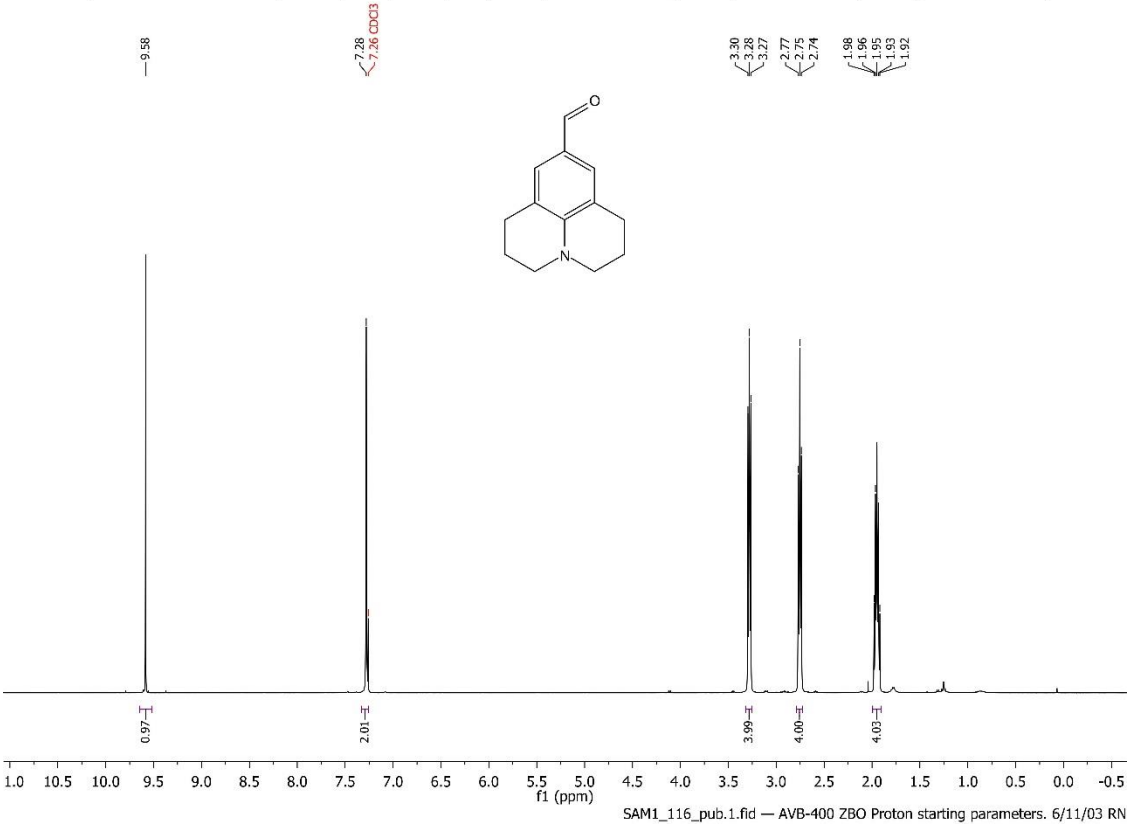

Spectrum S2. ^{13}C spectrum of 2,3,6,7-tetrahydro-1H,5H-pyrido[3,2,1-ij]quinoline-9-carbaldehyde, 1:

^{13}C NMR (101 MHz, $CDCl_3$) δ 190.22, 147.98, 129.60, 124.05, 120.39, 50.11, 27.74, 21.33.

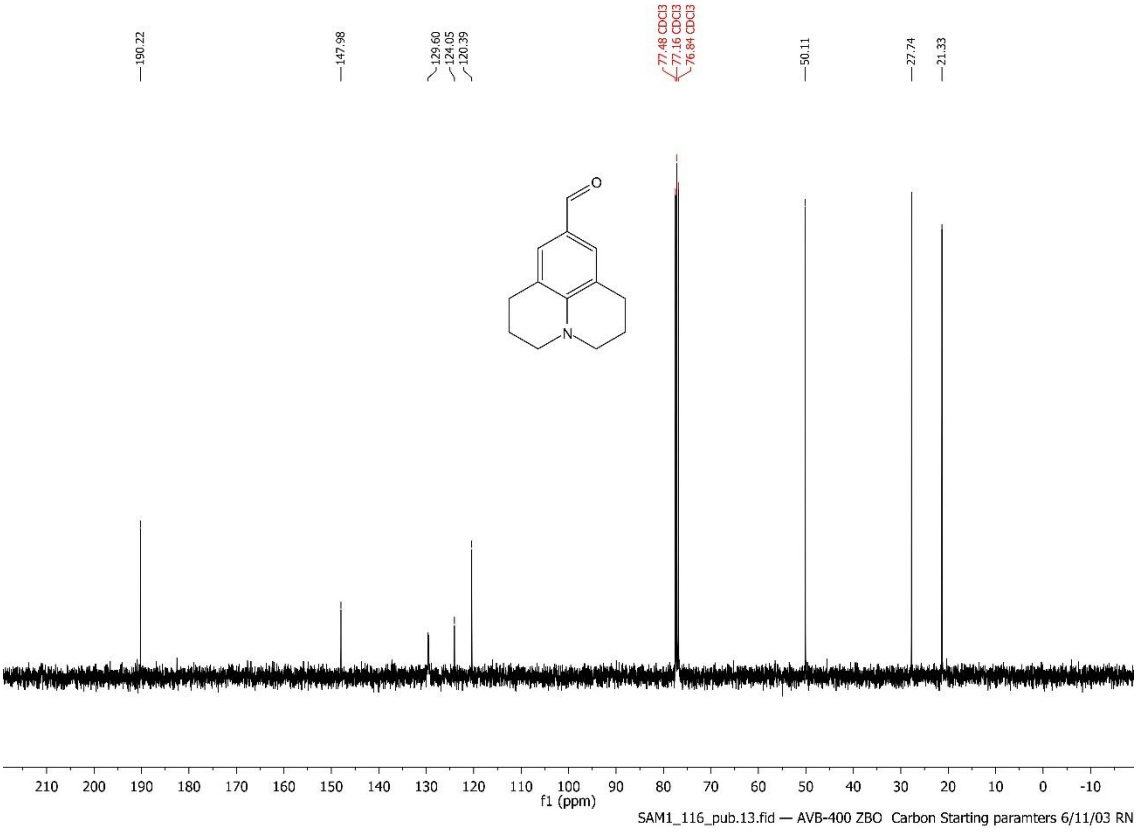

Spectrum S3. ^{1}H spectrum of (E)-4-(2-(2,3,6,7-tetrahydro-1H,5H-pyrido[3,2,1-ij]quinolin-9-yl)vinyl)benzaldehyde, 2:

^{1}H NMR (400 MHz, Chloroform-*d*) δ 9.94 (s, 1H), 7.81 (d, *J* = 8.4 Hz, 2H), 7.56 (d, *J* = 8.2 Hz, 2H), 7.12 (d, *J* = 16.2 Hz, 1H), 7.01 (s, 2H), 6.86 (d, *J* = 16.2 Hz, 1H), 3.20 (t, *J* = 5.6 Hz, 4H), 2.78 (t, *J* = 6.4 Hz, 4H), 1.98 (p, *J* = 6.3 Hz, 4H).

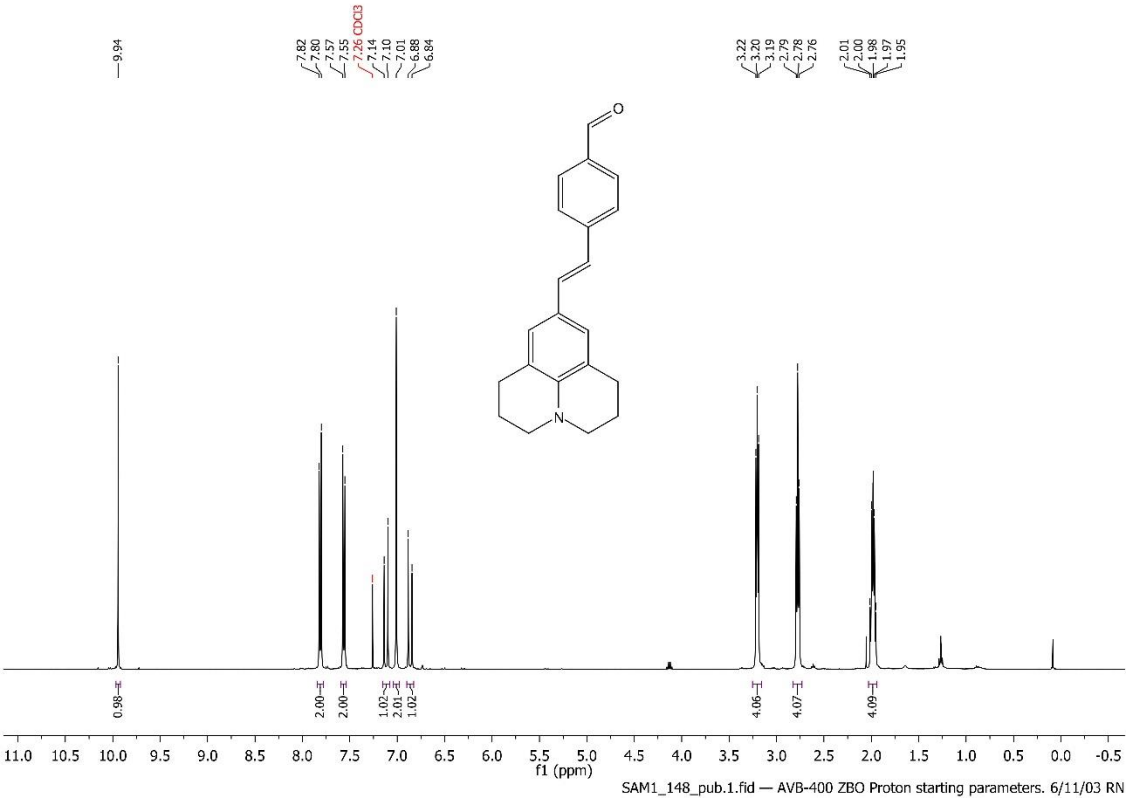

Spectrum S4. ^{13}C spectrum of (E)-4-(2-(2,3,6,7-tetrahydro-1H,5H-pyrido[3,2,1-ij]quinolin-9-yl)vinyl)benzaldehyde, 2:

^{13}C NMR (101 MHz, $CDCl_3$) δ 191.73, 144.96, 143.56, 134.30, 133.00, 130.38, 126.16, 126.13, 123.80, 121.76, 121.39, 50.05, 27.85, 21.95.

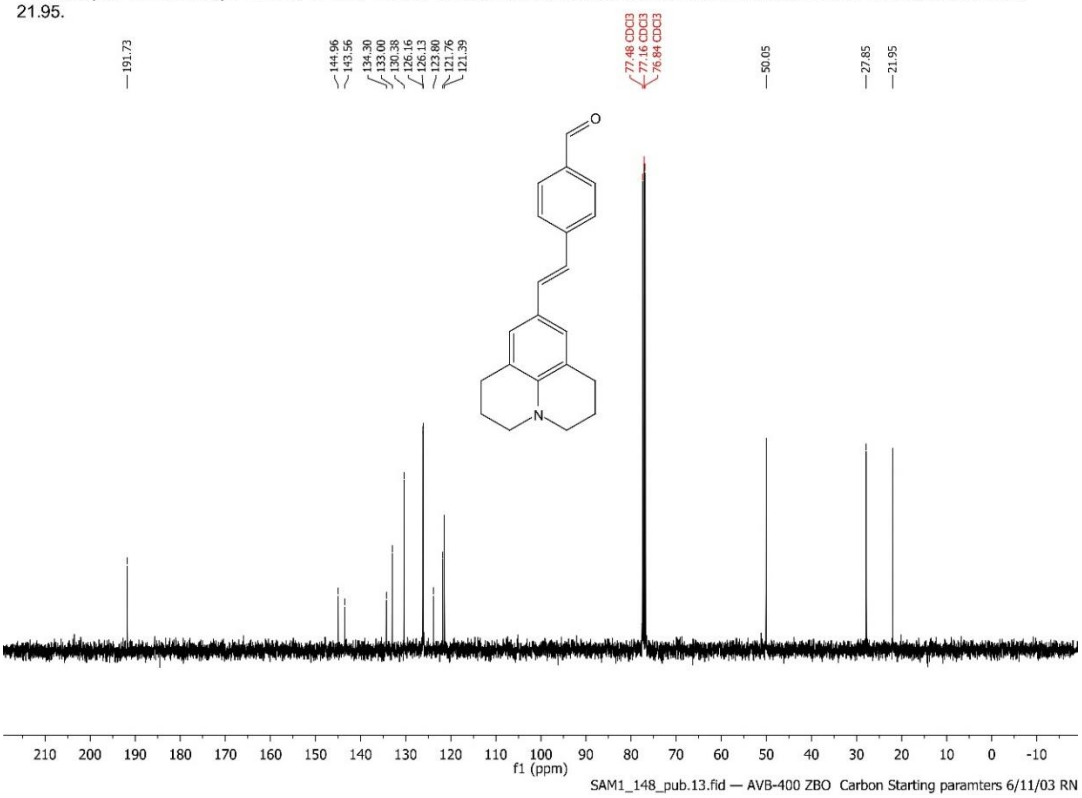

Spectrum S5. ^{1}H spectrum of 1-methyl-5-vinylindoline, 3:

^{1}H NMR (400 MHz, Chloroform-*d*) δ 7.22 (q, *J* = 1.3 Hz, 1H), 7.14 – 7.10 (m, 1H), 6.63 (dd, *J* = 17.5, 10.9 Hz, 1H), 6.42 (d, *J* = 8.0 Hz, 1H), 5.52 (dd, *J* = 17.5, 1.0 Hz, 1H), 5.00 (dd, *J* = 10.9, 1.1 Hz, 1H), 3.33 (t, *J* = 8.2 Hz, 2H), 2.95 (t, *J* = 8.1 Hz, 2H), 2.77 (s, 3H).

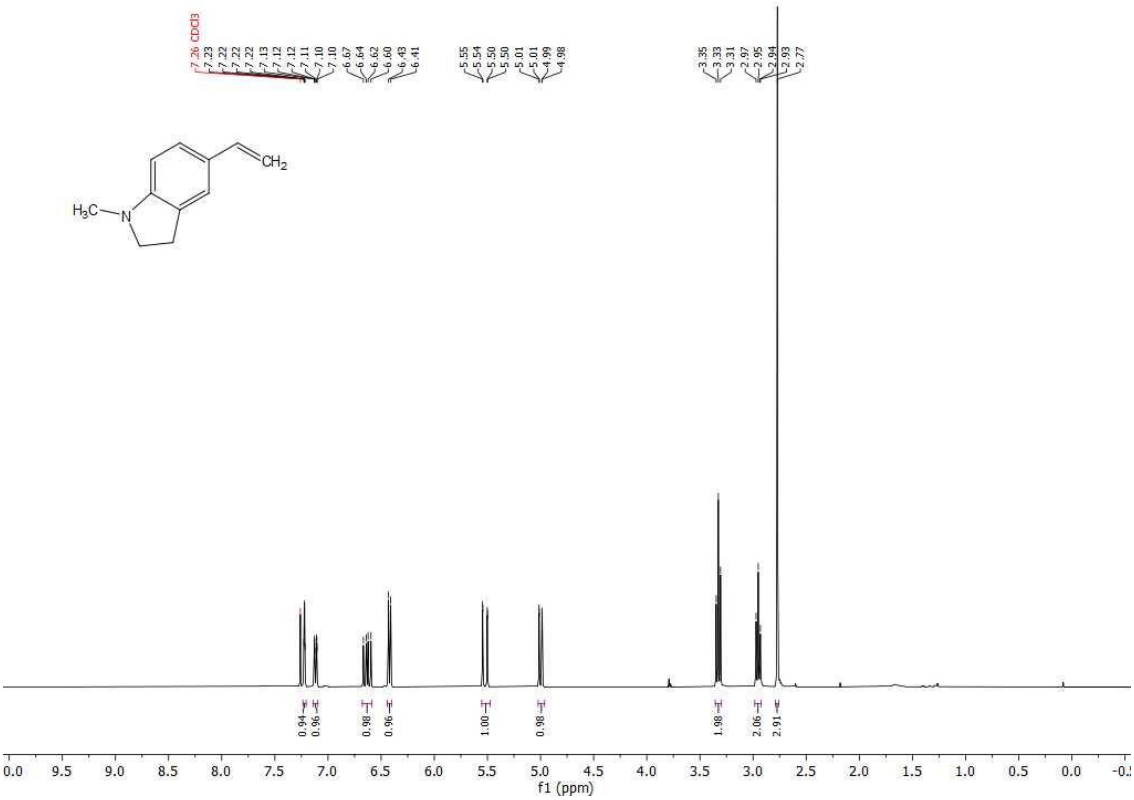

Spectrum S6. ^{13}C spectrum of 1-methyl-5-vinylindoline, 3:

^{13}C NMR (101 MHz, $CDCl_3$) δ 153.33, 137.05, 130.73, 127.82, 126.57, 121.66, 109.10, 106.64, 56.12, 36.07, 28.54.

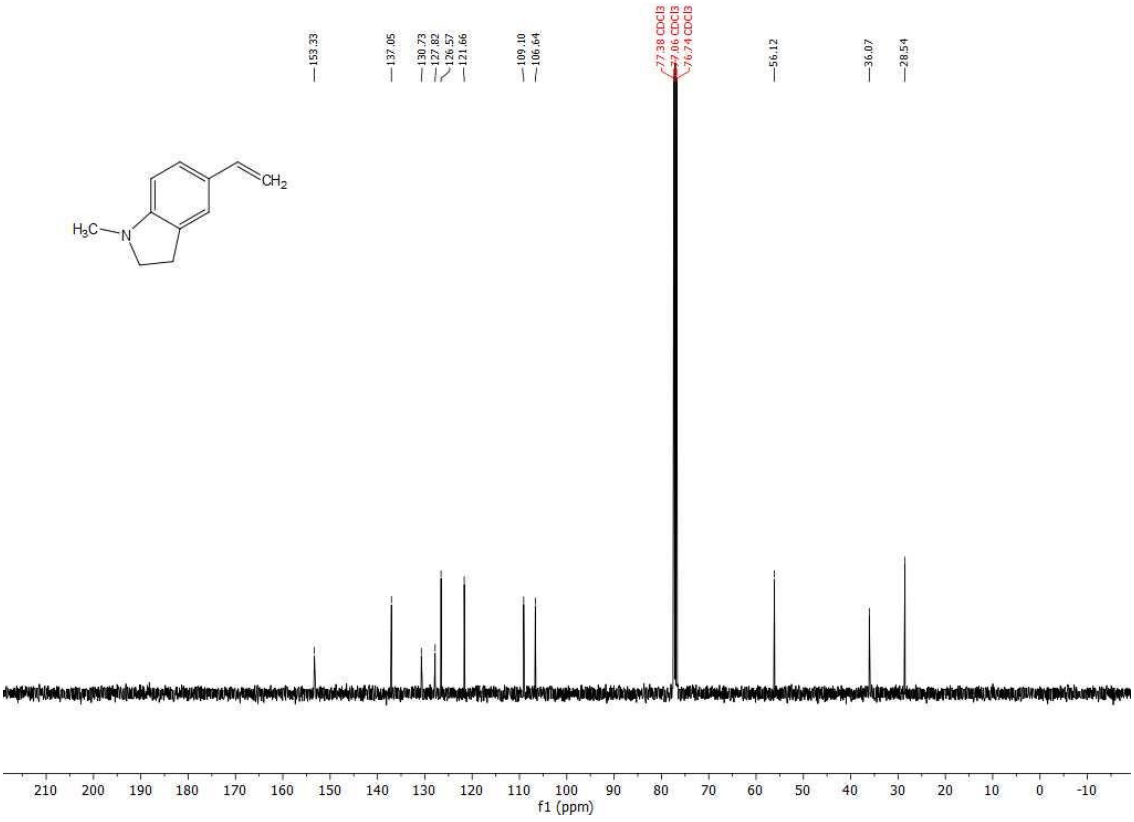

Spectrum S7. ^{1}H spectrum of (E)-4-(2-(1-methylindolin-5-yl)vinyl)benzaldehyde, 4:

^{1}H NMR (600 MHz, Chloroform-*d*) δ 9.95 (s, 1H), 7.82 (dd, 2H), 7.58 (d, *J* = 8.2 Hz, 2H), 7.34 (d, *J* = 1.8 Hz, 1H), 7.24 (dd, *J* = 8.0, 1.8 Hz, 1H), 7.19 (d, *J* = 16.2 Hz, 1H), 6.91 (d, *J* = 16.1 Hz, 1H), 6.43 (d, *J* = 8.1 Hz, 1H), 3.39 (t, *J* = 8.2 Hz, 2H), 2.99 (t, *J* = 8.2 Hz, 2H), 2.81 (s, 3H).

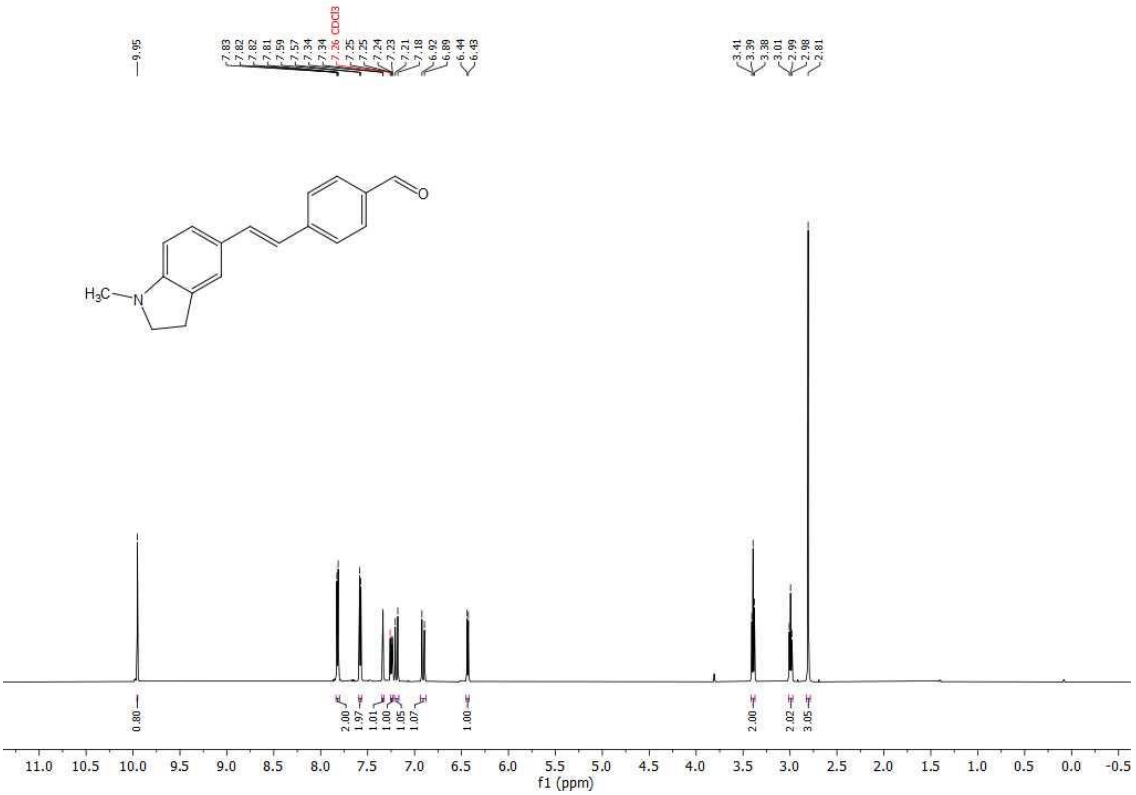

Spectrum S8. ^{1}H spectrum of (E)-4-(2-(1-methylindolin-5-yl)vinyl)benzaldehyde, 4:

^{13}C NMR (151 MHz, $CDCl_3$) δ 191.59, 153.96, 144.64, 134.46, 132.99, 130.97, 130.27, 128.13, 126.33, 126.21, 122.39, 122.26, 106.44, 55.74, 35.50, 28.35.

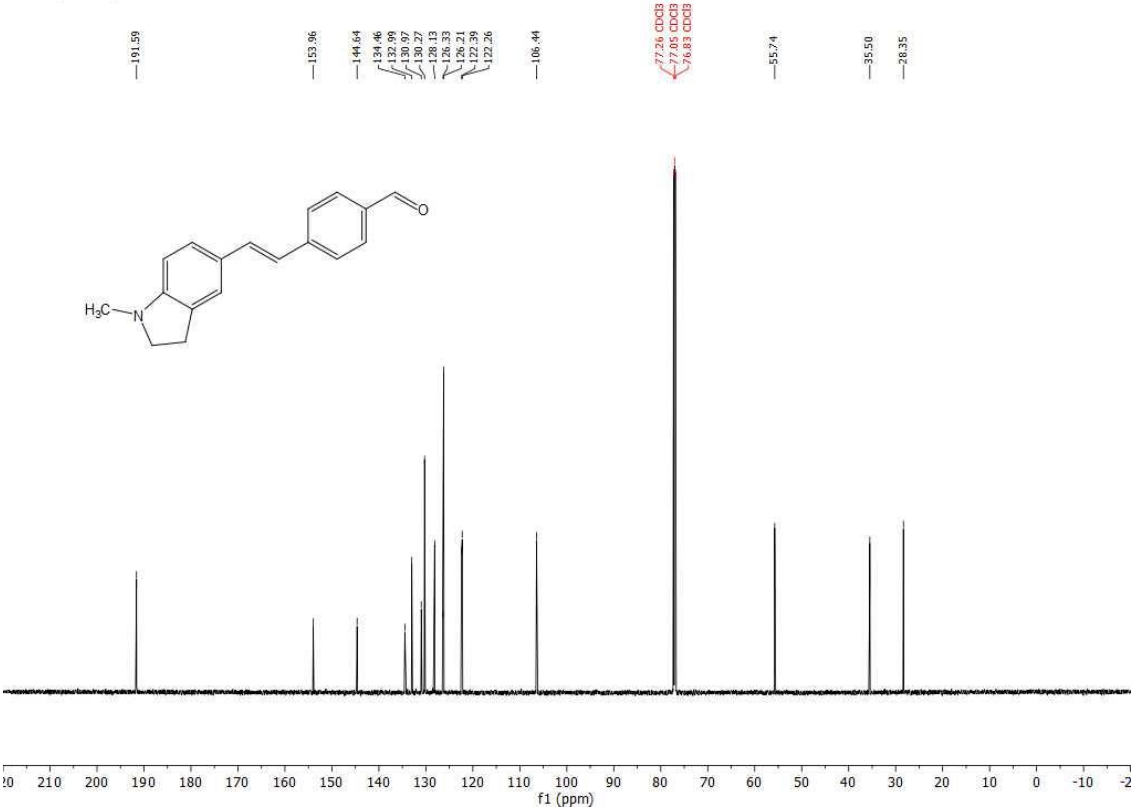

Spectrum S9. ^{1}H spectrum of (E)-1-methyl-5-(4-vinylstyryl)indoline, 5:

^{1}H NMR (600 MHz, Chloroform-*d*) δ 7.44 (d, *J* = 8.3 Hz, 2H), 7.39 (d, *J* = 8.3 Hz, 2H), 7.33 (s, 1H), 7.23 (dd, *J* = 8.0, 1.8 Hz, 1H), 7.06 (d, *J* = 16.2 Hz, 1H), 6.90 (d, *J* = 16.2 Hz, 1H), 6.72 (dd, *J* = 17.6, 10.9 Hz, 1H), 6.45 (d, *J* = 8.0 Hz, 1H), 5.78 – 5.72 (m, 1H), 5.25 – 5.21 (m, 1H), 3.37 (t, *J* = 8.1 Hz, 2H), 2.99 (t, *J* = 8.2 Hz, 2H), 2.80 (s, 3H).

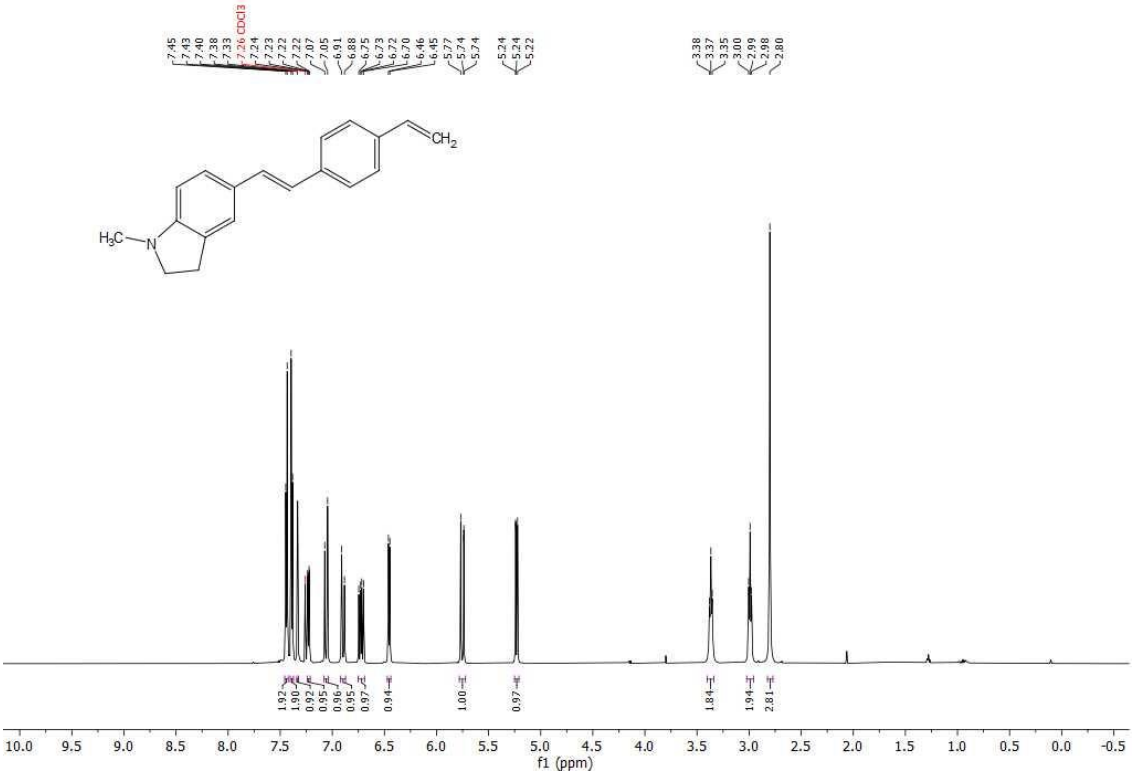

Spectrum S10. ^{13}C spectrum of (E)-1-methyl-5-(4-vinylstyryl)indoline, 5:

^{13}C NMR (151 MHz, $CDCl_3$) δ 153.29, 137.89, 136.64, 135.96, 130.91, 129.29, 127.36, 127.21, 126.51, 126.13, 123.74, 121.96, 113.09, 106.73, 55.98, 35.88, 28.51.

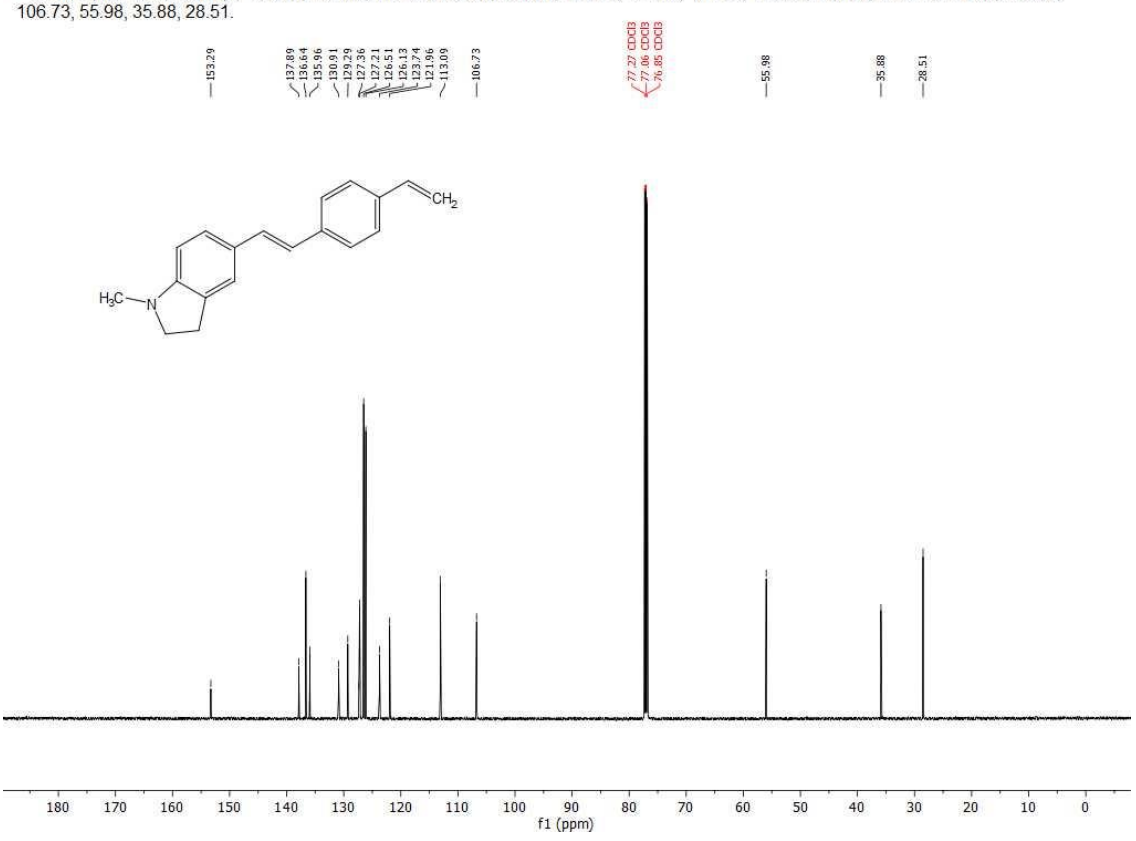

Spectrum S11. ^{1}H spectrum of N-isopropyl-N-methylaniline, 6:

^{1}H NMR (400 MHz, Chloroform-*d*) δ 7.23 (dd, *J* = 8.9, 7.2 Hz, 2H), 6.83 – 6.76 (m, 2H), 6.69 (tt, *J* = 7.1, 1.1 Hz, 1H), 4.10 (hept, *J* = 6.6 Hz, 1H), 2.73 (s, 3H), 1.16 (d, *J* = 6.6 Hz, 6H).

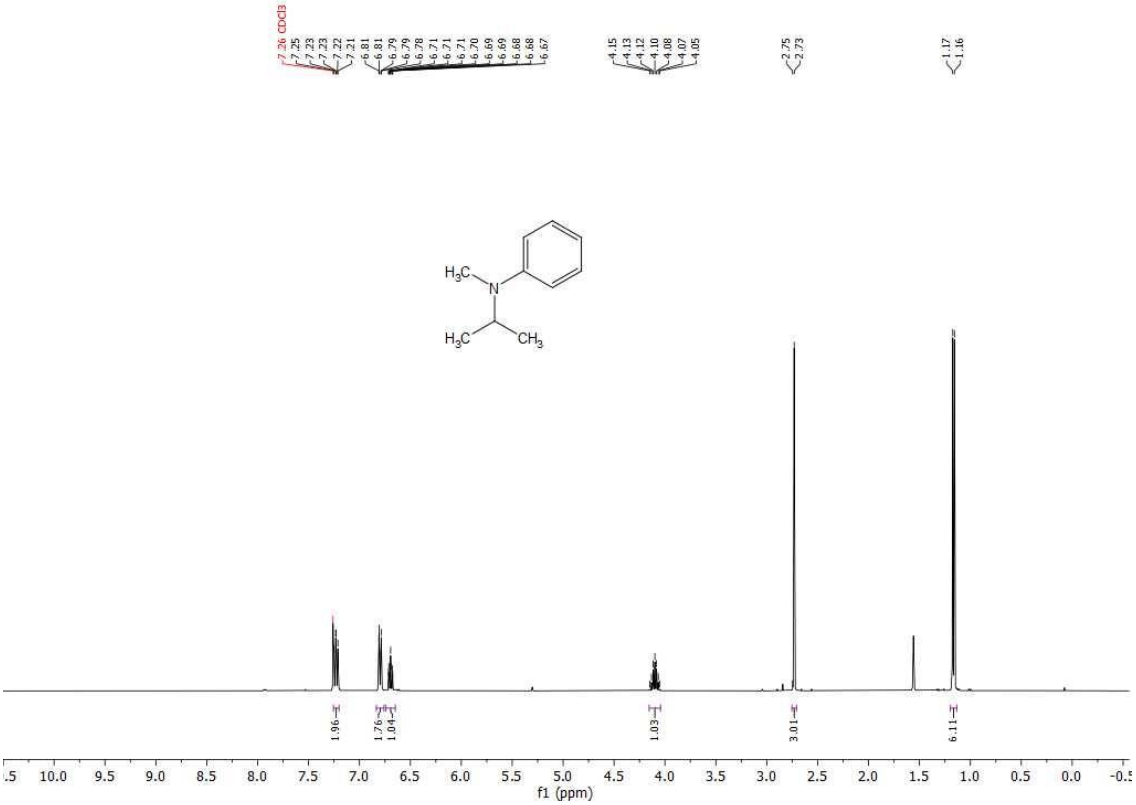

Spectrum S12. ^{13}C spectrum of N-isopropyl-N-methylaniline, 6:

^{13}C NMR (101 MHz, $CDCl_3$) δ 150.28, 129.15, 116.45, 113.39, 48.96, 29.81, 19.35.

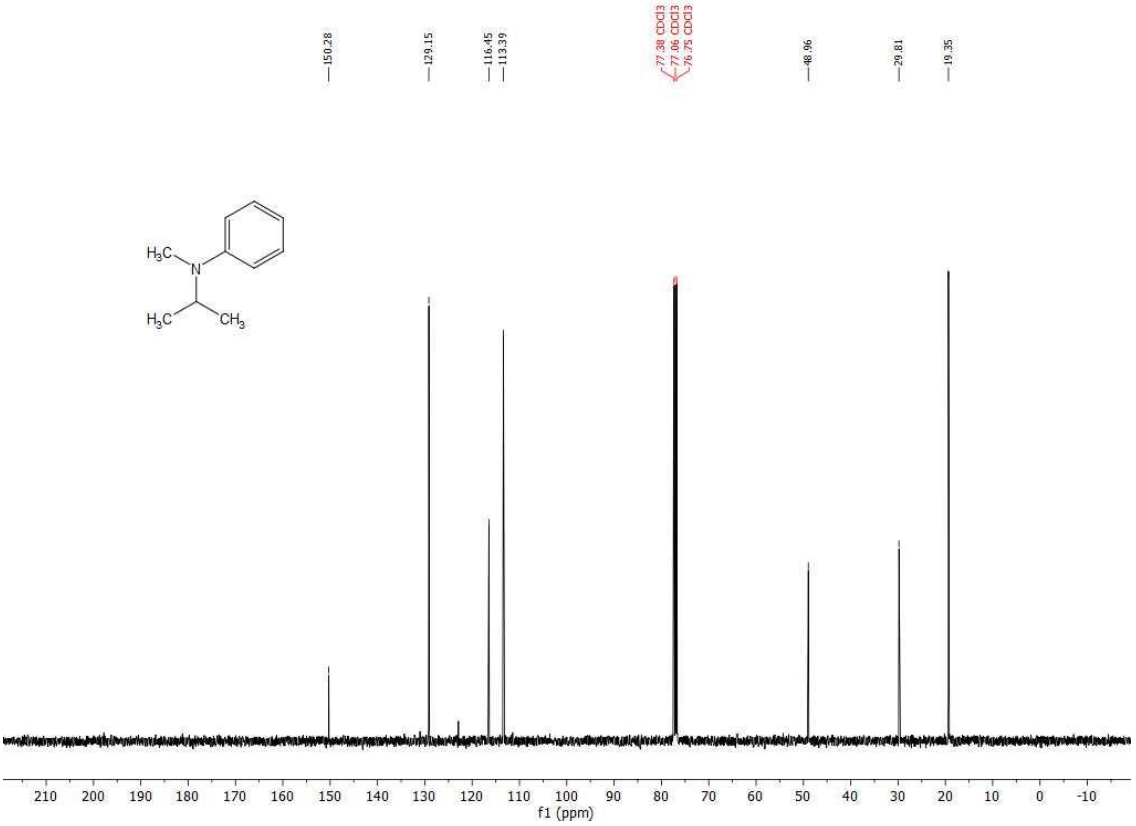

Spectrum S13. ^{1}H spectrum of 4-(isopropyl(methyl)amino)benzaldehyde, 7:

^{1}H NMR (400 MHz, Chloroform-*d*) δ 9.72 (s, 1H), 7.72 (dd, *J* = 8.9 Hz, 2H), 6.76 (dd, 2H), 4.23 (hept, *J* = 6.6 Hz, 1H), 2.85 (s, 3H), 1.22 (d, *J* = 6.6 Hz, 6H).

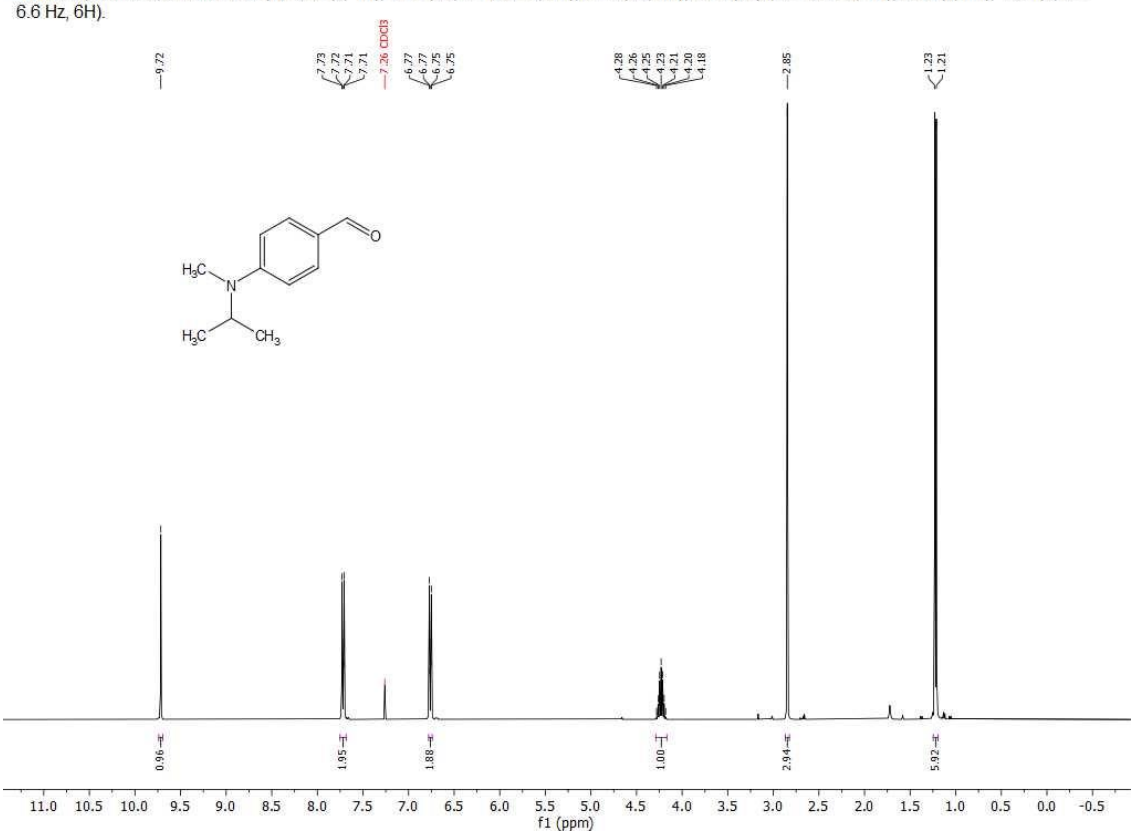

Spectrum S14. ^{13}C spectrum of 4-(isopropyl(methyl)amino)benzaldehyde, 7:

^{13}C NMR (101 MHz, $CDCl_3$) δ 190.10, 154.15, 132.14, 125.08, 111.27, 48.42, 29.94, 19.66.

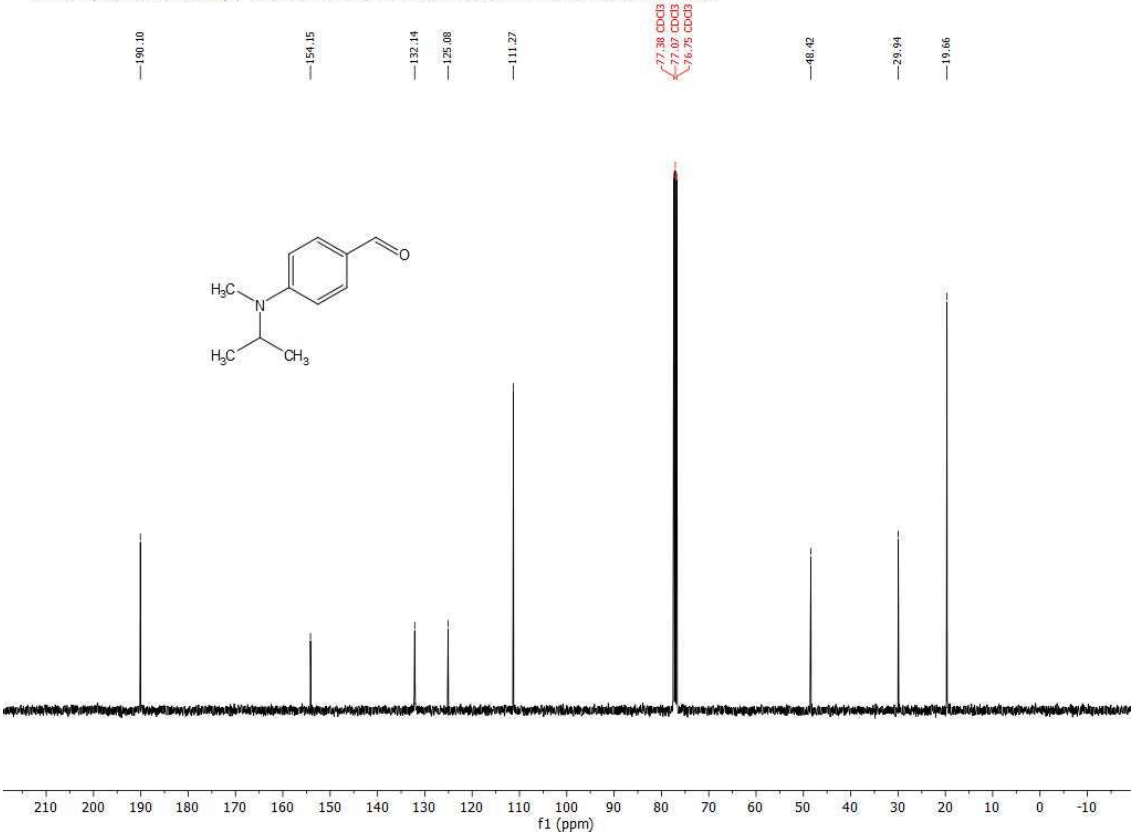

Spectrum S15. ^{1}H spectrum of N-isopropyl-N-methyl-4-vinylaniline, 8:

^{1}H NMR (400 MHz, Chloroform-*d*) δ 7.33 – 7.27 (m, 2H), 6.77 – 6.71 (m, 2H), 6.63 (dd, *J* = 17.6, 10.9 Hz, 1H), 5.53 (dd, *J* = 17.6, 1.1 Hz, 1H), 5.01 (dd, *J* = 10.9, 1.1 Hz, 1H), 4.11 (hept, *J* = 6.6 Hz, 1H), 2.74 (s, 3H), 1.17 (d, *J* = 6.6 Hz, 6H).

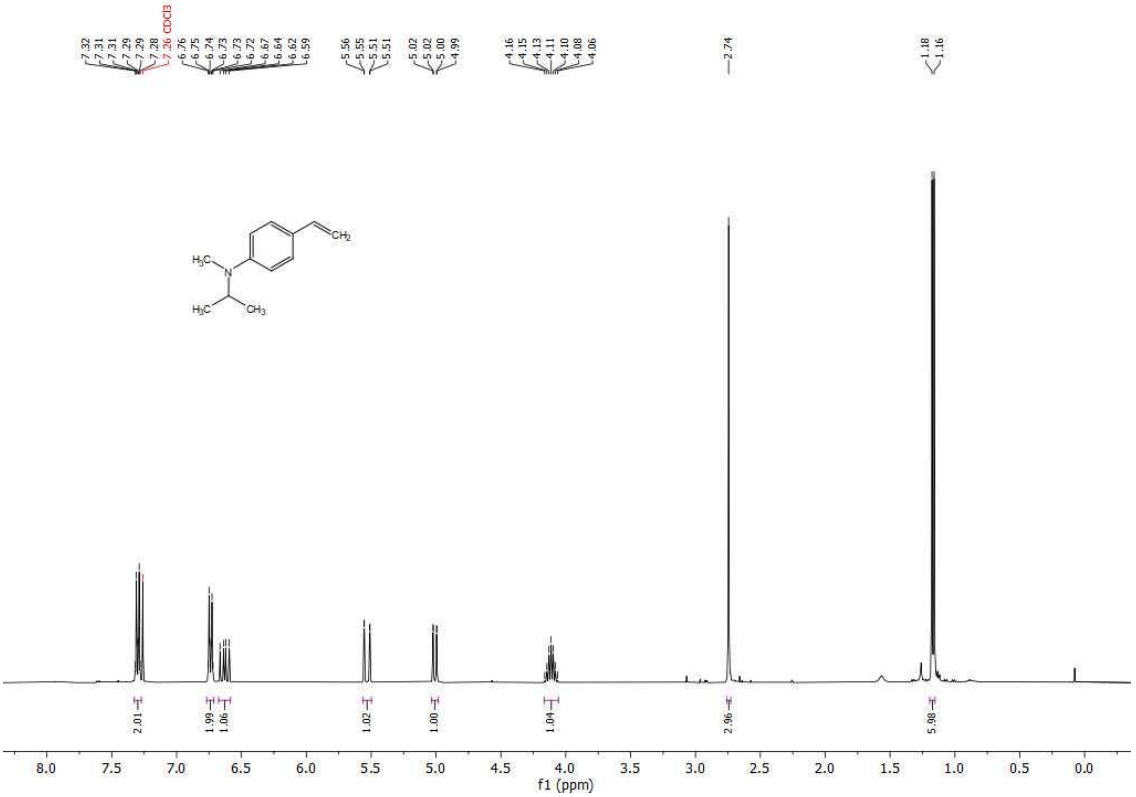

Spectrum S16. ^{13}C spectrum of N-isopropyl-N-methyl-4-vinylaniline, 8:

^{13}C NMR (101 MHz, $CDCl_3$) δ 149.88, 136.62, 127.23, 126.03, 112.91, 109.17, 48.81, 29.81, 19.37.

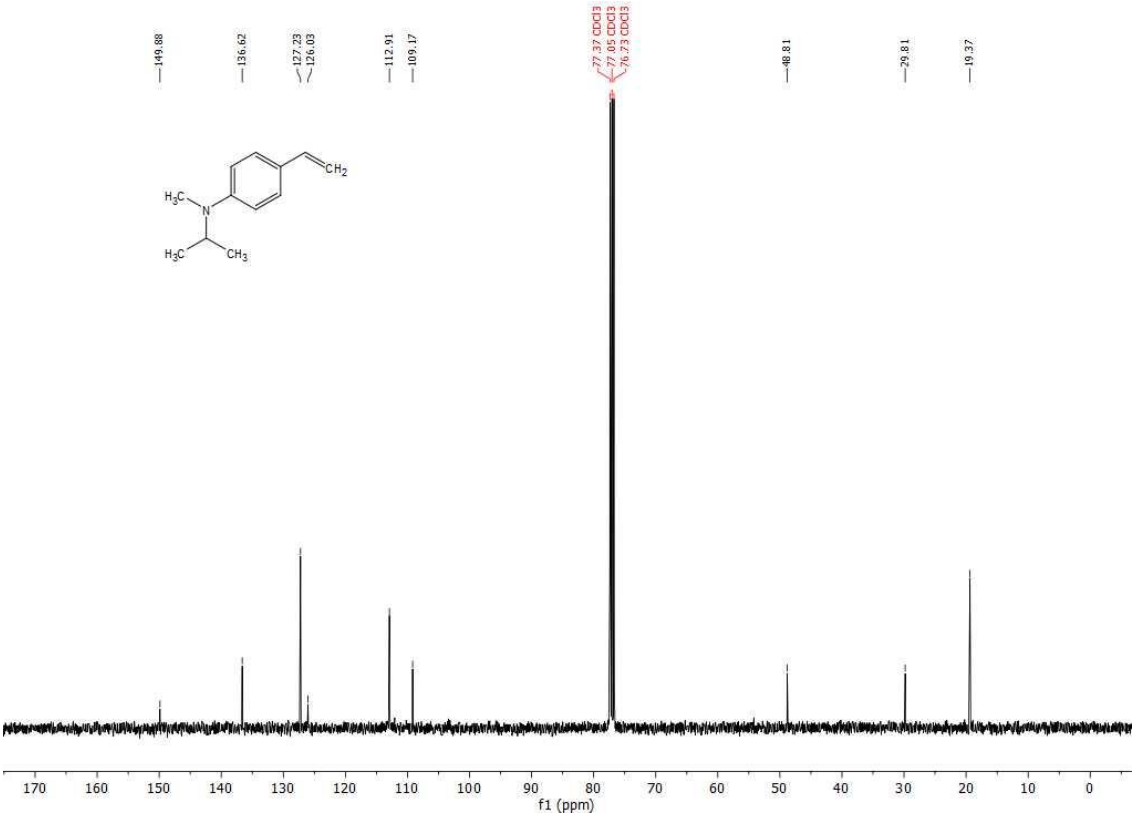

Spectrum S17. ^{1}H spectrum of (E)-4-(4-(isopropyl(methyl)amino)styryl)benzaldehyde, 9:

^{1}H NMR (600 MHz, Chloroform-*d*) δ 9.96 (s, 1H), 7.83 (d, *J* = 8.3 Hz, 2H), 7.59 (d, *J* = 8.2 Hz, 2H), 7.46 – 7.42 (m, 2H), 7.20 (d, *J* = 16.2 Hz, 1H), 6.93 (d, *J* = 16.2 Hz, 1H), 6.77 (d, *J* = 8.9 Hz, 2H), 4.16 (hept, *J* = 6.6 Hz, 1H), 2.79 (s, 3H), 1.20 (d, *J* = 6.6 Hz, 6H).

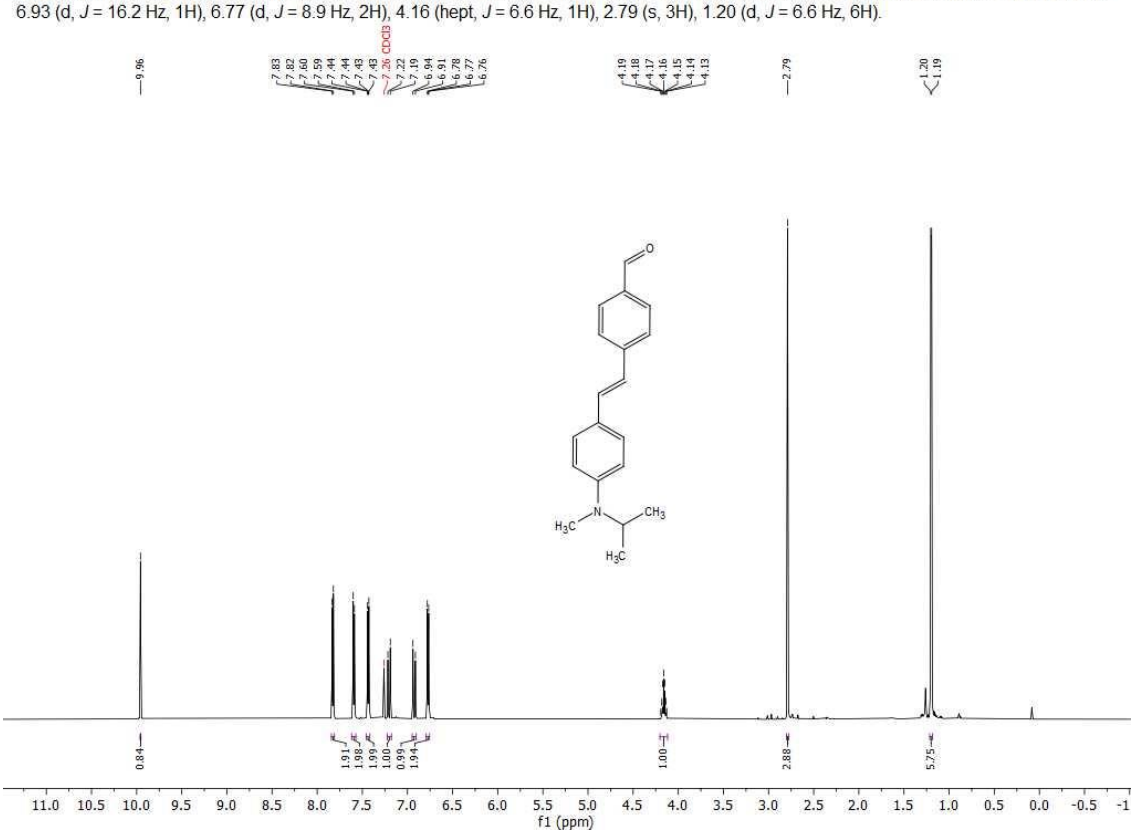

Spectrum S18. ^{13}C spectrum of (E)-4-(4-(isopropyl(methyl)amino)styryl)benzaldehyde, 9:

^{13}C NMR (151 MHz, $CDCl_3$) δ 191.56, 150.25, 144.59, 134.39, 132.49, 130.22, 128.25, 126.17, 124.47, 122.42, 112.65, 77.21, 77.00, 76.79, 48.54, 29.74, 19.45.

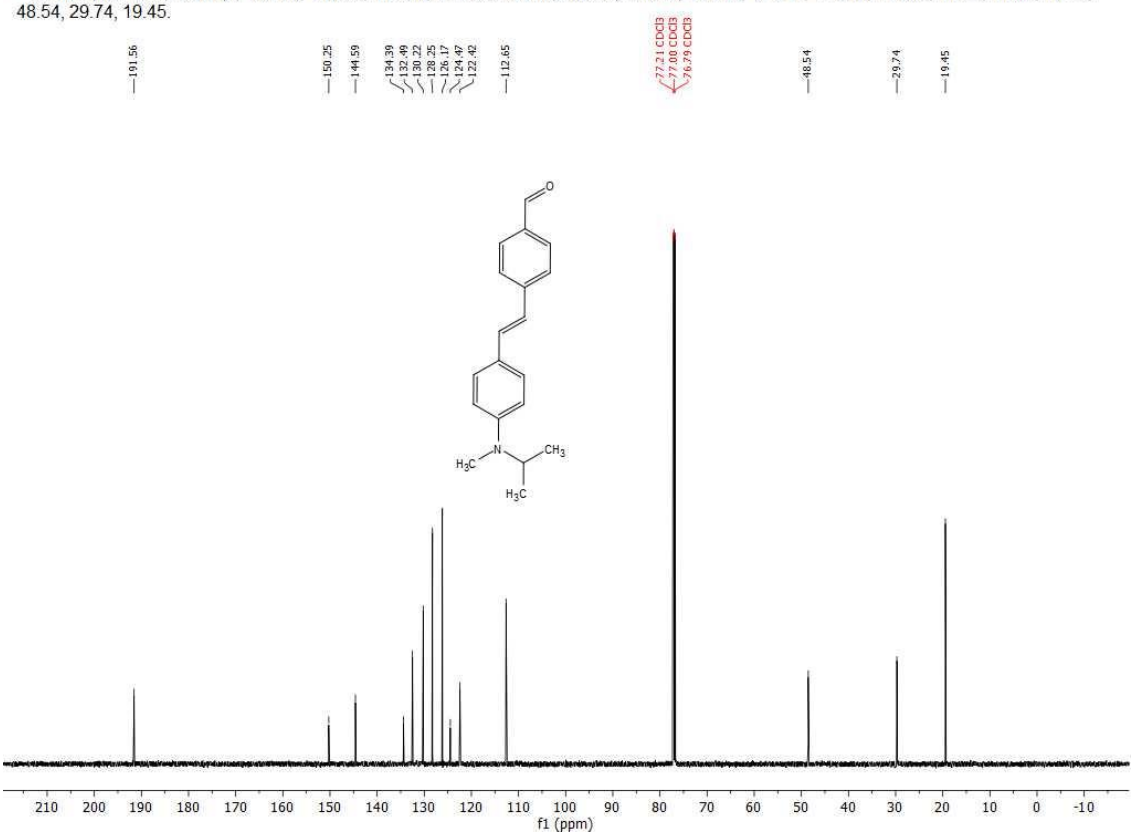

Spectrum S19. ^{1}H spectrum of (E)-N-isopropyl-N-methyl-4-(4-vinylstyryl)aniline, 10:

^{1}H NMR (600 MHz, Chloroform-*d*) δ 7.45 – 7.42 (m, 2H), 7.41 – 7.35 (m, 4H), 7.04 (d, *J* = 16.2 Hz, 1H), 6.89 (d, *J* = 16.2 Hz, 1H), 6.79 – 6.75 (m, 2H), 6.71 (dd, *J* = 17.6, 10.9 Hz, 1H), 5.74 (dd, *J* = 17.6, 0.9 Hz, 1H), 5.21 (dd, *J* = 10.8, 0.9 Hz, 1H), 4.14 (p, *J* = 6.6 Hz, 1H), 2.77 (s, 3H), 1.19 (d, *J* = 6.6 Hz, 6H).

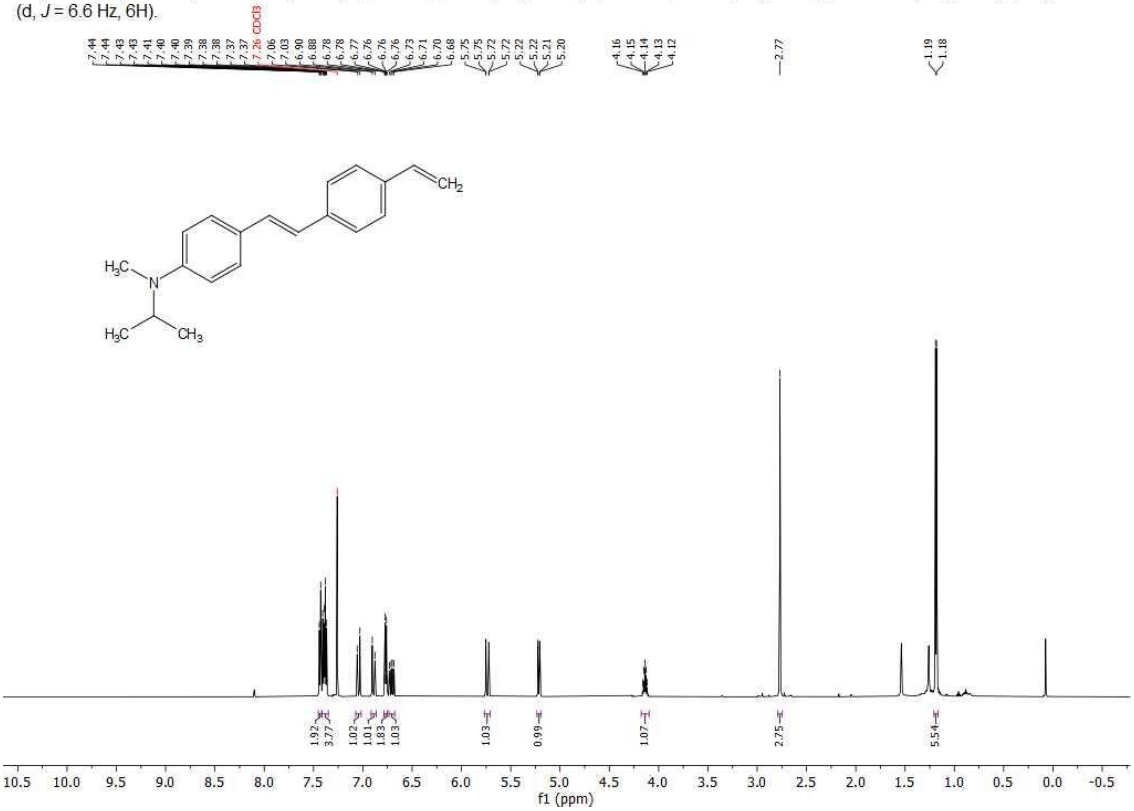

Spectrum S20. ^{13}C spectrum of (E)-N-isopropyl-N-methyl-4-(4-vinylstyryl)aniline, 10:

^{13}C NMR (151 MHz, $CDCl_3$) δ 149.78, 137.89, 136.62, 135.92, 128.82, 127.67, 126.48, 126.10, 125.53, 123.77, 113.05, 112.96, 48.73, 29.78, 19.41.

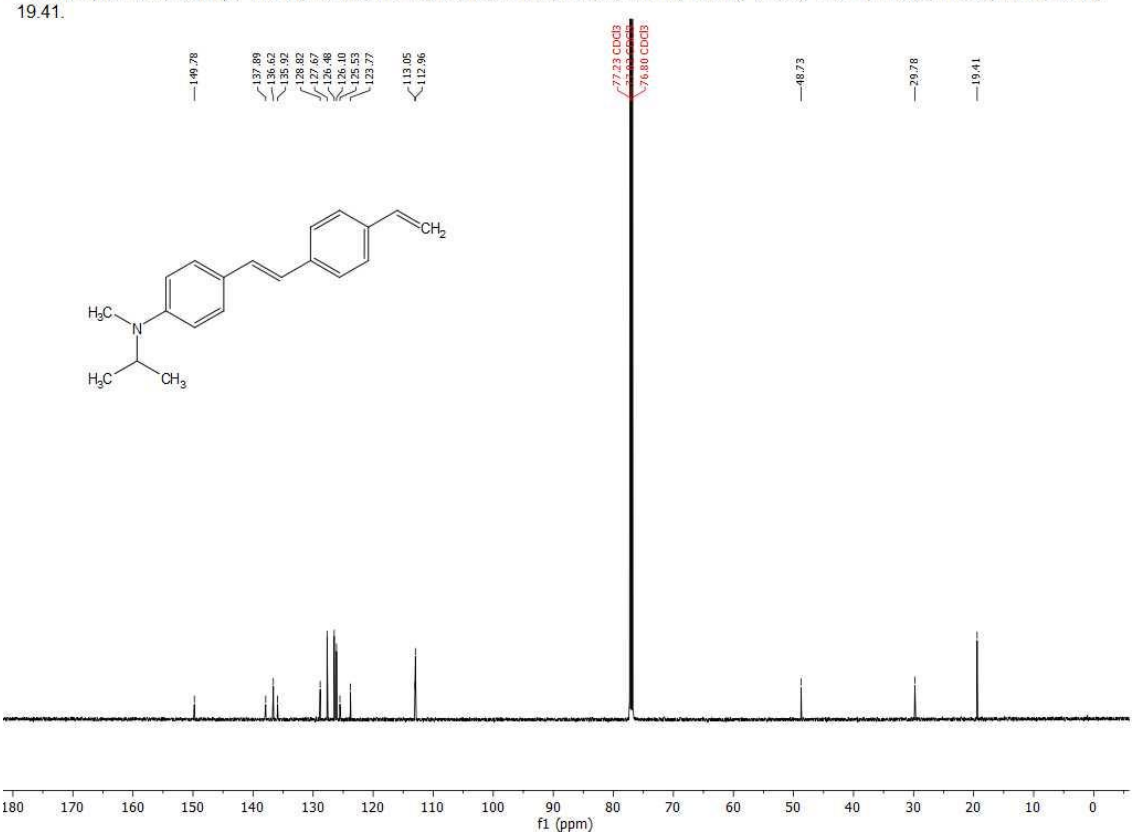

Spectrum S21. ^{1}H spectrum of 4-iodo-2,6-dimethylaniline, 11:

^{1}H NMR (500 MHz, Chloroform-*d*) δ 7.24 (s, 2H), 3.58 (s, 2H), 2.13 (s, 6H).

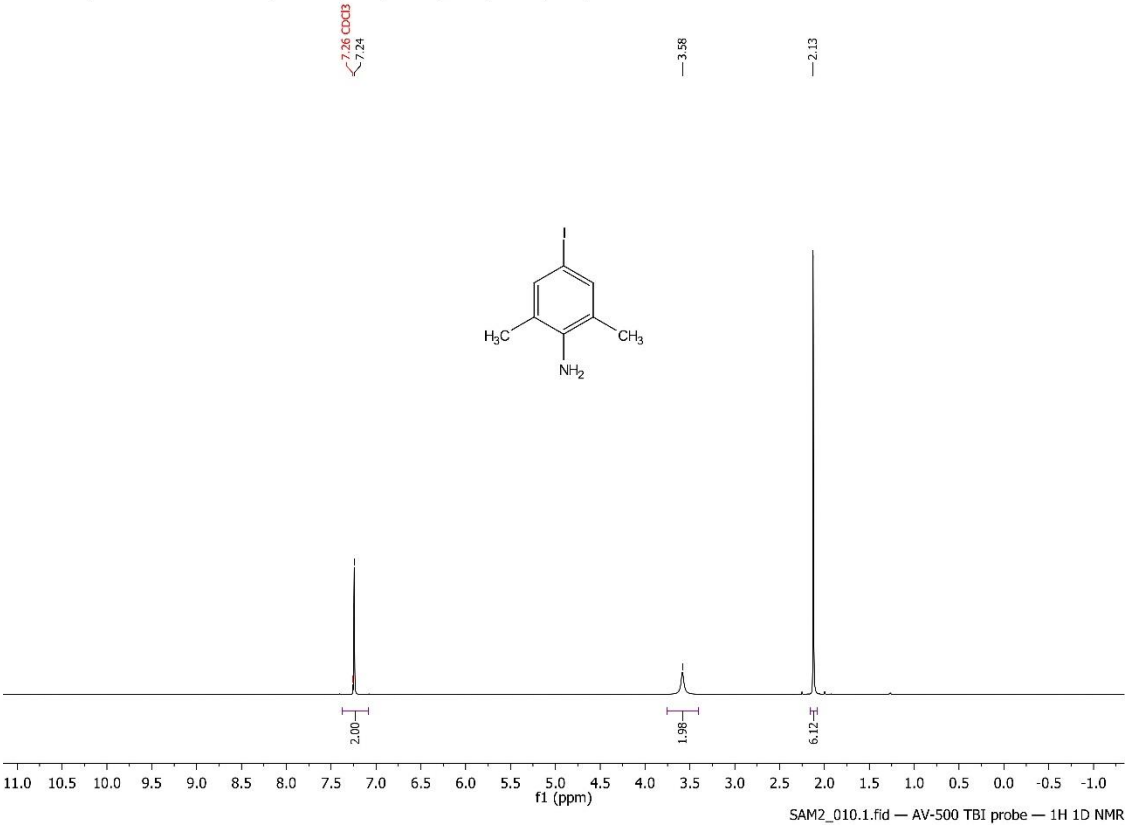

Spectrum S22. ^{13}C spectrum of 4-iodo-2,6-dimethylaniline, 11:

^{13}C NMR (126 MHz, $CDCl_3$) δ 142.67, 136.54, 124.21, 79.23, 17.36.

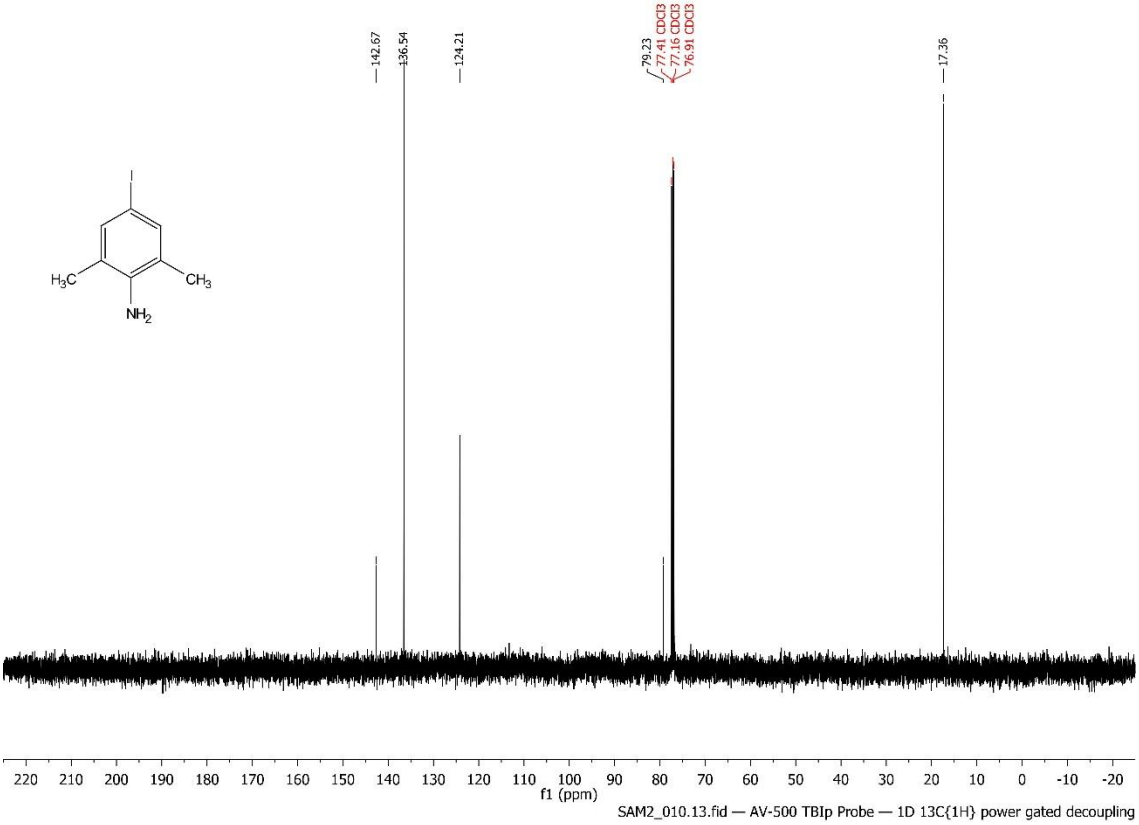

Spectrum S23. ^{1}H spectrum of 4-iodo-N,N,2,6-tetramethylaniline, 12:

^{1}H NMR (500 MHz, Chloroform-*d*) δ 7.32 (s, 2H), 2.78 (s, 6H), 2.23 (s, 6H).

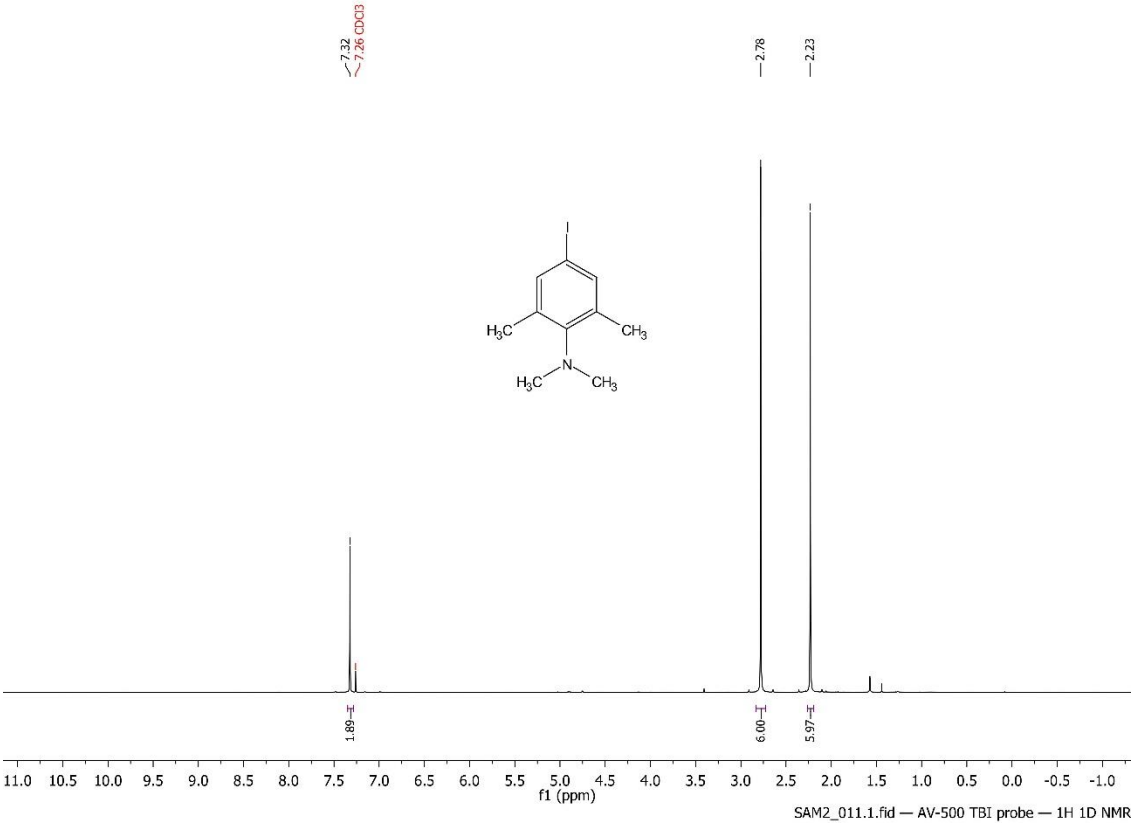

Spectrum S24. ^{13}C spectrum of 4-iodo-N,N,2,6-tetramethylaniline, 12:

^{13}C NMR (126 MHz, $CDCl_3$) δ 149.77, 139.70, 137.55, 89.31, 42.45, 18.89.

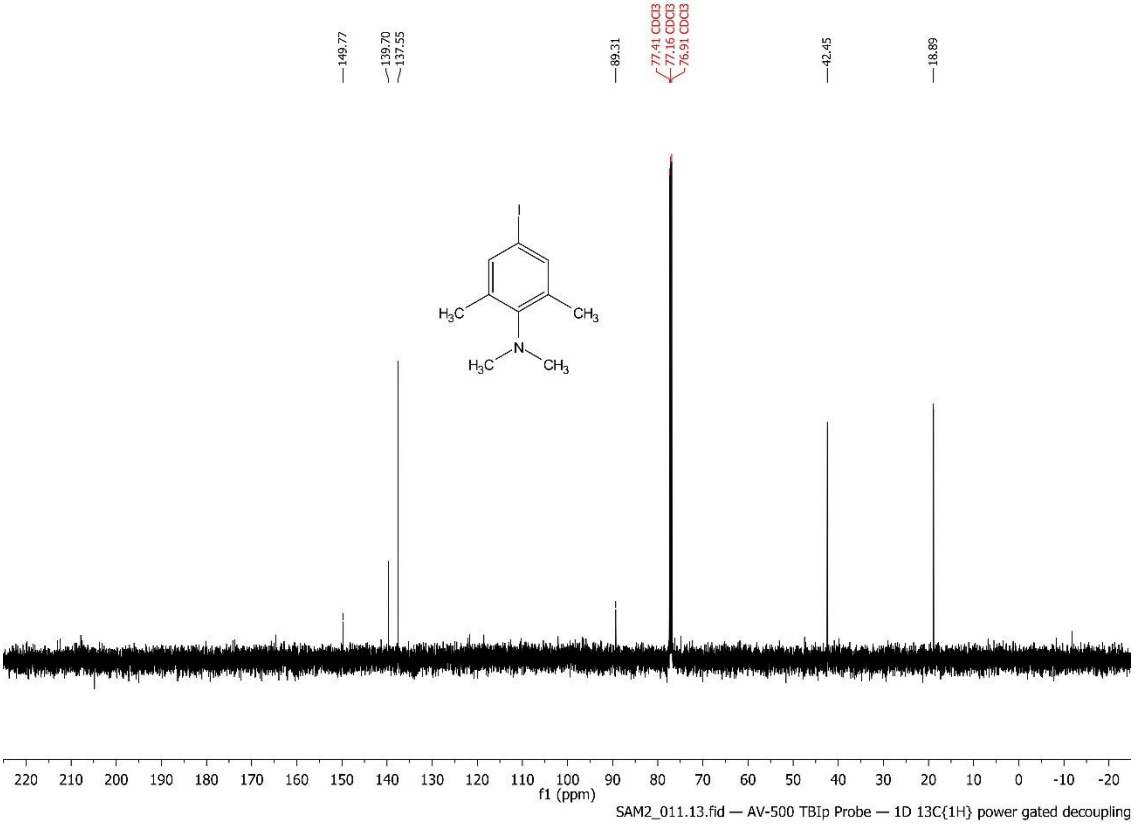

Spectrum S25. ^{1}H spectrum of 4-(dimethylamino)-3,5-dimethylbenzaldehyde, 13:

^{1}H NMR (500 MHz, Chloroform-*d*) δ 9.86 (s, 1H), 7.50 (s, 2H), 2.87 (s, 6H), 2.34 (s, 6H).

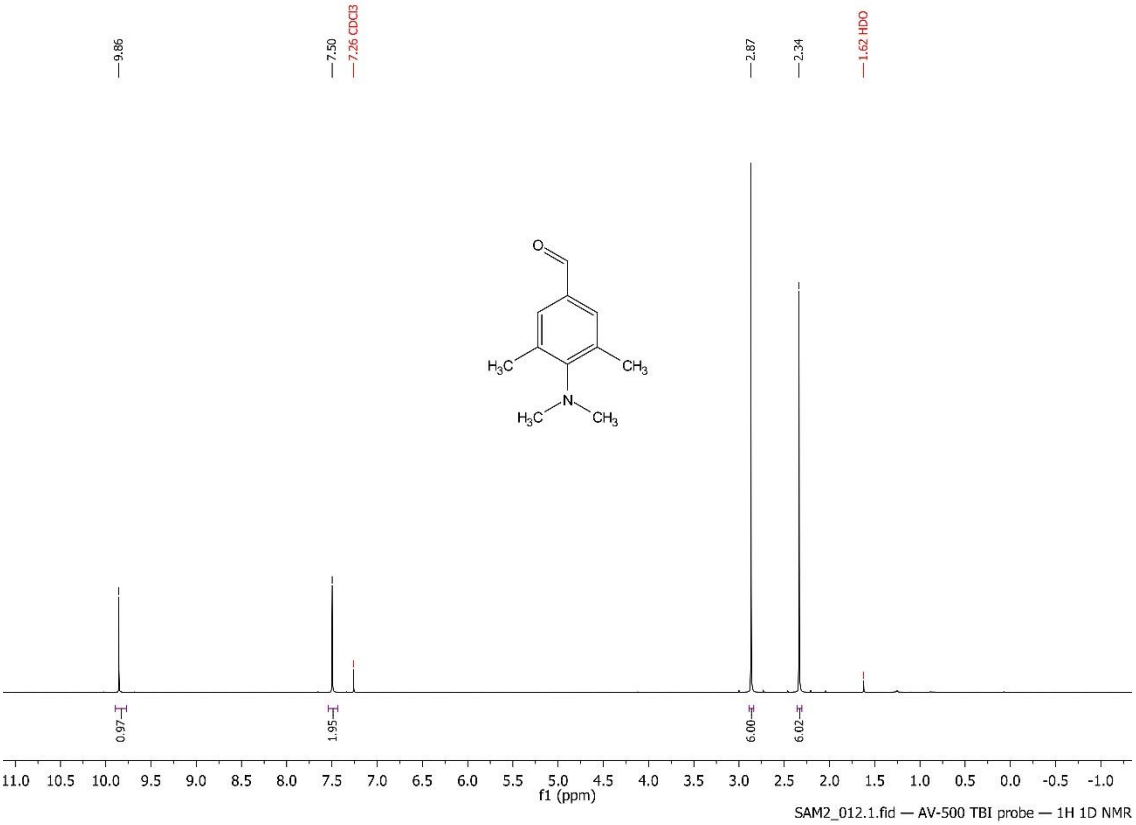

Spectrum S26. ^{13}C spectrum of 4-(dimethylamino)-3,5-dimethylbenzaldehyde, 13:

^{13}C NMR (126 MHz, $CDCl_3$) δ 191.99, 156.38, 136.70, 132.28, 130.83, 42.55, 19.66.

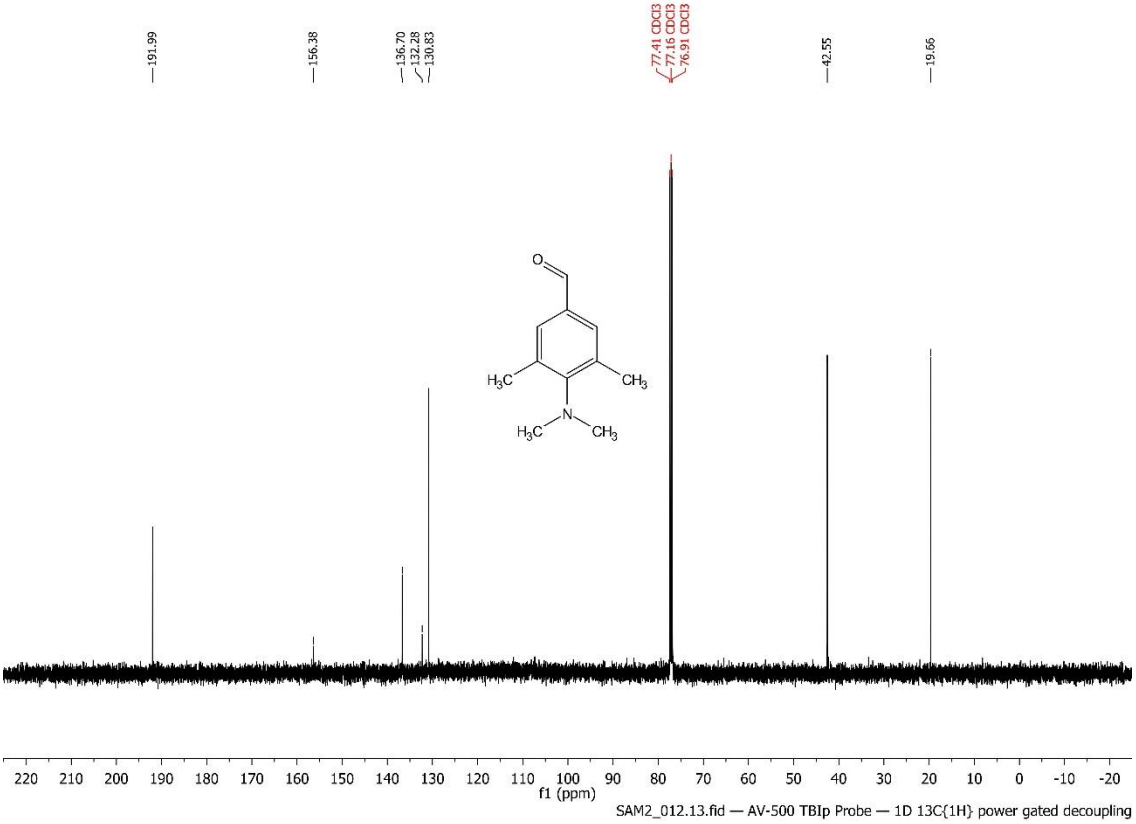

Spectrum S27. ^{1}H spectrum of N,N,2,6-tetramethyl-4-vinylaniline, 14:

^{1}H NMR (500 MHz, Chloroform-*d*) δ 7.05 (s, 2H), 6.62 (dd, *J* = 17.6, 10.9 Hz, 1H), 5.64 (d, *J* = 17.6 Hz, 1H), 5.14 (d, *J* = 10.9 Hz, 1H), 2.81 (s, 6H), 2.29 (s, 6H).

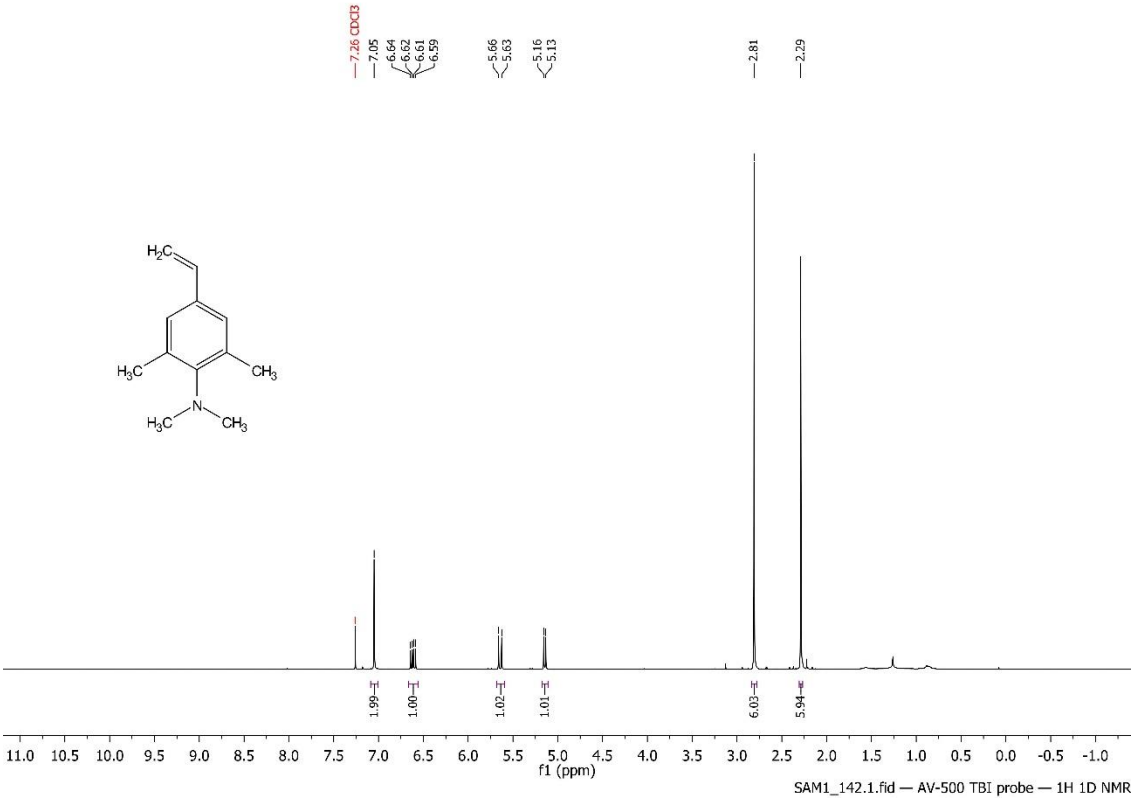

Spectrum S28. ^{13}C spectrum of N,N,2,6-tetramethyl-4-vinylaniline, 14:

^{13}C NMR (126 MHz, $CDCl_3$) δ 137.14, 136.67, 133.94, 126.77, 112.70, 42.64, 19.34.

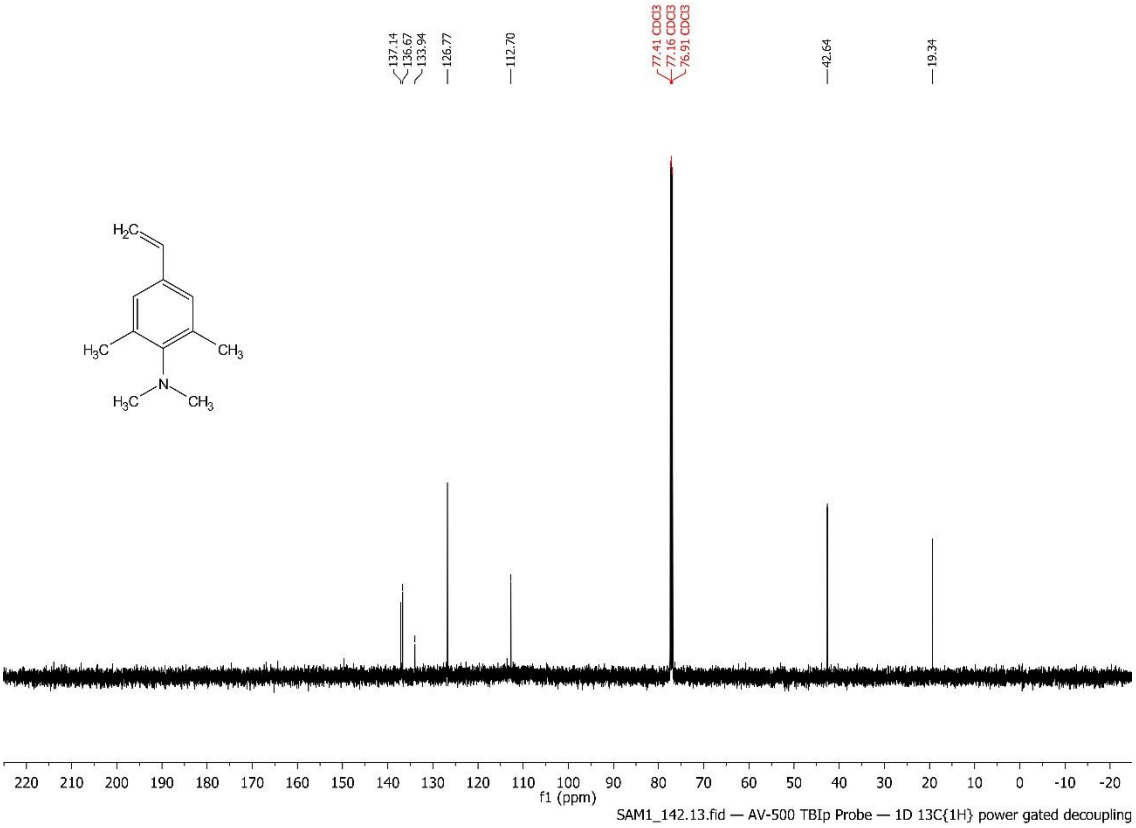

Spectrum S29. ^{1}H spectrum of (E)-4-(4-(dimethylamino)-3,5-dimethylstyryl)benzaldehyde, 15:

^{1}H NMR (400 MHz, Chloroform-*d*) δ 9.98 (s, 1H), 7.85 (d, *J* = 8.2 Hz, 2H), 7.62 (d, *J* = 8.2 Hz, 2H), 7.22 – 7.00 (m, 4H), 2.84 (s, 6H), 2.33 (s, 6H).

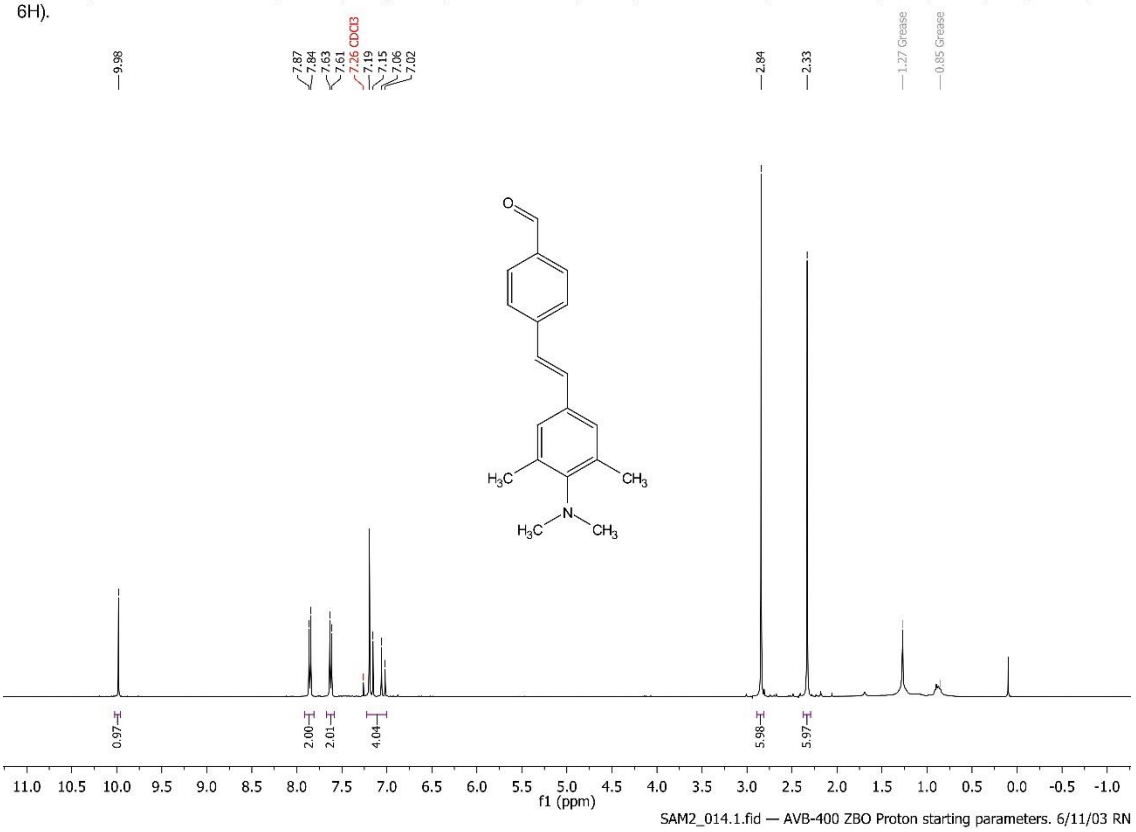

Spectrum S30. ^{13}C spectrum of (E)-4-(4-(dimethylamino)-3,5-dimethylstyryl)benzaldehyde, 15:

^{13}C NMR (101 MHz, $CDCl_3$) δ 191.72, 150.60, 143.98, 137.28, 135.10, 132.71, 132.17, 130.34, 127.57, 126.78, 126.10, 42.63, 19.43.

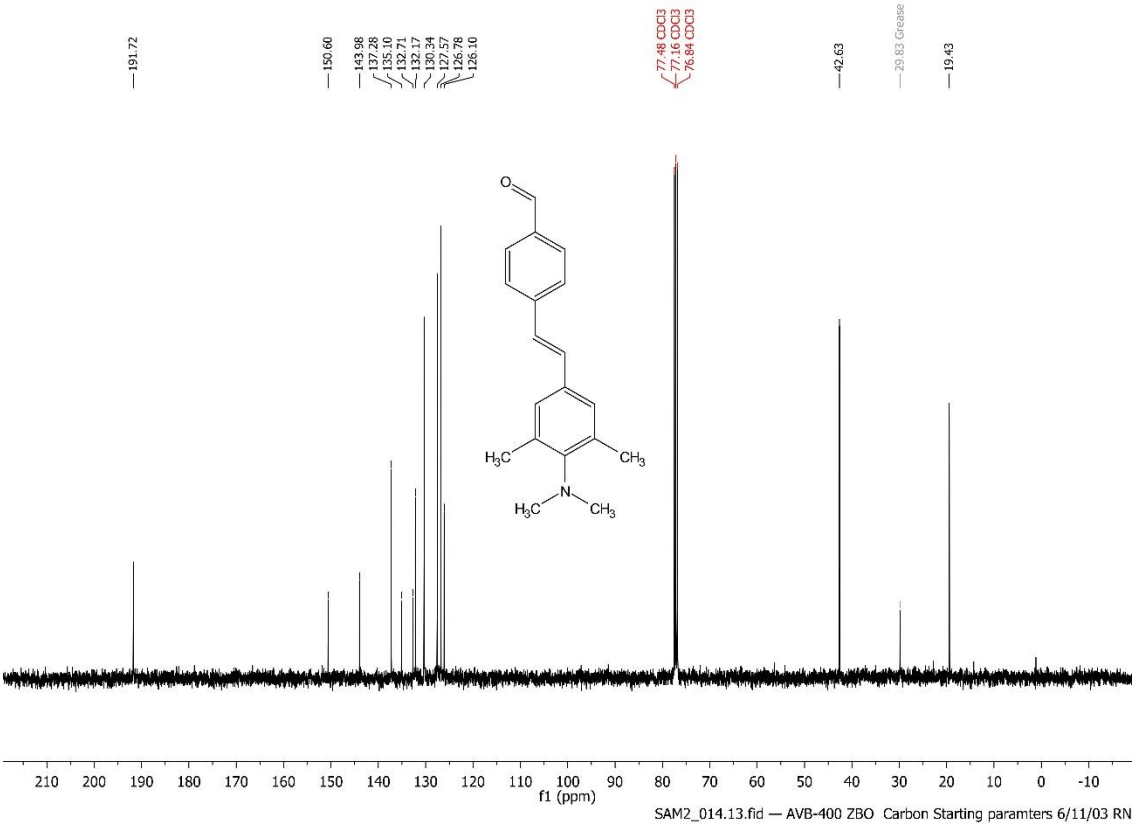

Spectrum S31. ^{1}H spectrum of (E)-N,N,2,6-tetramethyl-4-(4-vinylstyryl)aniline, 16:

^{1}H NMR (500 MHz, Chloroform-*d*) δ 7.48 – 7.38 (m, 4H), 7.16 (s, 2H), 7.01 (d, *J* = 3.0 Hz, 2H), 6.72 (dd, *J* = 17.6, 10.9 Hz, 1H), 5.76 (d, *J* = 17.6 Hz, 1H), 5.24 (d, *J* = 10.9 Hz, 1H), 2.83 (s, 6H), 2.32 (s, 6H).

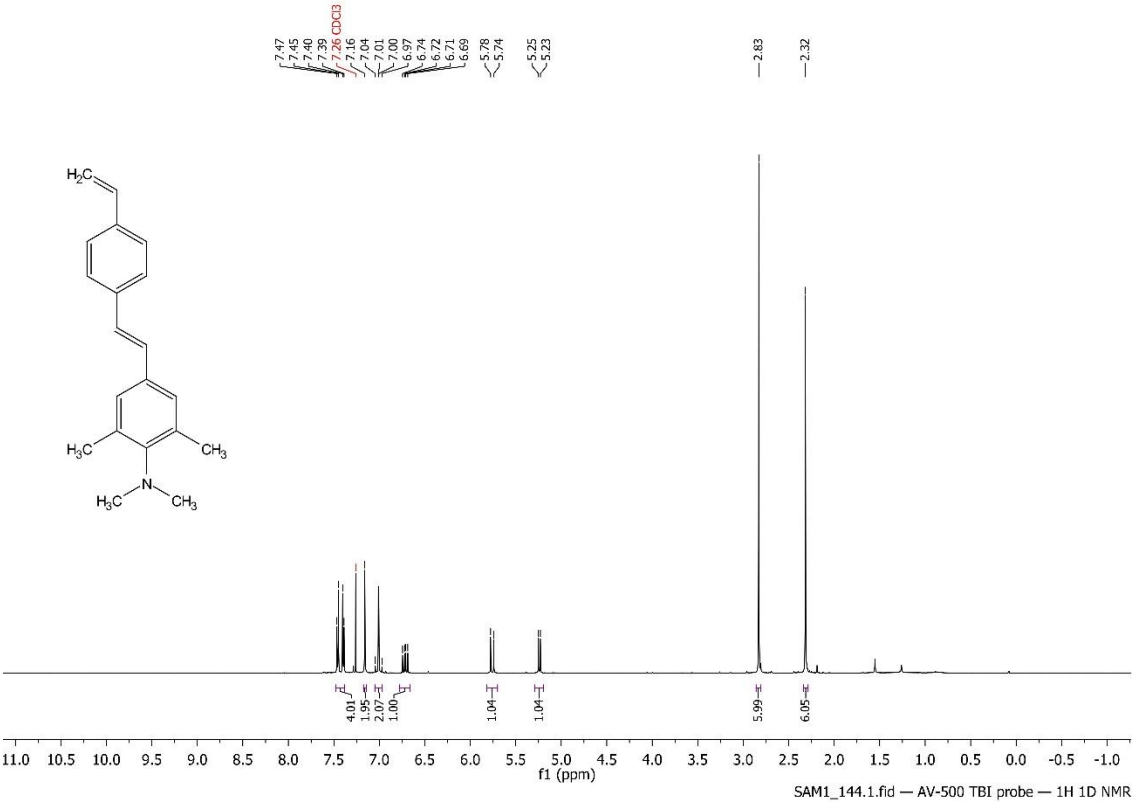

Spectrum S32. ^{13}C spectrum of (E)-N,N,2,6-tetramethyl-4-(4-vinylstyryl)aniline, 16:

^{13}C NMR (126 MHz, $CDCl_3$) δ 149.76, 137.41, 137.26, 136.63, 128.54, 127.18, 127.11, 126.65, 126.62, 113.64, 42.68, 19.42.

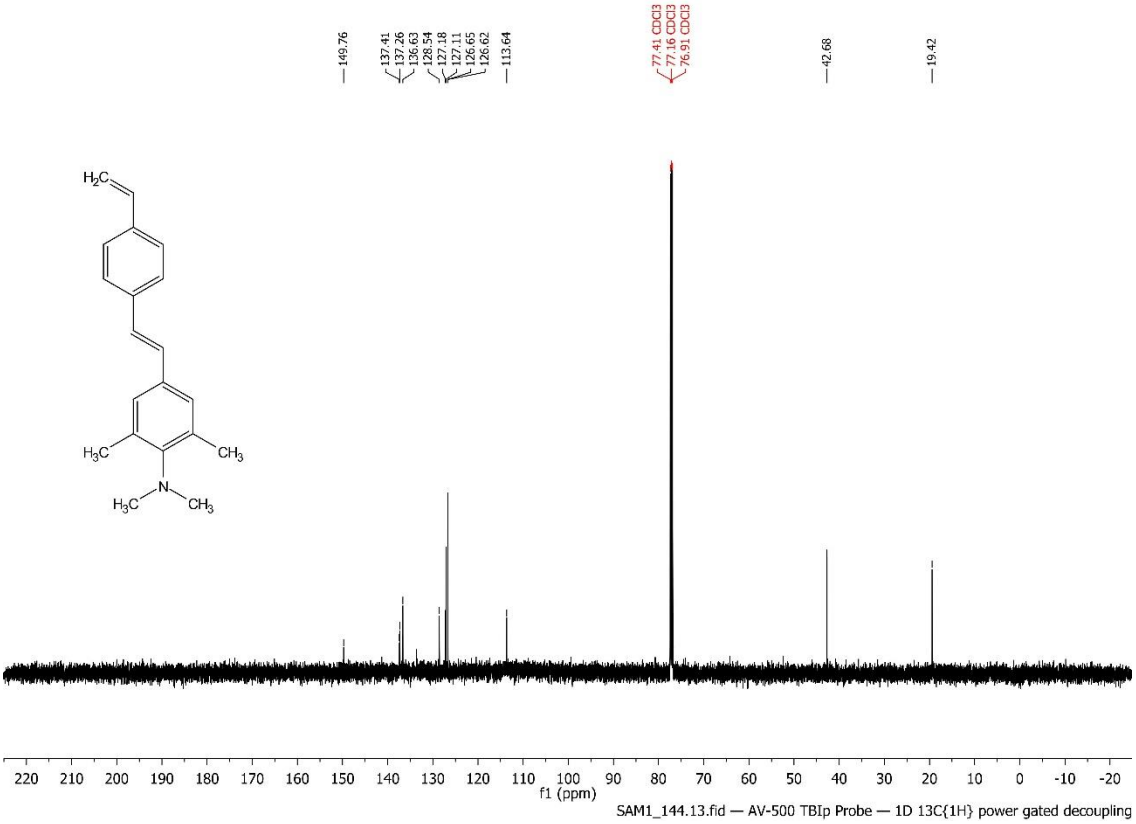

Spectrum S33. ^{1}H spectrum of 17 (JuloVF):

^{1}H NMR (400 MHz, DMSO-d_6) δ 8.17 (s, 1H), 7.79 (d, J = 8.0 Hz, 1H), 7.66 (d, J = 7.7 Hz, 2H), 7.54 (d, J = 7.8 Hz, 2H), 7.48 – 7.35 (m, 2H), 7.25 (d, J = 7.9 Hz, 1H), 7.18 – 6.82 (m, 6H), 6.77 (s, 2H), 3.28 – 3.01 (m, 4H), 2.87 – 2.58 (m, 4H), 1.99 – 1.78 (m, 4H).

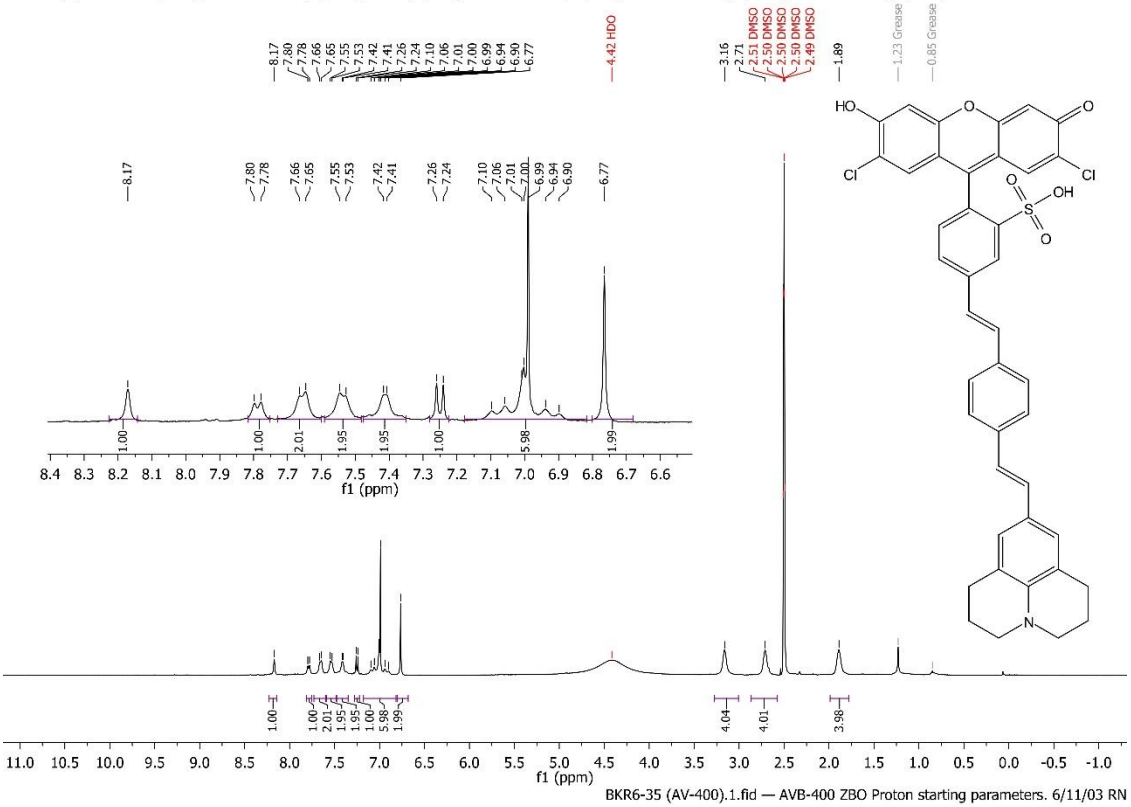

Spectrum S34. HPLC of 17 (JuloVF)

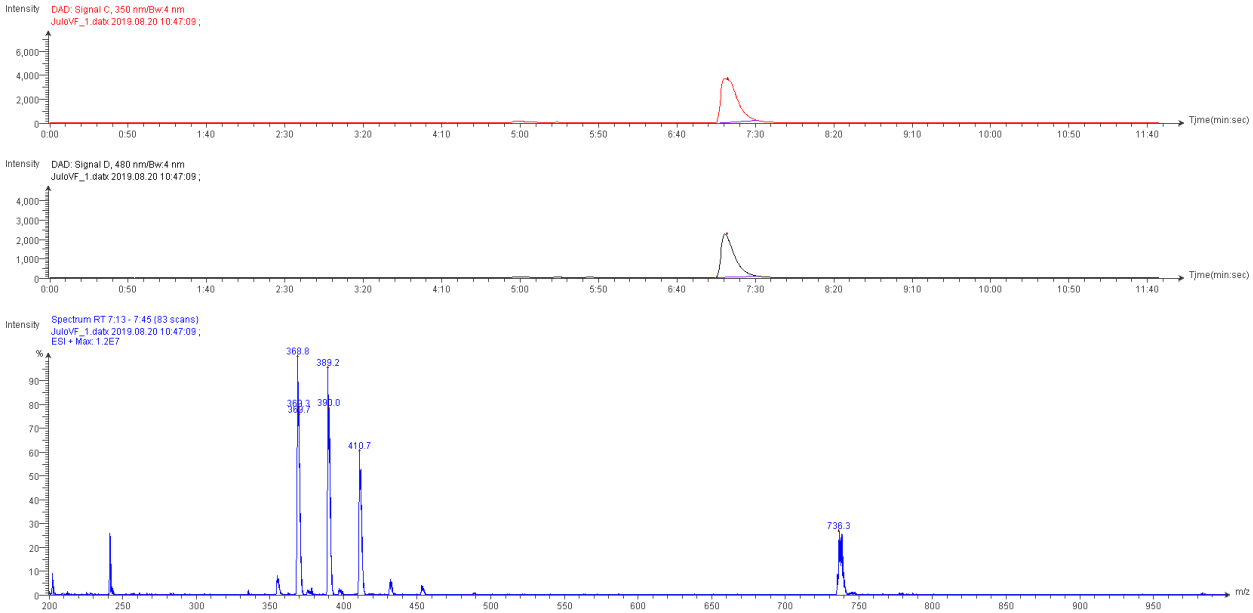

Low-resolution ESI(+) mass spectrum of **17** (JuloVF)
Calculated for $[M + H^+]^+$ = 736.1
Found: 736.3

Calculated for $[M + 2Na^+ + CH_3CN]^{2+}$ = 822.1 / 2 = 411.0
Found: 410.7

Calculated for $[M + 2H^+ + CH_3CN]^{2+}$ = 778.2 / 2 = 389.1
Found: 389.2

Calculated for $[M + 2H^+]^{2+}$ = 737.1 / 2 = 368.6
Found: 368.8

Spectrum S35. ^{1}H spectrum of 18 (IndoVF):

^{1}H NMR (400 MHz, DMSO-d_6) δ 8.15 (s, 1H), 7.76 (d, *J* = 7.8 Hz, 1H), 7.64 (d, *J* = 8.0 Hz, 2H), 7.53 (d, *J* = 7.9 Hz, 2H), 7.42 – 7.32 (m, 3H), 7.22 (dd, *J* = 8.1, 4.2 Hz, 2H), 7.16 (d, *J* = 16.5 Hz, 1H), 6.97 (d, *J* = 10.3 Hz, 3H), 6.73 (s, 2H), 6.47 (d, *J* = 8.0 Hz, 1H), 3.29 (t, *J* = 8.2 Hz, 3H), 2.89 (t, *J* = 8.3 Hz, 2H), 2.71 (s, 3H).

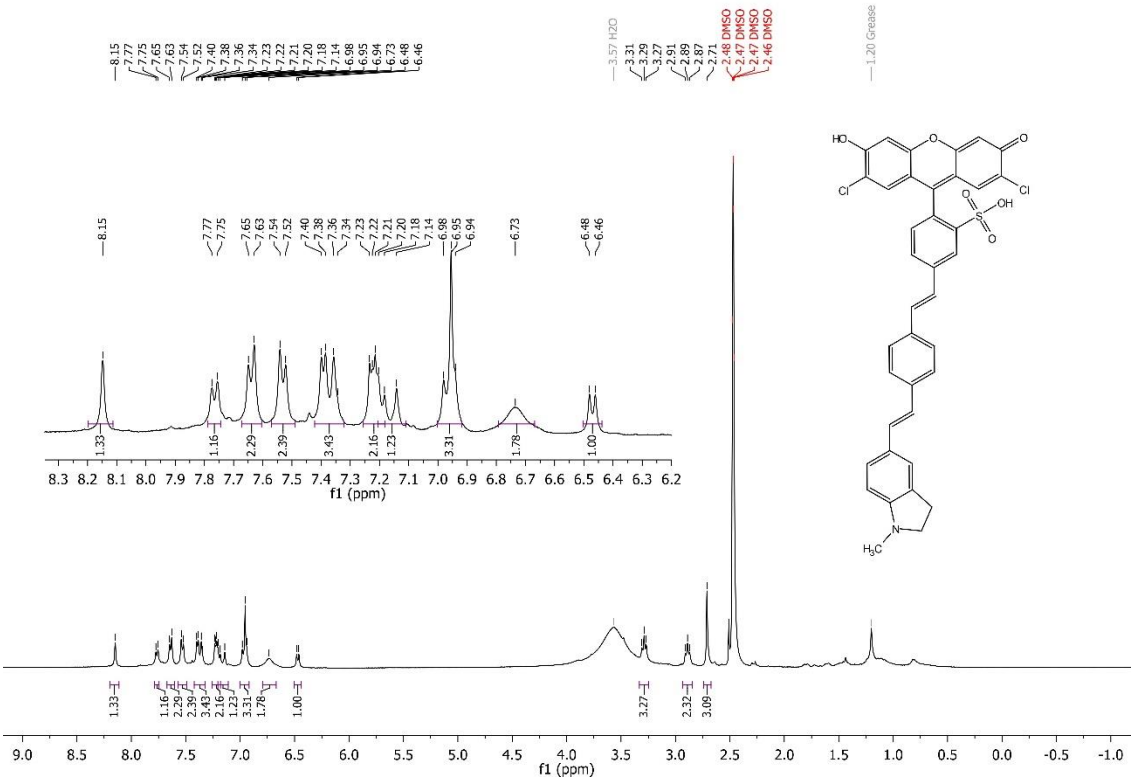

Spectrum S36. HPLC of 18 (IndoVF)

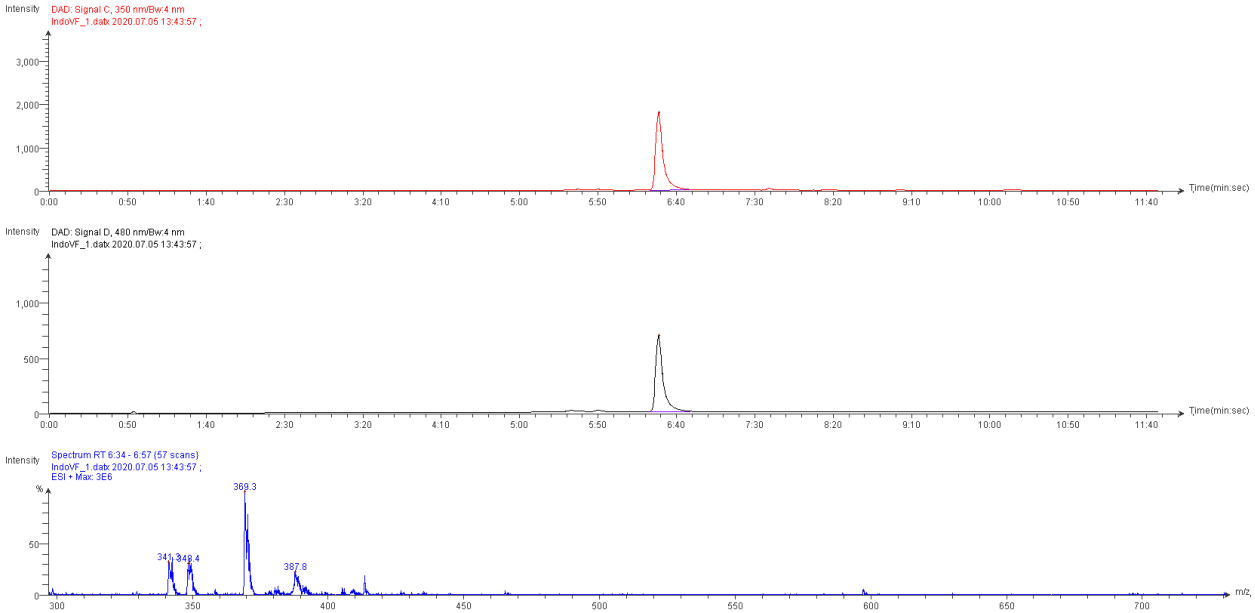

Low-resolution ESI(+) mass spectrum of **18** (IndoVF)
Calculated for $[M + 2H^+]^{2+}$ = 697.0 / 2 = 348.5;
Found: 348.4

Calculated for $[M + 2H^+ + CH_3CN]^{2+}$ = 738.1 / 2 = 369.0
Found: 369.3

Calculated for $[M + H^+ + K^+ + CH_3CN]^{2+}$ = 776.1 / 2 = 388.0
Found: 387.8

Spectrum S37. ^{1}H spectrum of 19 (^{i}PrVF):

^{1}H NMR (900 MHz, DMSO-d_6) δ 8.16 (d, J = 1.9 Hz, 1H), 7.71 (dd, J = 7.9, 1.9 Hz, 1H), 7.66 (d, J = 7.9 Hz, 2H), 7.56 (d, J = 8.0 Hz, 2H), 7.44 (d, J = 8.3 Hz, 2H), 7.41 (d, J = 16.3 Hz, 1H), 7.37 – 7.34 (m, 1H), 7.18 (d, J = 16.3 Hz, 1H), 7.12 (d, J = 7.7 Hz, 1H), 6.99 (d, J = 16.3 Hz, 1H), 6.79 (d, J = 8.5 Hz, 2H), 6.74 (s, 2H), 6.12 (s, 2H), 4.16 (q, J = 6.6 Hz, 1H), 2.72 (s, 3H), 1.13 (d, J = 6.5 Hz, 6H).

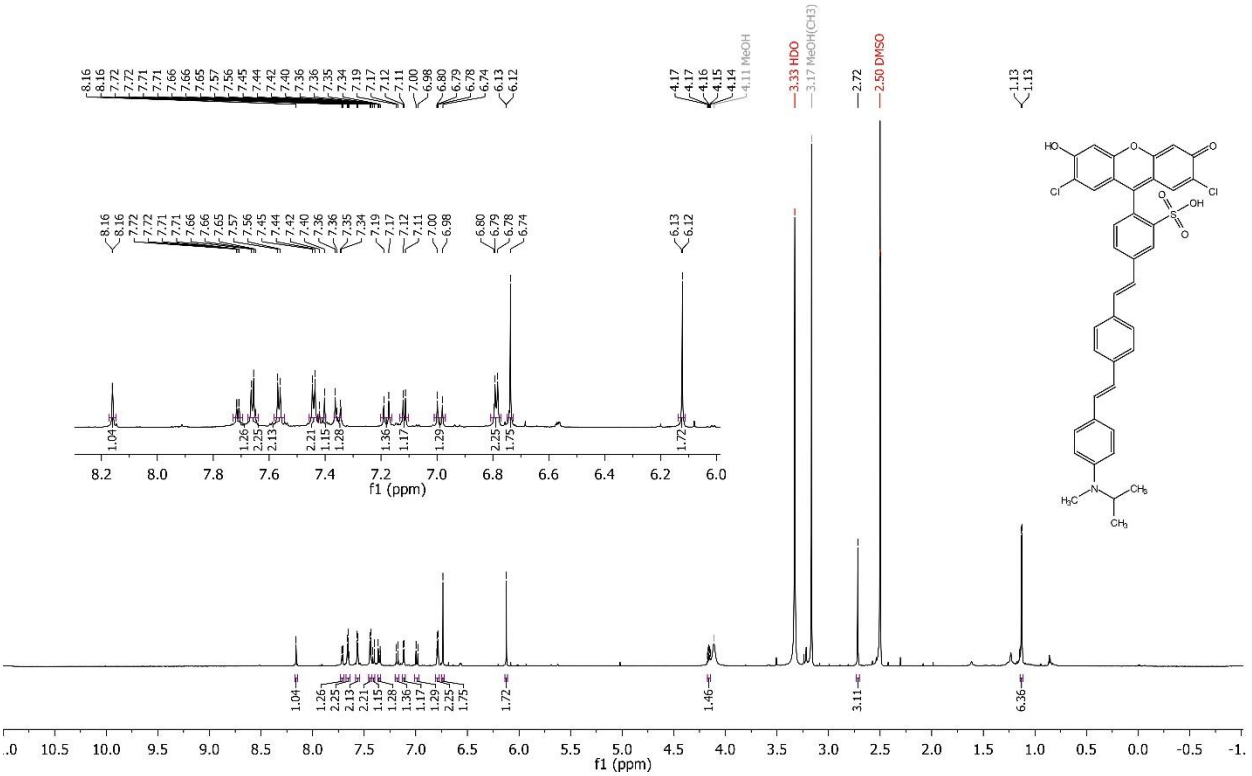

Spectrum S38. HPLC of 19 (^{i}PrVF)

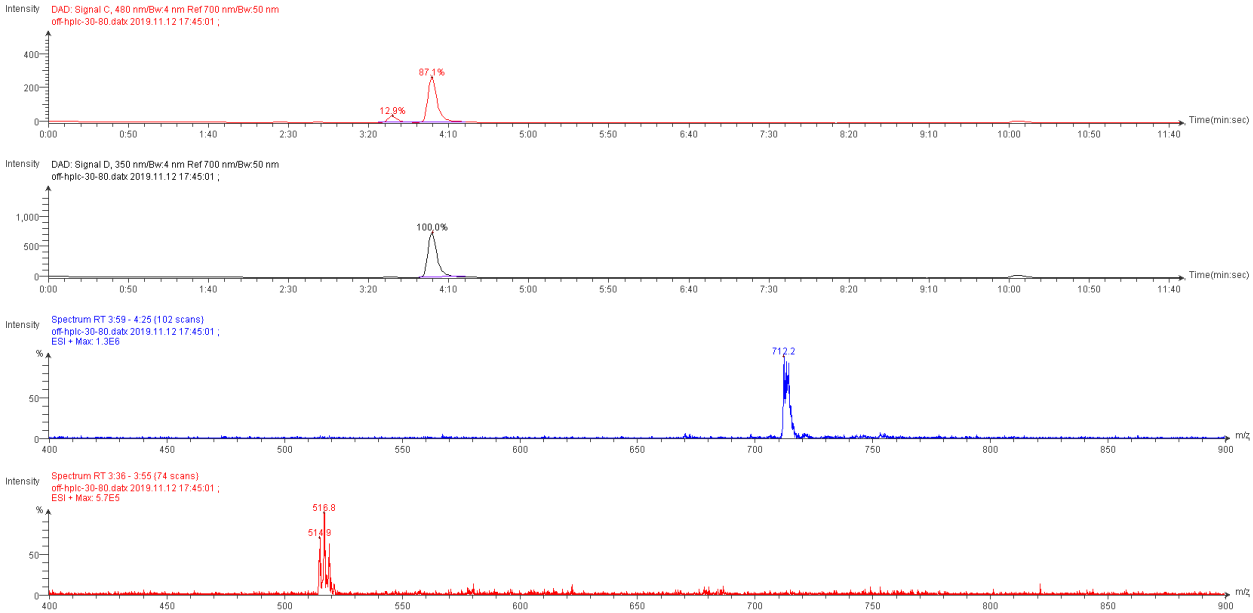

Low-resolution ESI(+) mass spectrum of **19** (^{i}PrVF)
Calculated for $[M + H^+]^+$ = 712.1 (retention time = 4:00 min)
Found: 712.2

Impurity at 3:35 is dichlorobromosulfonofluorescein **A**
Calculated for $[M + H^+]^+$ = 514.9
Found: 514.8

Spectrum S39. ^{1}H spectrum of 20 (NN26VF):

^{1}H NMR (900 MHz, DMSO-d_6) δ 8.17 (d, J = 1.8 Hz, 1H), 7.73 (dd, J = 7.8, 1.8 Hz, 1H), 7.69 (d, J = 7.9 Hz, 2H), 7.61 (d, J = 7.9 Hz, 2H), 7.44 (d, J = 16.4 Hz, 1H), 7.37 (d, J = 16.4 Hz, 1H), 7.24 (s, 2H), 7.19 – 7.15 (m, 2H), 7.13 (d, J = 7.8 Hz, 1H), 6.75 (s, 2H), 6.16 (s, 2H), 2.78 (s, 6H), 2.28 (s, 6H).

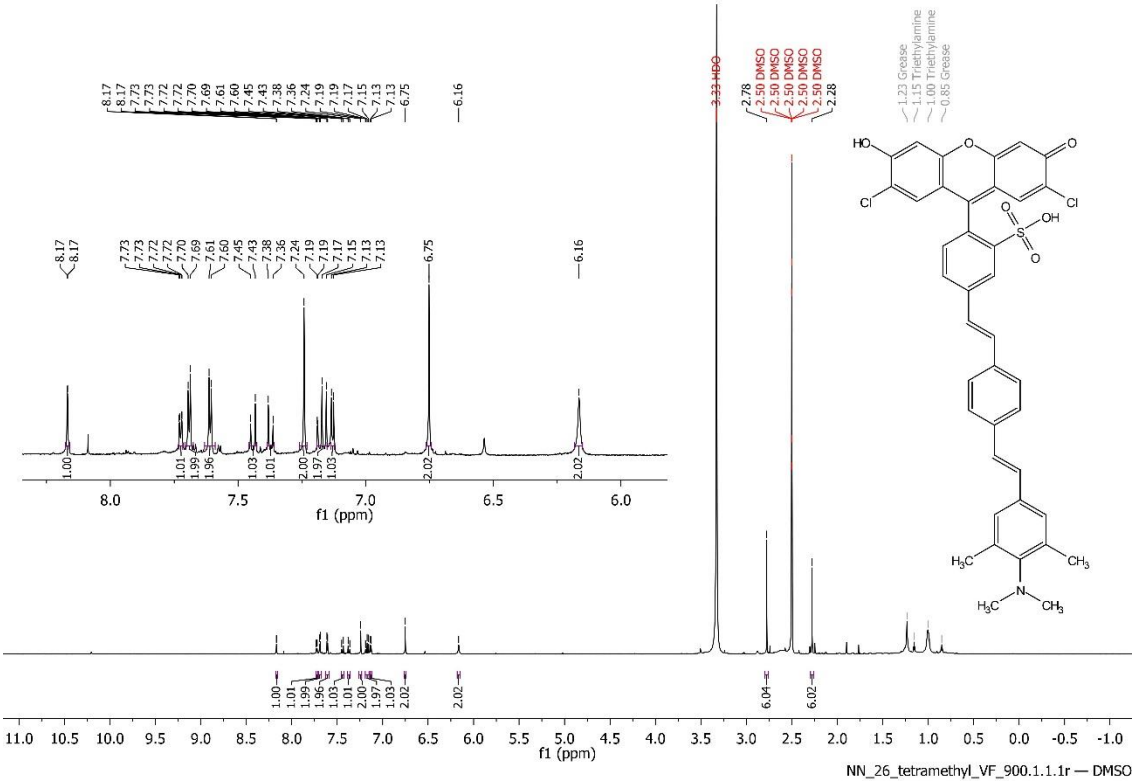

Spectrum S40. HPLC of 20 (NN26VF)

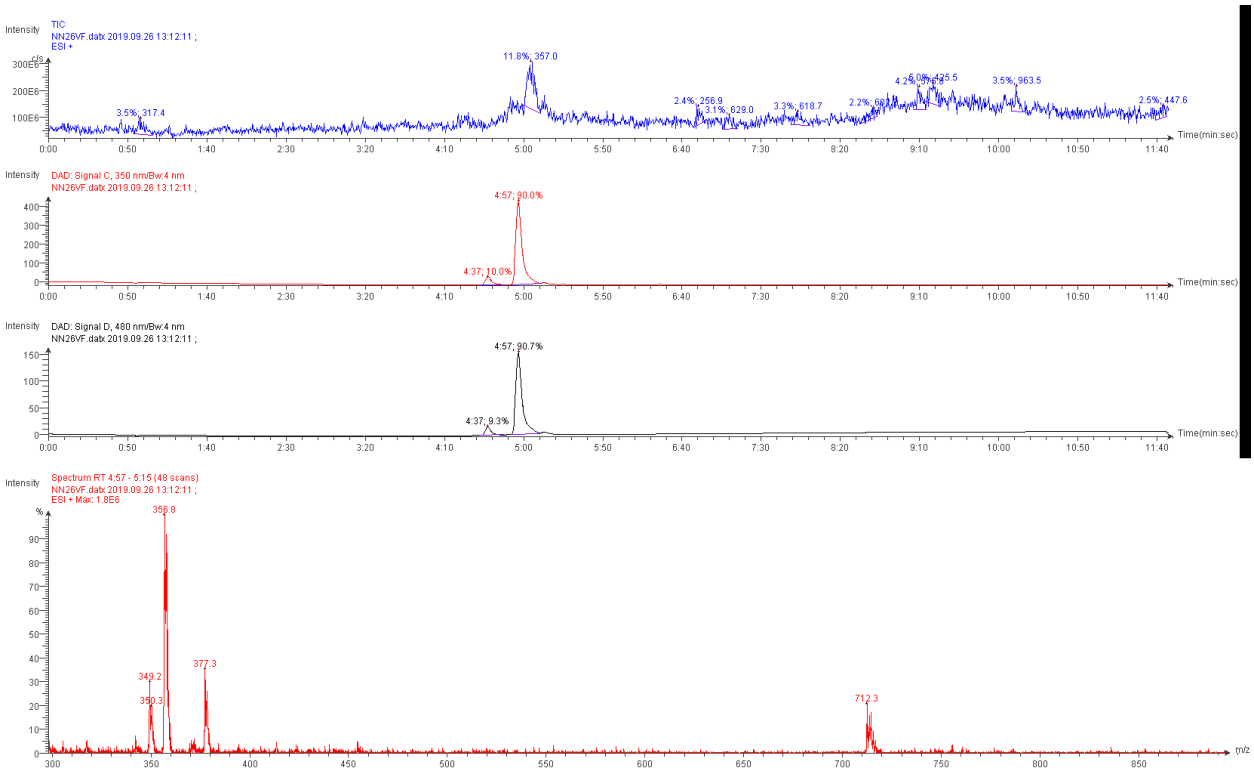

Low-resolution ESI(+) mass spectrum of **20** (JuloVF)
Calculated for $[M + H^+]^+$ = 712.1 (retention time = 4:57 min)
Found: 712.3

Calculated for $[M + 2H^+ + CH_3CN]^{2+}$ = 754.2 / 2 = 377.1
Found: 377.3

Calculated for $[M + 2H^+]^{2+}$ = 713.1 / 2 = 356.6
Found: 356.8

Spectrum S41. Comparison of NN26VF with dichlorobromosulfonofluorescein.

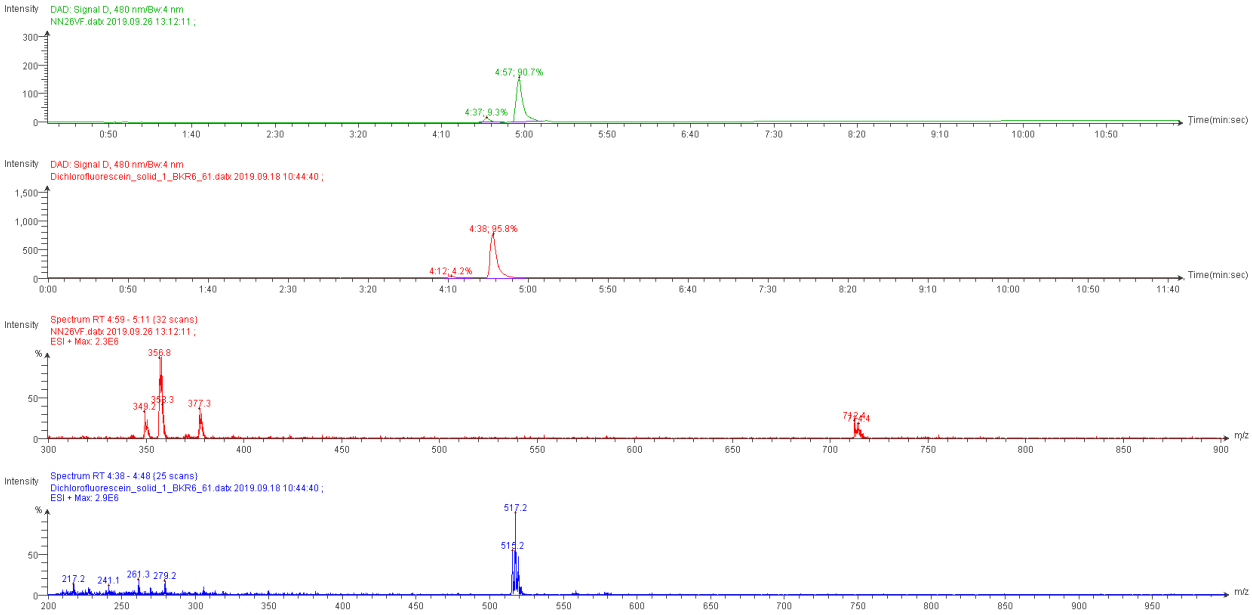

Spectrum S42. HPLC of VF2.1.Cl

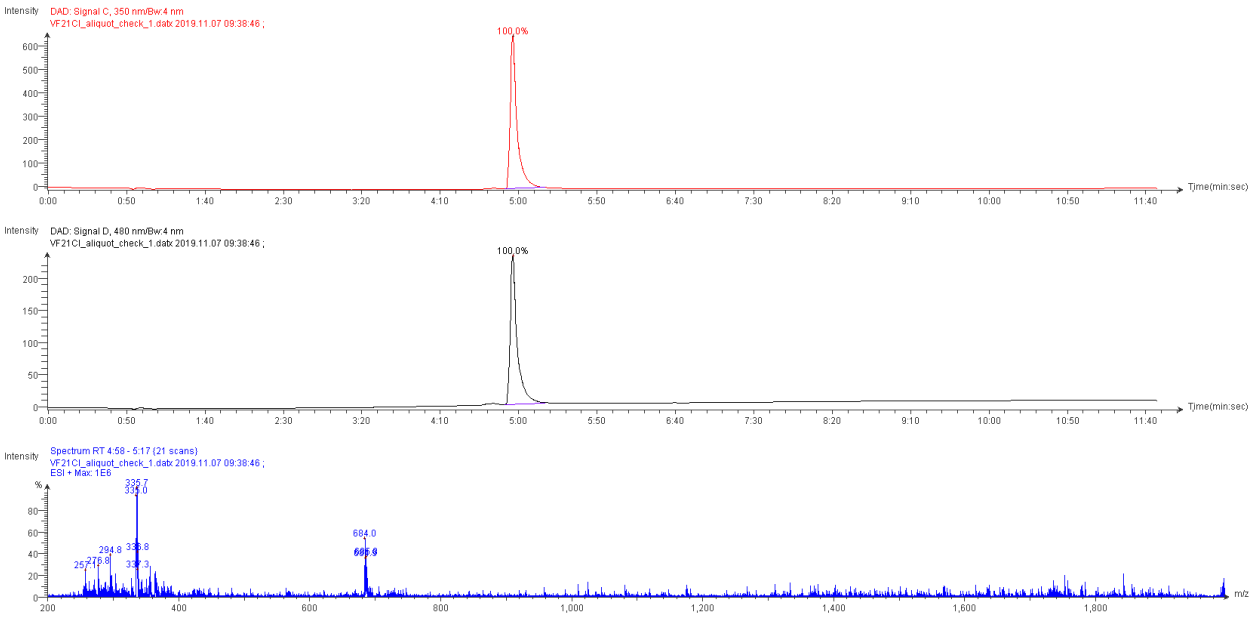

Low-resolution ESI(+) mass spectrum of VF2.1.Cl
Calculated for $[M + H^+]^+$ = 684.1
Found: 684.0

Spectrum S43. HPLC of VF2.0.Cl

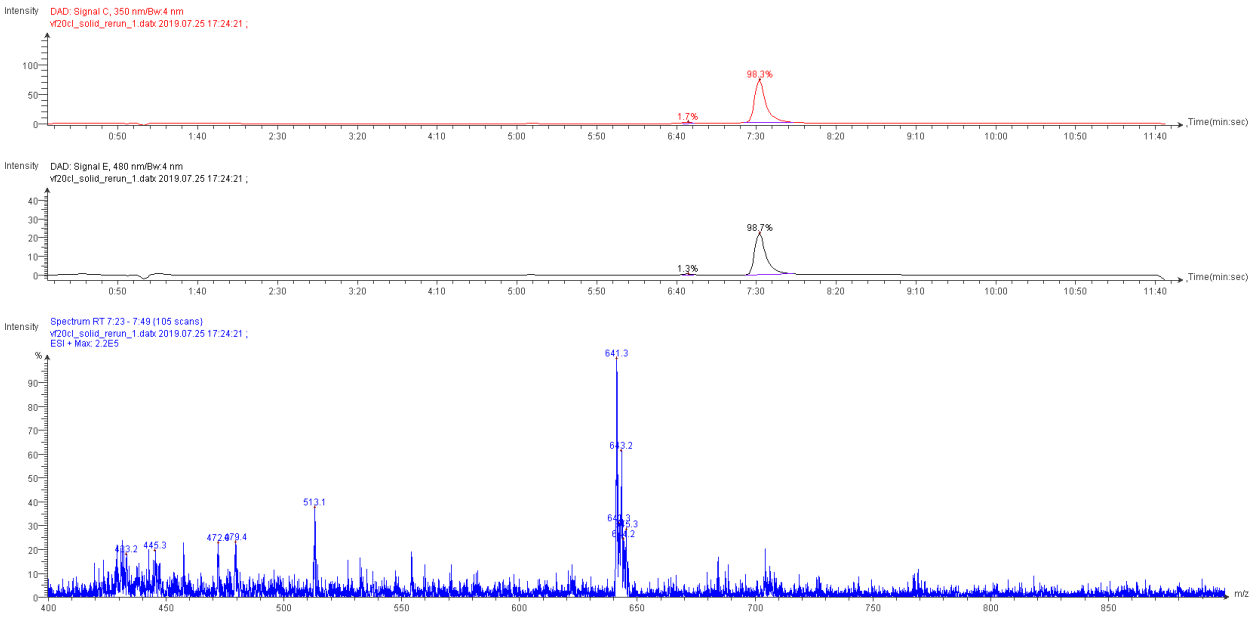

Low-resolution ESI(+) mass spectrum of VF2.0.Cl
Calculated for $[M + H^+]^+$ = 641.0
Found: 641.3

Spectrum S44. ^{13}C spectrum of 1-methylindoline-5-carbaldehyde (Figure S2):

^{13}C NMR (101 MHz, $CDCl_3$) δ 189.95, 157.96, 134.31, 130.44, 126.67, 124.33, 104.44, 54.79, 33.94, 27.34.

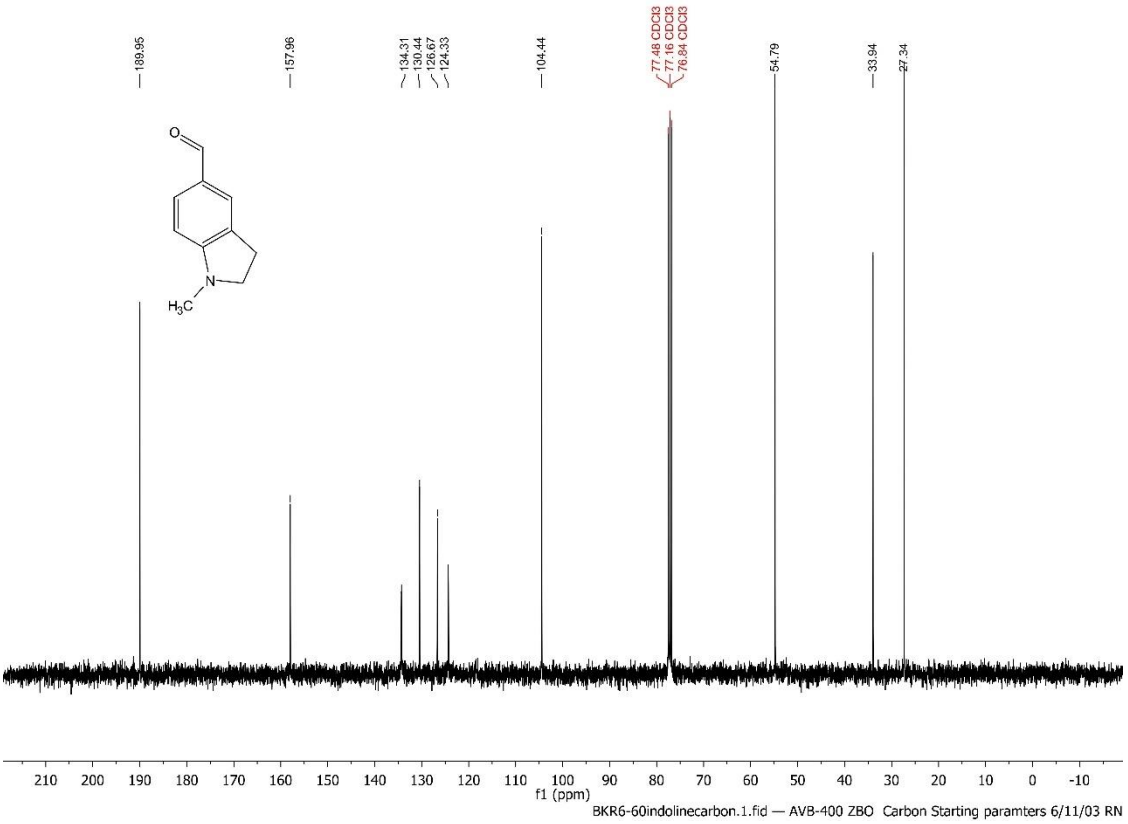

Spectrum S45. $^{1}H,^{13}C$-HMBC spectrum of 1-methylindoline-5-carbaldehyde (Figure S2):

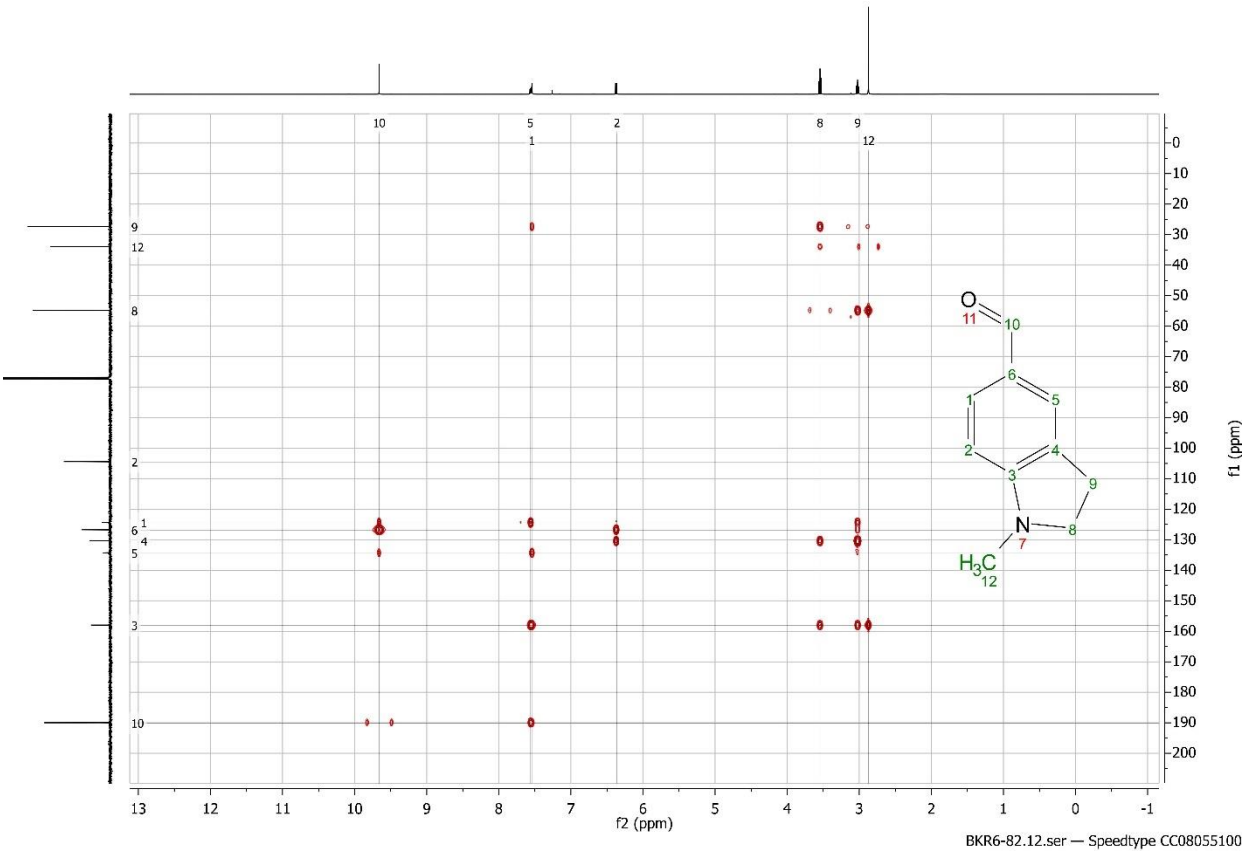

Spectrum S46. ^{1}H-^{13}C HSQC spectrum of 1-methylindoline-5-carbaldehyde (Figure S2):

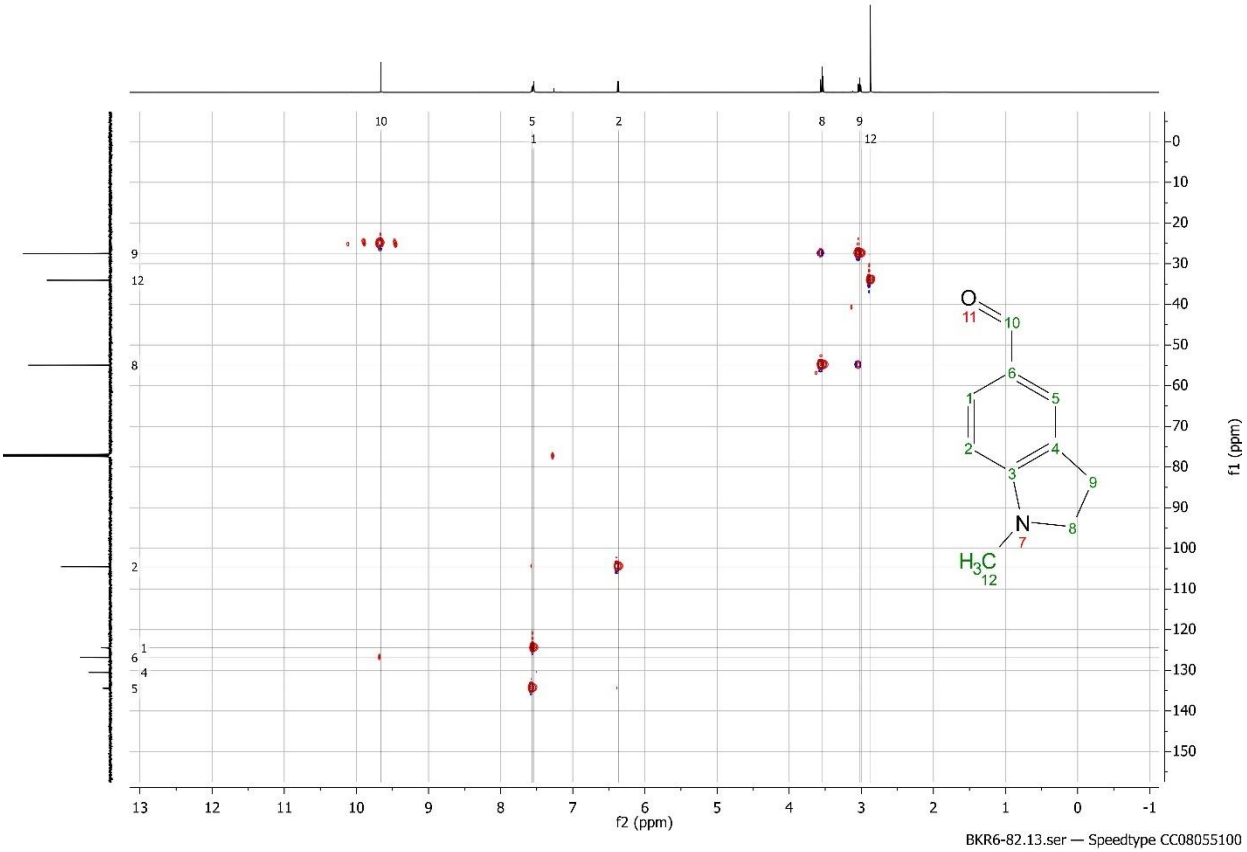

Spectrum S47. ^{13}C spectrum of 4-(dimethylamino)benzaldehyde (Figure S2):

^{13}C NMR (101 MHz, $CDCl_3$) δ 190.38, 154.29, 132.03, 125.33, 111.20, 40.23.

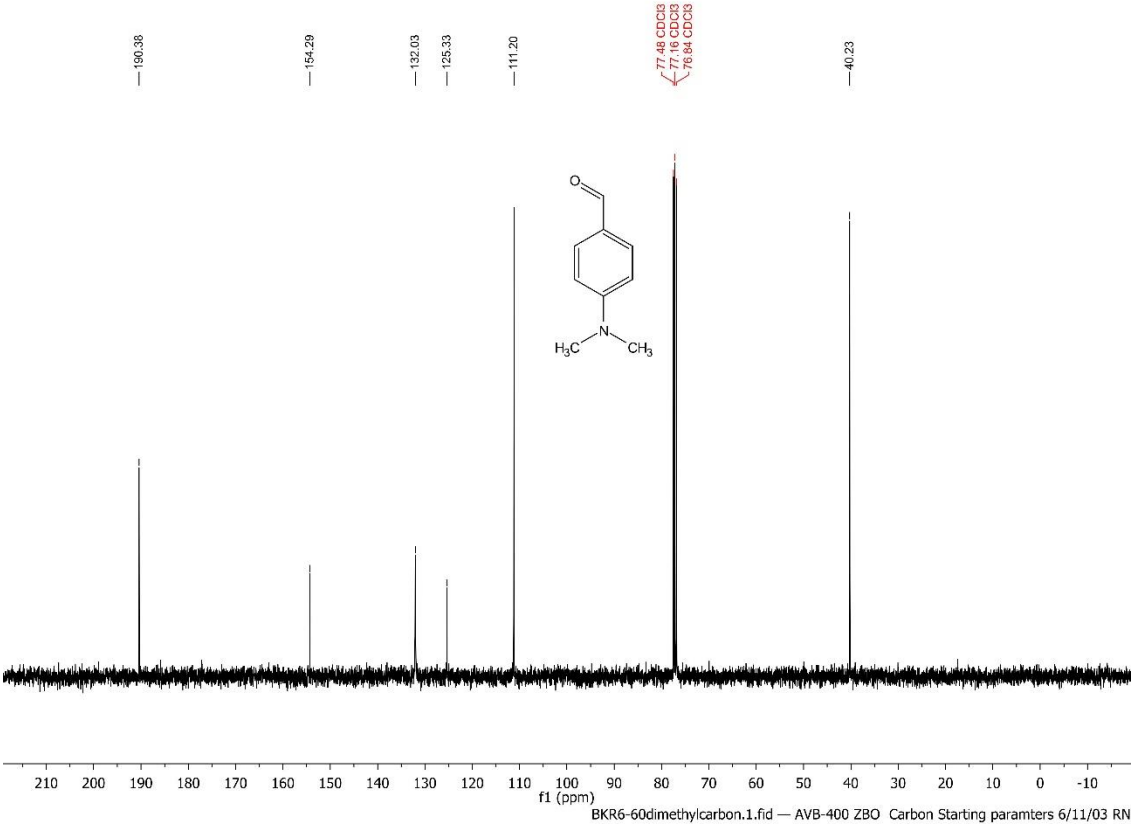

Spectrum S48. ^{13}C spectrum of benzaldehyde (Figure S2):

^{13}C NMR (101 MHz, $CDCl_3$) δ 192.51, 136.48, 134.57, 129.84, 129.10.

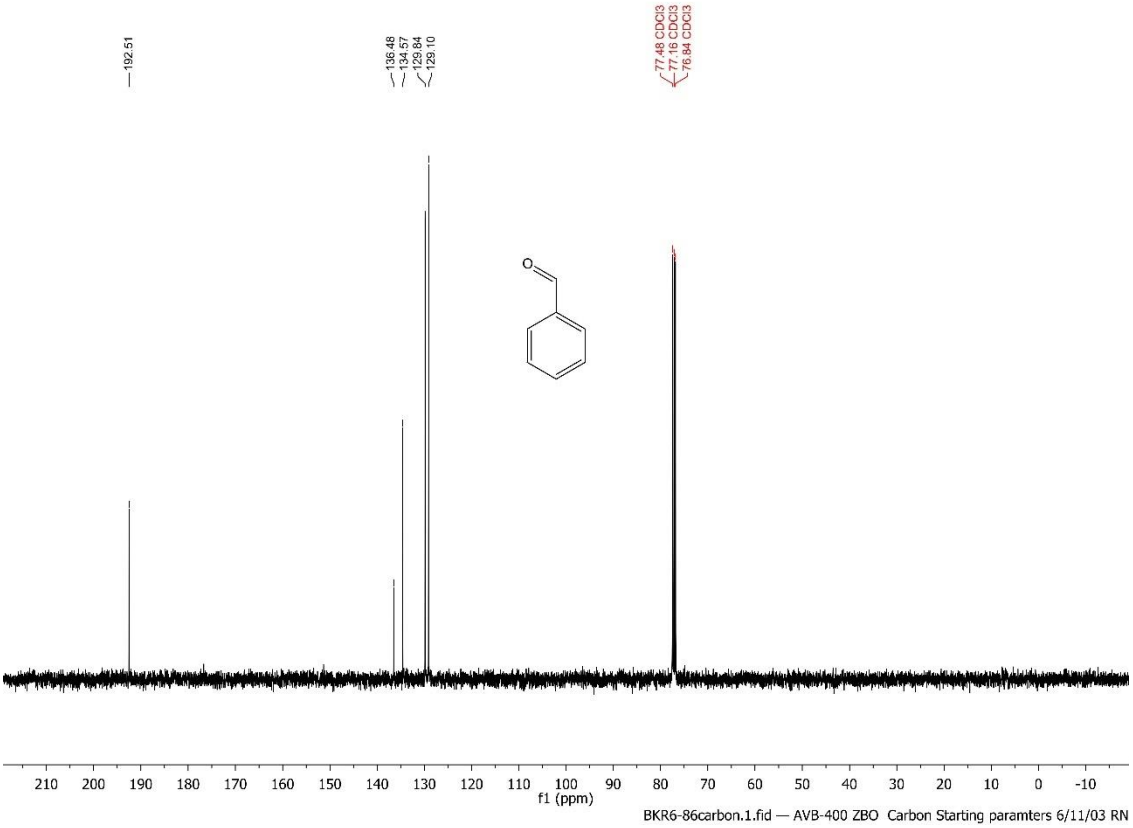

14. References

(1) Miller, E. W.; Lin, J. Y.; Frady, E. P.; Steinbach, P. A.; Kristan, W. B.; Tsien, R. Y. Optically Monitoring Voltage in Neurons by Photoinduced Electron Transfer through Molecular Wires. *Proc. Natl. Acad. Sci. U. S. A.* **2012**. https://doi.org/10.1073/pnas.1120694109.

(2) Magde, D.; Wong, R.; Seybold, P. G. Fluorescence Quantum Yields and Their Relation to Lifetimes of Rhodamine 6G and Fluorescein in Nine Solvents: Improved Absolute Standards for Quantum Yields¶. *Photochem. Photobiol.* **2002**. https://doi.org/10.1562/0031-8655(2002)075<0327:fqyatr>2.0.co;2.

(3) Zhang, X. F.; Zhang, J.; Liu, L. Fluorescence Properties of Twenty Fluorescein Derivatives: Lifetime, Quantum Yield, Absorption and Emission Spectra. *J. Fluoresc.* **2014**. https://doi.org/10.1007/s10895-014-1356-5.

(4) Fischer, M.; Georges, J. Fluorescence Quantum Yield of Rhodamine 6G in Ethanol as a Function of Concentration Using Thermal Lens Spectrometry. *Chem. Phys. Lett.* **1996**, *260*, 115–118.

(5) Wall, K. P.; Dillon, R.; Knowles, M. K. Fluorescence Quantum Yield Measurements of Fluorescent Proteins: A Laboratory Experiment for a Biochemistry or Molecular Biophysics Laboratory Course. *Biochem. Mol. Biol. Educ.* **2015**, *43* (1), 52–59. https://doi.org/10.1002/bmb.20837.

(6) Kreitzer, F. R.; Salomonis, N.; Sheehan, A.; Huang, M.; Park, J. S.; Spindler, M. J.; Lizarraga, P.; Weiss, W. A.; So, P.; Conklin, B. R. A Robust Method to Derive Functional Neural Crest Cells from Human Pluripotent Stem Cells. *Am. J. Stem Cell* **2013**, *2* (2), 119–131.

(7) Lian, X.; Zhang, J.; Azarin, S. M.; Zhu, K.; Hazeltine, L. B.; Bao, X.; Hsiao, C.; Kamp, T. J.; Palecek, S. P. Directed Cardiomyocyte Differentiation from Human Pluripotent Stem Cells by Modulating Wnt/β-Catenin Signaling under Fully Defined Conditions. *Nat. Protoc.* **2013**, *8* (1), 162–175. https://doi.org/10.1038/nprot.2012.150.

(8) Tohyama, S.; Hattori, F.; Sano, M.; Hishiki, T.; Nagahata, Y.; Matsuura, T.; Hashimoto, H.; Suzuki, T.; Yamashita, H.; Satoh, Y.; et al. Distinct Metabolic Flow Enables Large-Scale Purification of Mouse and Human Pluripotent Stem Cell-Derived Cardiomyocytes. *Cell Stem Cell* **2013**, *12*, 127–137.

(9) Lazzari-Dean, J. R.; Gest, A. M. M.; Miller, E. W. Optical Estimation of Absolute Membrane Potential Using Fluorescence Lifetime Imaging. *Elife* **2019**, *8*, e44522. https://doi.org/10.7554/elife.44522.

(10) Edelstein, A. D.; Tsuchida, M. A.; Amodaj, N.; Pinkard, H.; Vale, R. D.; Stuurman, N. Advanced Methods of Microscope Control Using MManager Software. *J. Biol. Methods* **2014**, *1* (2), 10. https://doi.org/10.14440/jbm.2014.36.

(11) Laughner, J. I.; Ng, F. S.; Sulkin, M. S.; Arthur, R. M.; Efimov, I. R. Processing and Analysis of Cardiac Optical Mapping Data Obtained with Potentiometric Dyes. *Am. J. Physiol. Heart Circ. Physiol.* **2012**, *303* (7), H753-65. https://doi.org/10.1152/ajpheart.00404.2012.

(12) Boggess, S. C.; Gandhi, S. S.; Siemons, B. A.; Huebsch, N.; Healy, K. E.; Miller, E. W. New Molecular Scaffolds for Fluorescent Voltage Indicators. *ACS Chem. Biol.* **2019**, *14* (3), 390–396. https://doi.org/10.1021/acschembio.8b00978.

(13) Boelens, H. F. M.; Dijkstra, R. J.; Eilers, P. H. C.; Fitzpatrick, F.; Westerhuis, J. A. New Background Correction Method for Liquid Chromatography with Diode Array Detection, Infrared Spectroscopic Detection and Raman Spectroscopic Detection. *J. Chromatogr. A* **2004**, *1057* (1–2), 21–30. https://doi.org/10.1016/j.chroma.2004.09.035.

(14) Luo, S.; Michler, K.; Johnston, P.; Macfarlane, P. W. A Comparison of Commonly Used QT Correction Formulae: The Effect of Heart Rate on the QTc of Normal ECGs. *J. Electrocardiol.* **2004**, *37* (SUPPL.), 81–90. https://doi.org/10.1016/j.jelectrocard.2004.08.030.

(15) Liu, M.; Jia, M.; Pan, H.; Li, L.; Chang, M.; Ren, H.; Argoul, F.; Zhang, S.; Xu, J. Instrument Response Standard in Time-Resolved Fluorescence Spectroscopy at Visible Wavelength: Quenched Fluorescein Sodium. *Appl. Spectrosc.* **2014**, *68* (5), 577–583. https://doi.org/10.1366/13-07236.

(16) Barry, P. H. JPCalc, a Software Package for Calculating Liquid Junction Potential Corrections in Patch-Clamp, Intracellular, Epithelial and Bilayer Measurements and for Correcting Junction Potential Measurements. *J. Neurosci. Methods* **1994**, *51* (1), 107–116. https://doi.org/10.1016/0165-0270(94)90031-0.

(17) Zakrzewska, A.; Gawinecki, R.; Kolehmainen, E.; Ośmiałowski, B. 13C-NMR Based Evaluation of the Electronic and Steric Interactions in Aromatic Amines. *Int. J. Mol. Sci.* **2005**. https://doi.org/10.3390/i6010052.

(18) Kulkarni, A.; Zhou, W.; Török, B. Heterogeneous Catalytic Hydrogenation of Unprotected Indoles in Water: A Green Solution to a Long-Standing Challenge. *Org. Lett.* **2011**. https://doi.org/10.1021/ol2019899.

(19) Maiti, D.; Fors, B. P.; Henderson, J. L.; Nakamura, Y.; Buchwald, S. L. Palladium-Catalyzed Coupling of Functionalized Primary and Secondary Amines with Aryl and Heteroaryl Halides: Two Ligands Suffice in Most Cases. *Chem. Sci.* **2011**. https://doi.org/10.1039/c0sc00330a.

(20) Ahlbrecht, H.; Düber, E. O.; Epsztajn, J.; Marcinkowski, R. M. K. Delocalisation, Conformation and Basicity of Anilines. *Tetrahedron* **1984**. https://doi.org/10.1016/S0040-4020(01)99321-4.

(21) Katritzky, A. R.; Yannakopoulou, K.; Lue, P.; Rasala, D.; Urogdi, L. The Chemistry of N-Substituted Benzotriazoles. Part 14. Novel Routes to Secondary and Tertiary Amines and to N,N-Disubstituted Hydroxylamines. *J. Chem. Soc. Perkin Trans. 1* **1989**. https://doi.org/10.1039/p19890000225.

(22) Bourke, D. G.; Collins, D. J. Synthesis and Some Reactions of 1-(Trimethoxymethyl)Cyclohexene. *Aust. J. Chem.* **1996**. https://doi.org/10.1071/CH9961287.

(23) Kitching, W.; Jonge, I. De; Adcock, W.; Abeywickrema, A. N. Inhibition and Enhancement of Resonance as Studied by 13C Nuclear Magnetic Resonance Spectroscopy. *Org. Magn. Reson.* **1980**. https://doi.org/10.1002/mrc.1270140615.

(24) G.R. Fulmer; A.J.M. Miller; N.H. Sherden; H.E. Gottlieb; A. Nudelman; B.M. Stoltz; J.E. Bercaw; Goldberg, K. I. NMR Chemical Shifts of Trace Impurities: Common Laboratory Solvents Relevant to the Organomettalic Chemist. *Organometallics* **2010**.